1-1-2017

Biomaterials Approaches For Utilizing The Regenerative Potential Of The Peripheral Nerve Injury Microenvironment

Melissa Renee Wrobel
Wayne State University,

BIOMATERIALS APPROACHES FOR UTILIZING THE REGENERATIVE POTENTIAL OF THE PERIPHERAL NERVE INJURY MICROENVIRONMENT

by

MELISSA RENEE WROBEL

DISSERTATION

Submitted to the Graduate School

of Wayne State University,

Detroit, Michigan

in partial fulfillment of the requirements

for the degree of

DOCTOR OF PHILOSOPHY

2017

MAJOR: BIOMEDICAL ENGINEERING

Approved By:

_____

Advisor Date

_____

_____

_____

_____

DEDICATION

In Loving Memory of Regina Stella Wrobel

1936-2017

ACKNOWLEDGEMENTS

A part of me always wanted to earn a PhD, but I lacked the self-confidence to make that goal a reality. So first and foremost, I have to thank Harini Sundararaghavan (aka “Dr.S”) for inviting me into her lab and affording me this opportunity. Without that invitation, this dissertation would not exist. Thank you Dr.S for encouraging me to pursue opportunities I would have otherwise passed up, for challenging me to step outside of my comfort zones (all those presentations!), and for reassuring me during times of disappointment. I am finishing this degree a more independent and more confident person than when I started and I owe that all to you.

Next, I need to thank my other committee members, Karen Beningo, Howard Matthew, and Weiping Ren for their guidance and perspective. I deeply admire you all and look forward to both professional and friendly relationships in the future. I also want to thank Wayne State University, the College of Engineering, and the Biomedical Engineering department for supporting me academically and financially. I have been beyond fortunate for the support provided to me by this institution, its faculty and its students. There truly is a sense of community here that I have never felt more strongly than I do now and that I will never forget.

I felt no greater sense of community than with my peers and colleagues in Dr.S’s lab, especially Tonya Whitehead, Beth Steel, and Lizzy Mays. As my time as a PhD candidate at Wayne State draws near, I have fallen victim to “senior-itis”, sometimes feeling desperate to move on and move out. Lizzy, seeing you finishing up your coursework and finally getting into your research, reminds me of how exciting science can be during those first experiments and why I wanted to do this in the first place. You’ve also taught me that I *am* the kind of person capable of making a fast friend. I’m sorry to be leaving after only a couple years with you. I really look forward to returning for your own dissertation defense!

Beth, you have taught me the importance of opening up to other people and the value of sharing my experiences. I could have gone through my entire college career doing everything on

my own and taking help from no one, but what a hollow education I would have received. “Bouncing” ideas off one another has produced some of our best, and potentially some of our worst too. Either way, I’m grateful to have had those times. You are passionate about life and science and I so admire your tenacity.

Tonya, you have “forced” me into a lot of different activities during my time at Wayne State. And I cannot thank you enough. You pressured me to participate in groups (including TBP, BMES, SWE, Journal clubs, teaching, etc) that resulted in leadership opportunities, professional experience, and lifelong friends. I’m not sure how I will ever repay you for helping me have such a rich experience here. Thank you for deciding to be my friend after all ;-) and for letting me by myself, but now a slightly better version thanks to you.

Tonya, Beth, and Lizzy, I can imagine no three better women to have gone through this PhD journey with than you. I feel so ridiculously lucky to have spent every day not just with lab mates but with true friends. Special thanks to the undergrads that have gone through the Sundararaghavan lab through the years. There are too many of you to name specifically but you know who you are and I thank you. Dr.S’s lab is truly the best group of people at Wayne State and if anyone wants to challenge us…bring it on!

I also need to thank my oldest and closest friends, my brother Matthew Wrobel and my “sister” Jennifer (Thomas) Miller. Jen, thank you for letting me type so obnoxiously loud on my keyboard during undergrad that it kept you awake at night. I needed those grades to get me where I am now. With you two I get to turn off the science for a few hours and just be silly. You two remind me to never take myself too seriously and to always have fun. So, as soon as I’m done with this degree, do you guys wanna play Mario Party?

I also need to thank my incredible boyfriend Mat Lutz. Having endured my senior year at Michigan and all 7 years of graduate school at Wayne State, you’ve truly tolerated all the ups and downs of this degree, and have somehow remained so unbelievably dependable. You’ve provided me with everything from comfort and calm to candy and caffeine (you literally delivered to me

whatever I asked for during grueling hours of writing and at all hours of the day!) You've kept me sane and probably alive (so klutzy!). As the street smarts to my books smarts, you are my indispensable other half. I am so grateful for you. Also, I begrudgingly thank you for making me get our two cats, Max and Kirby. I never knew I could love two fur balls so much. Thankfully, they are good listeners. Every person mentioned here should probably thank the cats because it means you had to listen to me complain at least one fewer time!

Finally, I need to thank my entire family. Thank you to every aunt, uncle, and cousin (there are too many of you to name!) Special thanks to my grandparents, Robert and Rosemarie Francis and Robert and Regina Wrobel. Thank you for your appearances at my school events throughout the years. Thank you for your unwavering support. I know that you are all my biggest fans. It may not have seemed like it, but I'm grateful to each one of you who has ever asked me "when will you graduate?" Your consistent reminders only showed how much you care. Most importantly, thank you to my parents, Ken and Renee ("Lady") Wrobel. You are the two most loving and generous parents, possibly in existence. Everything I have, everything I am, and everything I will ever be, I owe to you two. I love you Mom and Dad and I hope I've made you proud.

Earning this degree has been more than I could have ever imagined. To anyone who had a part in my life the past several years, no matter how small, I thank you.

TABLE OF CONTENTS

LIST OF TABLES

LIST OF FIGURES

CHAPTER 1: INTRODUCTION AND BACKGROUND

Prevalence and Significance of Peripheral Nerve Injuries

Trauma is the most common cause of peripheral nerve injuries (PNI) comprising nearly 3% of all traumatic injuries in the United States. In combat, however, PNI comprises up to 30% of injuries to the extremities.[1-3] Drug regimens (e.g. chemotherapy) and disease (e.g. diabetes) present additional causes of PNI, bringing the potential number of affected patients into the millions.[4] In 2012, the number of PNI surgical procedures in the United States was estimated at 560,000 and the market for PNI repair was estimated at $1.3-1.9 billion.[5]

All peripheral nerves have the potential to regenerate, even following complete nerve transection, if the gap between the two nerve ends is short.[6] As the gap length exceeds a critical size of ~3cm, however, the intrinsic regeneration process becomes delayed or deficient requiring surgical treatment. Current treatments (e.g. coaptation, grafting, and nerve guide conduits) are either unavailable or insufficient to achieve full functional recovery in large (>3cm) peripheral nerve gaps. PNI recovery diminishes with each additional centimeter of separation in a transected nerve. Failed recovery may come at the cost of life-long morbidity, paralysis, and/or vulnerability to other risks.

This thesis focuses on understanding the complex molecular and cellular environment that develops following PNI, including the presence of inhibitory signaling molecules and inflammatory cell responses. This thesis explores the use of different tissue engineering strategies to direct the behavior and phenotype not only of neurons, but glia (Schwann cells) and immune cells (macrophages). The overall hypothesis is that biomaterials-based adhesive and topographical cues, designed to mimic the innate regenerative capacity in short injuries, can be used to accelerate regeneration and repair. The strategies explored here can ultimately help improve the design of treatments for large PNI. To understand the complexity of the PNI environment, a detailed description of peripheral nerve anatomy and physiology follows.

Nerve Anatomy and Physiology

The human nervous system is divided into the central nervous system (CNS), composed of the spinal cord and brain, and is connected to the rest of the body by the peripheral nervous system (PNS). Communication between the PNS and CNS is coordinated by neurons, the major cell type of the nervous system. The PNS is composed of two types of neurons. Motor neurons transmit signals from their cell bodies in the spinal cord out to distant target organs.[7] Alternatively, sensory neurons transmit signals from their cell bodies in the periphery towards the spinal cord to synapse with central neurons. Neurons transmit these signals via long cytoplasmic extensions, called axons. Most axons are wrapped in an insulating coating, called the myelin sheath, which allows for faster conduction of nerve impulses compared to unmyelinated axons.[8]

In the PNS, myelin sheath is produced by Schwann cells specifically associated with individual axons. Schwann cells are non-neuronal, supportive glial cells making up approximately 80% of the cells in adult peripheral nerves.[9] The Schwann cells are surrounded by a thin, continuous layer of basal lamina (mostly collagen fibrils and a few fibroblasts), called the endoneurium. Non-myelinated axons are embedded directly within Schwann cell cytoplasm.[10]

Axons, and their Schwann cells, are arranged in motor and sensory bundles, called nerve fascicles, which are separated by another connective tissue layer called the perineurium. The perineurium consists of many longitudinally aligned collagen fibrils and layers of flattened perineurial cells.[11] Finally, the epineurium is the outermost layer of connective tissue which holds many fascicles, as well as loose connective tissue, adipose tissue, and blood vessels together into a whole nerve.

Peripheral Nerve Injury Classifications

In the 1940s, a British orthopedic surgeon, Sir Herbert Seddon, offered the earliest classifications of nerve injury. He described three nerve injury grades: neurapraxia, axonotmesis, and neurotmesis, each defined by increasing severity of axon and connective tissue layer damage. In

1951, Australian professor of anatomy and neurology, Sydney Sunderland, used histological sections to expand these classifications into injury grades I through V. **Table 1-1** combines Seddon and Sunderland's work. The remainder of this thesis will discuss strategies specifically aimed at improving nerve regeneration following complete transection injuries (neurotmesis; grade V) that result in large nerve gaps (>3cm) for which spontaneous recovery is impossible and surgical interventions still fail to produce full functional recovery.

Seddon	Sunderland	Typical Etiology	Injured Tissues	Injury Characteristics	Spontaneous Recovery Potential
Neurapraxia	I	Compression Injury	Myelin	Axon intact, conduction block	Full; weeks to months
Axonotmesis	II	Crush Injury	Myelin, axon	Axon discontinuity, conduction failure	Full; 2 to 4 months
Axonotmesis/ Neurotmesis	III	Transection Injury	Myelin, axon, endoneurium	Nerve is still continuous, tissue stiffening and enlargement	Slow, incomplete
Axonotmesis/ Neurotmesis	IV	Transection Injury	Myelin, axon, endoneurium, perineurium	Same as III + fascicle damage	Poor without surgical intervention
Neurotmesis	V	Transection Injury	Myelin, axon, endoneurium, perineurium, epineurium	Same as IV + substantial hemorrhaging and scarring	None without surgical intervention

Table 1-1. Peripheral Nerve Injury Grades

The severity of PNI increases from grades I-V. The table defines the tissue layers involved and the probable clinical outcomes for each class of injury.

Characterization of the Peripheral Nerve Injury Microenvironment

Following peripheral neurotmesis, a cascade of degenerative cellular and molecular changes occurs at the site of injury.

Neuronal Responses

In the proximal nerve stump (part of the axon still connected to the neuron's cell body), neurons undergo morphological changes to allow for intrinsic regeneration, most importantly, the

reformation of the growth cone (**Figure 1-1**). The growth cone is a specialized structure at the tip of an advancing axon primarily comprised of actin filaments and microtubules. Growth cones are highly motile structures that explore the extracellular environment using sheet-like (lamellipodia) and finger-like (filopodia) extensions to sense biochemical and physical guidance cues. Growth cones are thus responsible for determining in which direction to grow and then must guide the axon in that direction.[12]

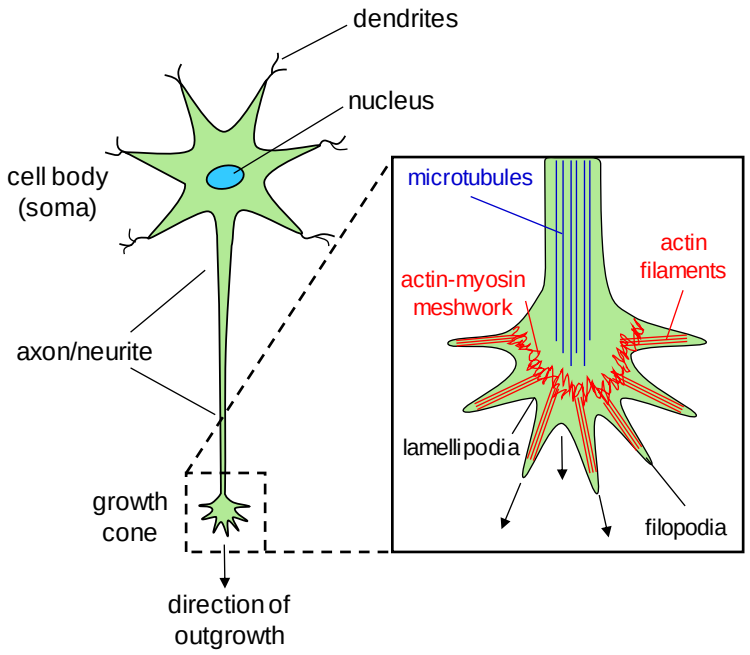

Figure 1-1. The growth cone

Schematic representation of a neuron and detailed view of the growth cone with its main cytoskeletal components.

The growth cone is responsible for mediating axon extension during normal embryonic development and following injury. In both instances, axon extension occurs through a well-defined three-step process: 1) protrusion and attachment of filopodia to a substrate, 2) engorgement of the growth cone by microtubules and organelles, and 3) consolidation of a new stretch of axon shaft behind the advancing growth cone.[13] The three stages of growth cone advance are all influenced by environmental factors, namely adhesive cues in the surrounding matrix. Growth cone

receptors bind to an adhesive substrate initiating intracellular signaling cascades to further anchor the cell cytoskeleton to the surface and advance the neurite outgrowth in a rate controlled manner.[14]

During the development and differentiation of the nervous system axons extend over exceedingly long distances (>1 meter).[15, 16] This development involves periods of axon elongation, retraction, and branching. Neurons extend processes in an excessive and redundant manner. Thus, some of these branches require selective removal to achieve a final organized and complex circuitry.[17] This removal of aberrant processes, called pruning, is important for proper nervous system development.[18] Within the first 2 days following injury, axons in the proximal stump also produce many sprouts or branches, from the terminal axon tip, that advance distally. However, most of these sprouts never make reconnections across the gap but rather undergo periods of extensive degeneration and retraction.[19]

Axon degeneration can occur as the result of several different physiological or pathological conditions. Some causes of degeneration include Wallerian degeneration (distal nerve stump retraction following transection, described next), toxic agent insult, trophic factor deprivation, and neurodegenerative disease.[17, 19] The father of modern neuroscience, Santiago Ramon y Cajal, was first to describe both long distance retraction, called "resorption," and the pathological morphology of retracting growth cones (he called them "sterile clubs").[20] In general, retracting growth cones have a smooth terminal bulb, while elongating growth cones are ruffled with filopodial extensions.[21] Retracting axon shafts can assume different morphologies including bead-like spherical blebbing or retracting as a sinusoidal curve.[22] One primary goal of this work was to reduce neurite retraction events using a novel, tissue engineered construct featuring topographical and adhesive, biochemical cues for guidance of the growth cones.

In the distal nerve stump (part of the axon separated from the neuron's cell body), axons undergo widespread disintegration of their cytoskeleton and internal organelles, primarily due to the lack of trophic support from the soma. This process is called Wallerian degeneration (WD),

after British physiologist, Augustus Volney Waller, who first described the phenomenon in the mid- 1800s. The first few hours of WD involve neurofilament break up and axonal fragmentation. Next the myelin sheath begins to break down into droplets over a few days, with complete denaturation of the myelin after a few weeks. Despite its seemingly catastrophic nature, this type of axonal degeneration is a normal part of the repair process, primarily because axonal breakdown initiates a pro-healing response from Schwann cells and macrophages in the injury site.

Glial and Immune Cell Responses

Following PNI, Schwann cells undergo a process, often referred to as de-differentiation, assuming the phenotype and gene expression of immature, pre-myelinating cells.[9] These post-injury Schwann cells also begin to hyperproliferate in response to myelin and axonal debris and the loss of physical axonal contact. Proliferating Schwann cells migrate along residual basement membrane forming longitudinal, cellular columns called the Bands of Bungner. These bands serve as cellular "bridges" that span the nerve gap and provide a substrate for regenerating axons. Schwann cells further support axon regeneration by depositing extracellular matrix (ECM) proteins and secreting neurotrophic factors (e.g. nerve growth factor, NGF). However, Schwann cells also express chondroitin sulfate proteoglycans (CSPGs) following injury, which are traditionally studied as physical and chemical inhibitors to axon regeneration in the CNS, but have more recently been discovered to inhibit axon outgrowth following PNI as well.

Denervated Schwann cells play an early role in removing this debris from the injury site and are the major phagocytic cells for the first few days after injury.[23] In additional to releasing factors for neuronal growth and survival, Schwann cells also release cytokines to recruit circulating macrophages to the injury site. Macrophages phagocytose myelin debris during the later stages of Wallerian degeneration. Macrophages are not only essential for effective myelin phagocytosis but also produce mitogenic factors for Schwann cell activation. Macrophages have even been shown to stabilize neurite outgrowth from dorsal root ganglia grown on pre-injured nerve

cryosections[24] and can remodel the distal nerve's ECM in preparation to receive the re-growing axons.[23]

Following less severe nerve injuries (Sunderland classifications I-III) or in very short nerve gaps, growth cones that extend into the defect site along the Bands of Bungner will eventually restore axon-Schwann cell contact. These renewed cell-cell interactions trigger the Schwann cells to 're-differentiate' and begin remyelinating the newly formed nerve fibers. Macrophage contact with this 'new' myelin can trigger the immune cells' exit from injury site and re-entry into circulation. Thus, interactions between Schwann cells and macrophages are imperative for this 'normal' peripheral nerve regeneration to proceed (**Figure 1-2**).

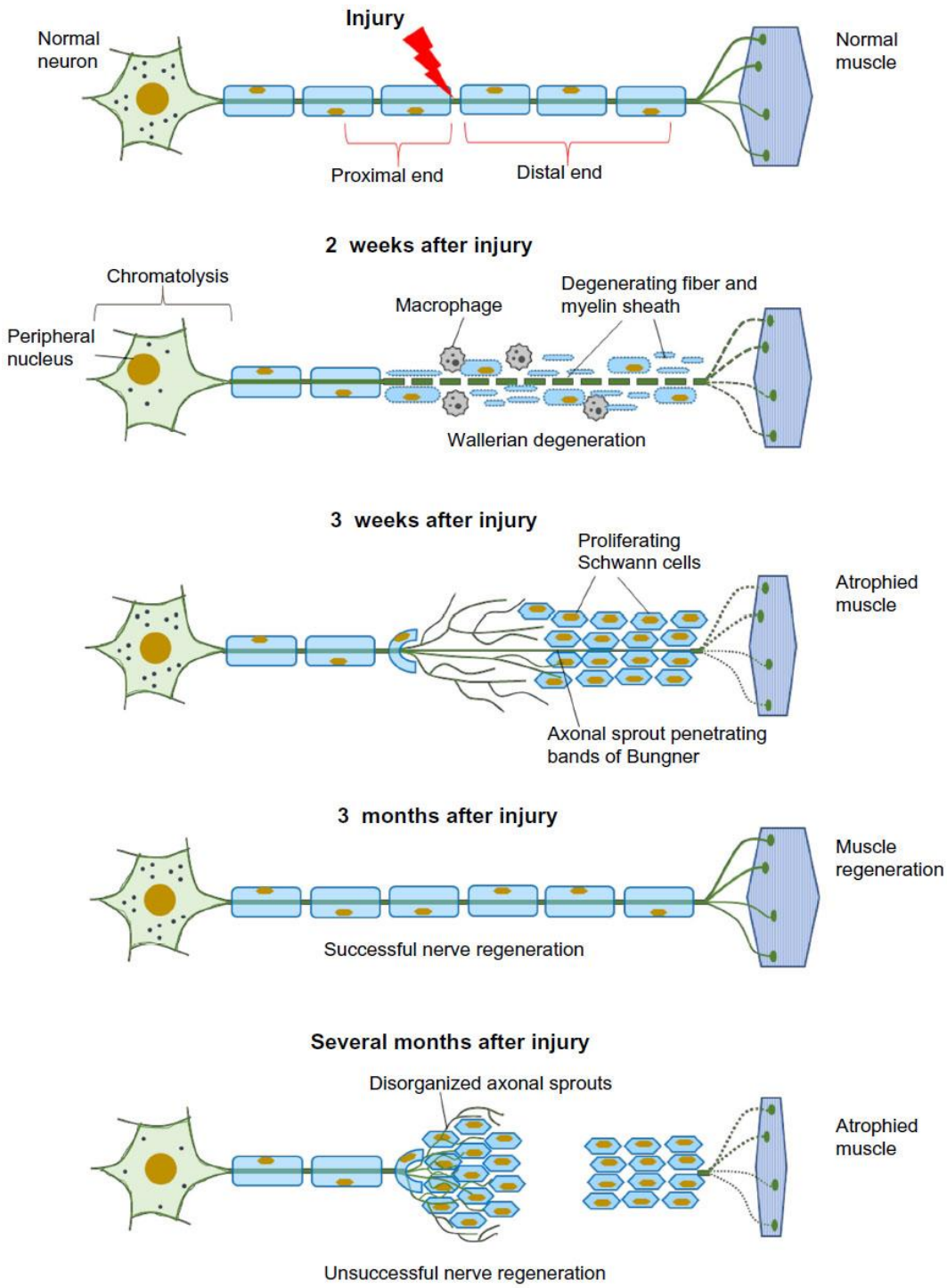

Figure 1-2. Typical repair schema following peripheral nerve injury
The "normal" regeneration program that proceeds in short peripheral nerve gaps includes dedifferentiatoin, hyperproliferation and alignment of Schwann cells into the Bands of Bungner. Infiltrating macrophages facilitate repair by cleaning up axonal and myelin debris. These non-neuronal responses are essential to successful nerve regeneration. (This figure has been reproduced freely under a Creative Commons Attribution license. © 2014 Arslantunali et al. Originally published by Dove Medical Press Limited DOI: https://doi.org/10.2147/MDER.S59124)

Chondroitin Sulfate Proteoglycans

Proteoglycans are complex molecules featuring a glycosylated core protein and one of three types of carbohydrate side chains (chondroitin, heparan or keratin sulfates).[25] Proteoglycans are found in the ECM where they often form large complexes with other proteoglycans and hyaluronan. Proteoglycans were initially believed to be "filler" in the ECM following their isolation in the 1890s but have since been shown to have important roles in cell migration and disease progression. In nerve ECM, proteoglycans play important roles in axonal guidance during development and following injury.[26] Individual functions of proteoglycans can be attributed to either the protein core or attached glycosaminoglycan (GAG) side chains.

Chondroitin sulfate proteoglycans (CSPGs) are the most well characterized of the proteoglycans for their inhibition of axon outgrowth following injury, especially in the CNS where CSPGs are studied as a physical barrier to axon regeneration as part of the glial scar. The role of CSPGs in the PNS is far less studied even though it is known that CSPG expression by endothelial cells and Schwann cells increases following PNI.[26] CSPGs in the PNS interact with outgrowing neurites via receptors on the neuron cell body and growth cone.[25] **Figure 1-3** illustrates CSPG structure and function following PNI.

In the PNI environment, CPSGs are primarily distributed in the Schwann cell endoneurium and surrounding newly formed Bands of Bungner.[26] Because of their ability to inhibit axon growth, CSPGs may help prevent aberrant growth into the extraperineurial space that could lead to neuroma formation. This would mimic nervous system development where CSPGs function as necessary guidance cues and are expressed temporally and spatially to guide neurons to appropriate targets by inhibiting them from entering inappropriate areas.[27, 28] In this thesis we will present results demonstrating the potential of CSPGs as a unique cue for PNI regeneration and not a molecule to be avoided.

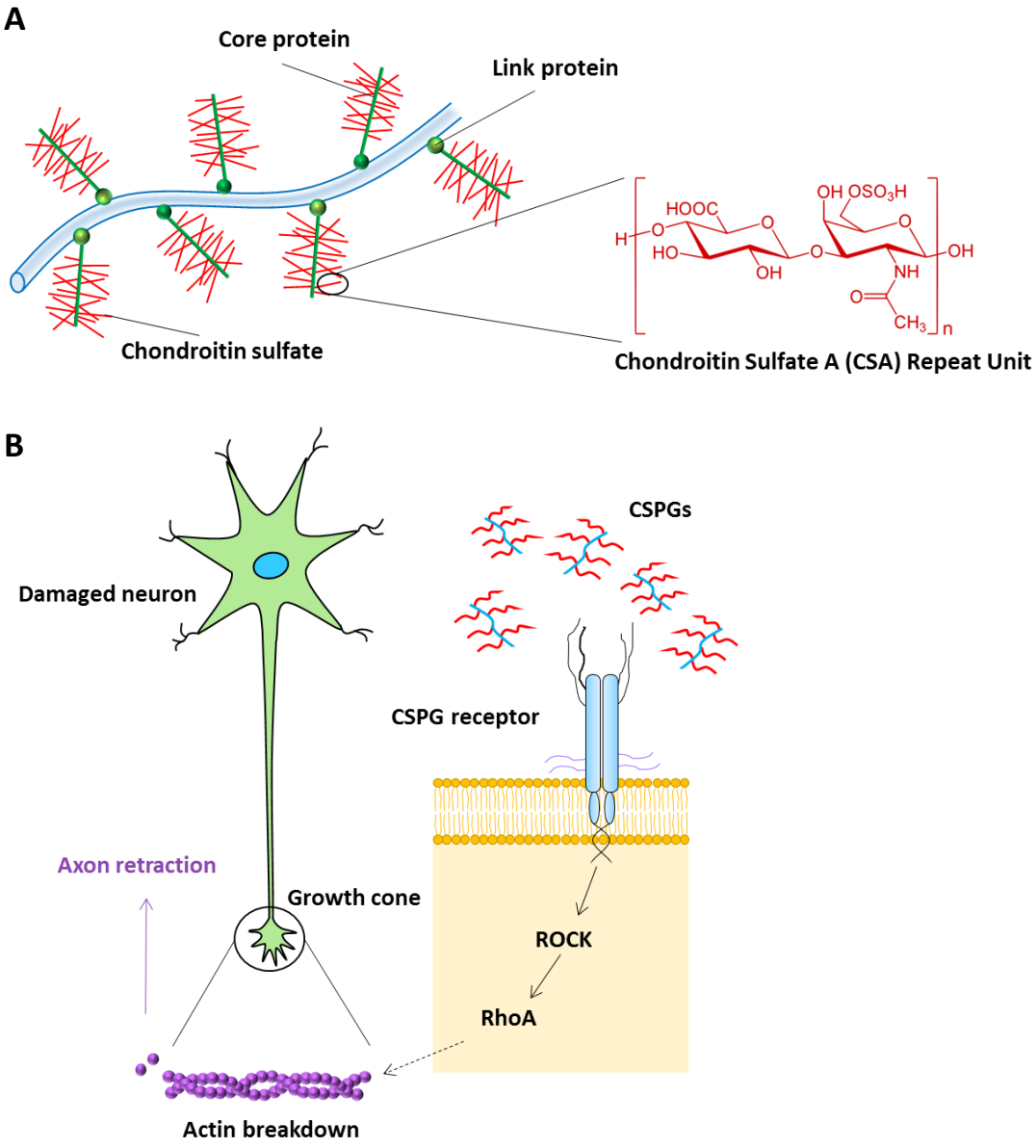

Figure 1-3. Chondroitin sulfate proteoglycans structure and function

Chondroitin sulfate proteoglycan (CSPG) structure **(A)** and function following peripheral nerve injury. Glycosaminoglycan (GAG) side chains are the inhibitory component of CSPGs and the GAG, Chondroitin sulfate A (CSA), was chosen as representative of injured nerve extracellular matrix in this study. **(B)** Intracellular signaling mechanism triggered by CSPGs. Binding of CSPG receptors present in axons initiates growth cone inhibition. RhoA activation eventually leads to actin de-polymerization and growth cone retraction.

Problem Statement: Current Treatments are Insufficient to Repair Large Nerve Gaps

Traditional treatments for PNI, including coaptation, autografting, and allografting are insufficient to achieve full functional recovery in large gaps (>3 cm in humans). Therefore, several research groups have focused on neural tissue engineering to replace grafting. The most popular tissue engineered strategies involve synthetic nerve guide conduits (NGCs), which are hollow tube devices designed to hold the two nerve ends in close proximity.[29] Unfortunately, NGCs have been unable to match the success of autografts *in vivo.* In this section, we discuss the drawbacks of current treatments and propose improvements to the current NGC model. We hypothesize that many neural tissue engineered strategies have failed because of a lack of study of the complete regenerative environment before going *in vivo*. **Figure 1-4** summarizes currently available PNI treatment options based on gap size.

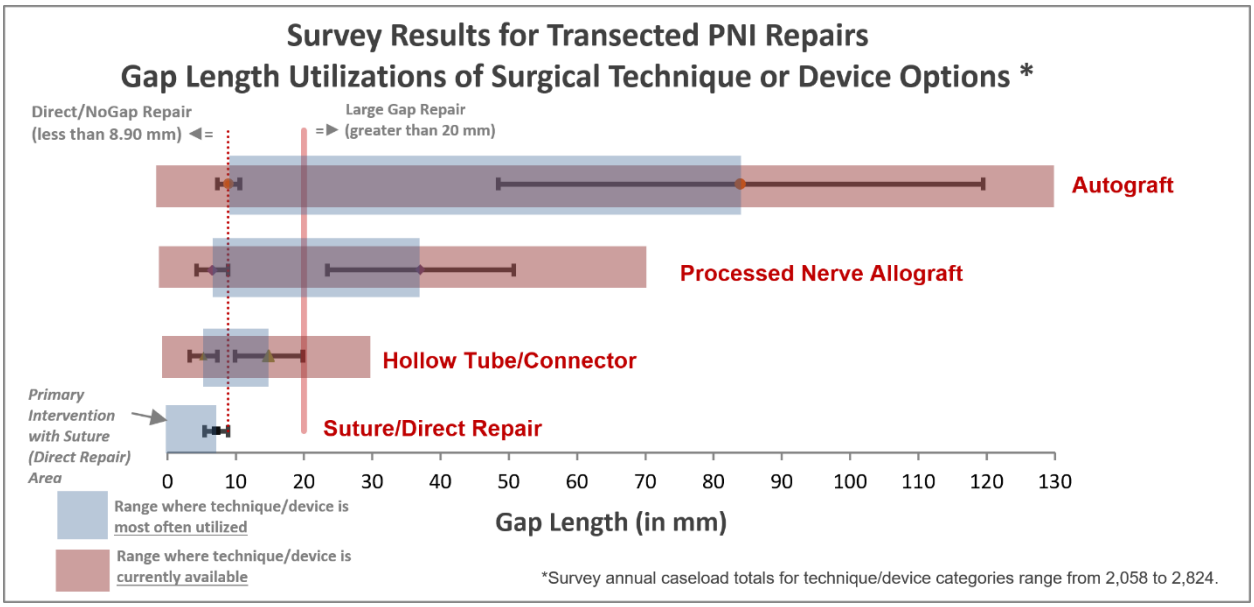

Figure 1-4. PNI repair options by size and availability

As PNI gap size increases, the availability (pink) and utilization (blue) of different treatment options diminishes. A critical need exists to develop nerve guide conduits that can treat large nerve gaps in the clinic. (This figure was originally published in the *Analysis of the Peripheral Nerve Repair Market in the United States*, 2012 by Magellan Medical Technology Consultants, Inc. and was reproduced freely as part of the public domain. Original file provided by the author Kurt Brattain).

Grafting

Coaptation, is defined as the joining or reuniting of two surfaces, in this case the two nerve stumps following nerve transection. This direct suturing of epineurial structures is the preferred surgical treatment because it allows for the gross lining up or matching of fascicles and blood vessels which produces the best functional outcomes.[7] When coaptation of the two nerve ends would result in destructive tension on the tissues, an autologous nerve graft is the favored treatment option. Autografting takes whole or partial donor nerve tissue from elsewhere in the patient's body to fill the defect site. A single graft is designed to join two nerve ends with a segment of donor nerve of similar diameter. Gaps in large diameter nerves may require cable grafts, where multiple fascicular sections of smaller diameter nerves are used to approximate the diameter of the injured one.[12] However, each nerve can contain between 1-100 fascicles each with a diameter ranging from 0.5-3.5 mm depending on nerve size and location within the body.[30] This diversity of peripheral nerves poses a significant challenge to treatment. Donor nerve is typically harvested from dispensable sensory nerves, especially the sural nerve made up of collateral branches of the tibial and common fibular nerve in the distal part of the leg.

All peripheral axons have the potential to regenerate following injury at rates of 2-5 mm/day.[31, 32] This rate should translate into bridging a critical gap injury (3 cm) in a matter of days; however, reinnervation of target tissues can actually take months, which delays functional recovery and leads to muscular atrophy.[17] As the nerve defect size increases, functional recovery diminishes. Singh et al.[33] performed a comprehensive analysis of 187 patients with complete transection of upper limb peripheral nerves treated with sural nerve autografts. Patients' motor and sensory recovery was analyzed 18 months after surgery. Outcomes of this study are summarized in **Table 1-2**. The percentage of patients achieving ‘good’ motor and sensory recovery (defined by the British Medical Research Council) diminished with increasing gap size.

Gap Size (cm)	% Motor Recovery	% Sensory Recovery
<2.5	100	57
2.5-5	79	45
5.1-7.5	64	37
7.6-10	43	14
>10	43	38

Table 1-2. Peripheral nerve autograft functional outcomes in a clinical trial

The percentage of patients with full motor and sensory recovery following an upper limb injury treated with a sural nerve autograft diminishes with increasing injury size. n = 187 patients; 18 month follow up. Data from Singh et al. 1992.

Despite these discouraging outcomes for large peripheral nerve transections, autografting has remained the "gold standard" treatment for PNI since the 1960s.[34] Furthermore, autografting is associated with a number of other drawbacks including multiple surgeries, donor site morbidity, size mismatch, and limited tissue availability.[35, 36] For patients with extensive nerve injuries and inadequate autologous donor tissue available, human cadaver nerve allografts have been used. However, allografting with donor tissue, typically from a cadaver, faces a different set of challenges including immune rejection and disease transfer.[4] Therefore, allograft recipients typically require several years of immunosuppressive therapy. These issues demand an alternative treatment option.

Neural Tissue Engineering

Tissue engineering utilizes biomaterials, cells, and growth factors (GFs), alone or in combination, to restore, maintain or improve tissue function. The traditional definition of tissue engineering involved isolating healthy cells from a patient, expanding them *in vitro*, seeding the cells onto a biodegradable scaffold (the NGC in nerves), implanting it into the patient, and allowing the body to eventually replace the scaffold with newly grown tissue.[37] Several NGCs have reached clinical trials and the market (FDA has approved 11 new devices in the past 20 years). Current

clinically approved NGCs are made from a variety of materials including: type I collagen, polyglycolic acid (PGA), poly (DL-lactic-co-caprolactone) (PLCL), polyvinyl alcohol (PVA) hydrogel, porcine small intestinal submucosa (SIS) or a combination of these.[38] Devices range in length from 2.5 to 6.35 cm and have degradation rates ranging from 4 months to 4 years (some devices are not bioresorbable). These devices have shown clinical outcomes comparable to autografts but only in small defect (<3cm), small diameter digital nerves. Unfortunately, these devices are all structurally similar to what was first introduced in the 1980s, hollow tubes lacking any internal structure that mimics native nerve tissue[39] and therefore they are not successful for treating larger injuries.

Neural tissue engineers have begun exploring modifications to the basic NGC to improve regeneration. Popular modifications include growth factor delivery, cell delivery (e.g. Schwann cells or stem cells), changes to material properties (e.g. porosity, stiffness, conductivity, and degradation) and material size/shape (e.g. micro- or nano-scale topography, gels, fibers, or patterns). Popular NGC modifications are illustrated in **Figure 1-5**.[39]

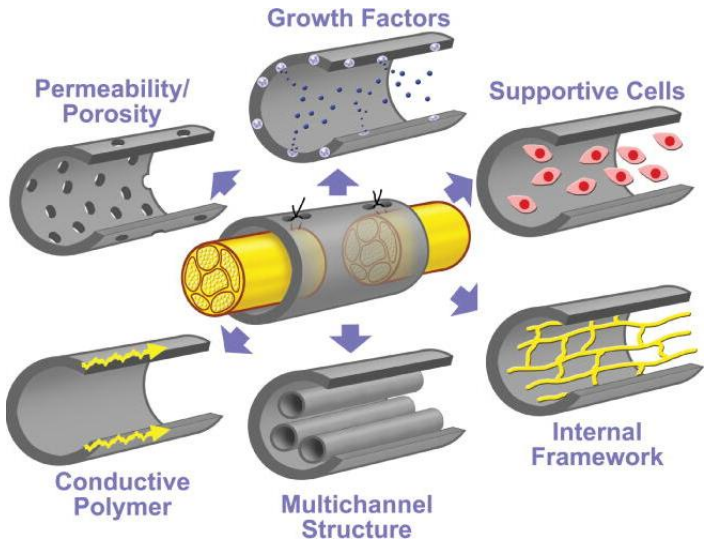

Figure 1-5. Neural tissue engineering strategies to improve NGCs

Modifications to the basic, hollow nerve guide conduit currently being explored by tissue engineers. (This figure has been reproduced with permission from Neurosurgical Focus and the Journal of Neurosurgery Publishing Group. DOI: 10.3171/FOC.2009.26.2.E5)

A full analysis of these modifications will not be described here, but we recommend several great reviews discussing the current state of NGC technology and comparing each of these modifications.[39-43] In this thesis, we have focused on what we believe to be the most promising modifications for future success based on previous studies, ease of delivery, and ease of clinical translation. Our objective is to model intrinsic topographical and adhesive cues, that form during regeneration in short PNI, with biomaterials. We specifically want to explore these cues in the context of the acute PNI environment. This environment contains inhibitory CSPGs and inflammatory glial and macrophage responses, often overlooked by tissue engineers in their pursuit to promote axon outgrowth. Therefore, we explore the effects of a representative inhibitory CSPG, Chondroitin sulfate A (CSA) on neuron, Schwann cell and macrophage responses, especially CSA-induced neurite retraction in real time. We isolate porcine spinal cord extracellular matrix proteins (SCM) and utilize it as a growth permissive substrate. We hypothesize that our matrix is a more complete ECM mimic than fibronectin or laminin cues alone. We then deliver the CSA and SCM cues as part of a tissue engineered scaffold. Our scaffold features electrospun hyaluronic acid (HA) nanofibers providing a topographical cue. Lastly, we explore the effects of the SCM and HA nanofibers on macrophage and Schwann cell response. We hypothesize that our cues can accelerate repair programs in the cells. These cells normally must spend time aligning and laying down matrix. By delivering aligned, ECM-containing fibers to the cells, they might be able to "skip a step" in the repair process. Some of the motivating studies for our work are highlighted below.

Literature Review and Motivating Work

Topographical Cues

Aligned fibers have a well-established benefit for enhancing neurite outgrowth in the fiber direction.[44, 45] Neurite outgrowth has been studied on a variety of natural and synthetic polymers including gelatin, chitosan, silk fibroin, poly-lactic-glycolic acid, polyurethane, poly-vinyl alcohol, poly-caprolactone, and any number of combinations of these polymers.[37, 46] Aligned fibers can also be fabricated using a variety of techniques including electrospinning or self-assembly.[47] In

this thesis, we utilize electrospinning to fabricate nanofibrous scaffolds because it is a simple fabrication method, which can be adapted to create fibers of different sizes from many different polymers. We use hyaluronic acid (HA) as our base polymer because it has previously been established as a useful polymer for neural tissue engineering[48] but more importantly, HA is easily modifiable and provides a great vehicle to deliver our adhesive cues (SCM and CSA).

Adhesive Cues

We have already discussed the importance of Schwann cell proliferation and alignment for *physically* guiding axon regeneration. However, research suggests that following axonal injury chemical cues are also released into the injury site.[49] These molecules are released by Schwann cells, endothelial cells, immune cells, and even the injured neurons themselves. Consequently, axon extension based on chemotactic (or diffusible) cues has been the primary approach for guiding axon regeneration since the late 19th century.[50, 51] Chemotaxis describes chemical-induced cell migration, typically the preferential movement of the cells up a concentration gradient of soluble chemoattractant molecules.[52-54] A family of growth factors (GFs) called neurotrophins are the most popular molecules being studied for promoting peripheral nerve regeneration.[55] Neurotrophins play a critical role in regeneration by promoting neuron survival, regulating Schwann cell differentiation, and organizing axon myelination.[56] Unfortunately, growth factor based therapies for peripheral nerve regeneration face a number of challenges. For example, GFs cannot be delivered *in vivo* via conventional methods because of systemic toxicity, slow tissue penetration, and short biological half-lives (minutes to hours).[55, 57] Despite these unresolved issues, the established guidance ability of the neurotrophins, has dictated that chemotaxis be at the forefront of neural tissue engineering research.[58]

While the study of chemotaxis has a longer history, other types of axonal guidance may offer benefits that chemotactic cues cannot provide[59], specifically establishing cues that last the lifetime of an implant. Haptotaxis, first described by Carter in 1965, describes directed cell migration along surface bound cues.[60, 61] Laminin and its derivatives, have been extensively studied *in*

vitro as haptotactic guidance molecules. Several studies have specifically identified the different concentration gradient thresholds of different surface bound cues necessary to initiate directed growth.[62] However, very few studies have combined permissive and inhibitory guidance molecules into one scaffold and only one study looked at a gradient of an inhibitory molecule (Slit-2).[63] Therefore, our approach is innovative because of the unique combination of SCM (permissive) and CSA (inhibitory) guidance cues and their immobilization within a scaffold. The study of soluble chemical cues is more popular but immobilized cues within the fibers are expected to more beneficial in large nerve gaps where they can last the duration of the scaffold.

Decellularized Extracellular Matrix

Processed nerve allografts have also gained recent popularity for treating large PNIs. The resulting decellularized extracellular matrix (ECM) has distinct advantages over synthetic guides (e.g. biochemical cues) and offers regeneration below autografts but better than NGCs in a 3-way comparison.[64, 65] One of the challenges to using whole acellular allografts, however, is preserving the nerve layers and ECM structure. Extensive tissue processing methods, including lyophilization, cold preservation, freeze–thaw cycling, detergent processing, and/or irradiation can lead to poor mechanical properties and frail grafts.[64] Here we still deliver ECM cues, using precipitated matrix proteins, but we allow the HA nanofibers to provide the structural component. Nanofibers are a good mimic of native ECM size and shape.

Residual CSPGs also present a potential source of inhibition in decellularized allografts. Groups have found success pre-treating their grafts with bacterial enzyme, Chondroitinase ABC.[66, 67] Most clinical and experimental studies have used ChABC to degrade and inactivate the entire family of CSPGs within the grafts. Unfortunately, this treatment negates any potential benefits of the CSPG cues. It has been suggested that selective de-inhibition of nerve grafts would be more beneficial to using them in PNI treatment.[68] However, there are no known Chondroitinases that selectively degrade different types of CS chains. CSPGs have the ability to up-regulate receptors in advancing growth cones enabling them to bind strongly to the surrounding

ECM molecules. In the designs proposed here we introduce chondroitin sulfate in a controlled way so that the cells can benefit from both the CS cues and the ECM.

Schwann-cell Inspired Designs

Another obvious issue with processed allografts is their lack of cells, especially Schwann cells, and the regenerative cues provided by them. Therefore, many research groups have focused on re-seeding decellularized donor tissue with the patient's Schwann cells prior to implantation.[69, 70] Many groups have worked on pre-seeding traditional tissue engineered scaffolds with Schwann cells or stem cells, allowing them time to form the Bands of Bungner, prior to implantation. Unfortunately, cell-based therapies, are time consuming, costly, and will be more rigorously evaluated by the FDA, making clinical translation difficult. Several approaches have been established methods to recreate the bands of Bungner following PNI.

Kofron et al. 2010 and Lopez-Fagundo et al. 2013 both used relief replicas of actual cultured Schwann cells to create microwells and 3D micropillars in the size and shape of these cell structures. Unfortunately, neither of these studies had significantly improved neurite outgrowth based on structure size or shape, it was only the presence of a topographical cue, as opposed to a flat surface, that improved neurite behavior. Furthermore, these approaches required several complicated fabrication steps and featured non-biologically relevant materials (e.g. PDMS).[71, 72]

In a study by Georgiou et al. the group designed engineered neural tissue or "ENTs" comprised entirely from aligned Schwann cells.[73] While support cells are absolutely critical to the success of an implanted device finding an appropriate delivery system to keep the cells alive is very difficult to achieve, maintain, and translate.[74] Pre-seeding tissue engineered scaffolds with cells prior to implantation, even if they are autologous cells, will face many challenges to reaching clinical translation. It is anticipated that the best chance to promote regeneration, and reach patients, is to develop an artificial scaffold that mimics these crucial cellular structures.

The Bands of Bungner have a striated appearance, due to not only the presence of elongated Schwann cells but connective tissue bundles.[60] Here we use electrospun nanofibers to

mimic this natural striated appearance as opposed to the smoothness of these other "bio-inspired" designs. The primary goal of this thesis is to control the phenotype and behavior of three key cell types in the peripheral nerve injury environment using naturally derived biomaterials cues to mimic the physical and adhesive guidance during normal axon regeneration.

Modulating Non-Neuronal Cell Phenotypes

Following PNI, Schwann cells undergo a process sometimes referred to as “dedifferentiation,” assuming a phenotype similar to embryonic development (**Figure 1-6A**). Macrophages can also assume distinct phenotypes with different biological activities (**Figure 1-6B**). Macrophage phenotype exists on a spectrum, but subpopulations of macrophages are broadly classified into two major groups: "classically activated" macrophages (M1) and alternatively active macrophages (M2). M1 macrophages arise immediately following PNI and have been shown *in vitro* to be neurotoxic, releasing pro-inflammatory cytokines. Conversely, M2 macrophages have reduced production of these cytokines and release factors that promote tissue repair and wound healing. M2 macrophages have been shown to be neuroprotective and to promote long distance axon growth even in the presence of inhibitory CSPGs.[75]

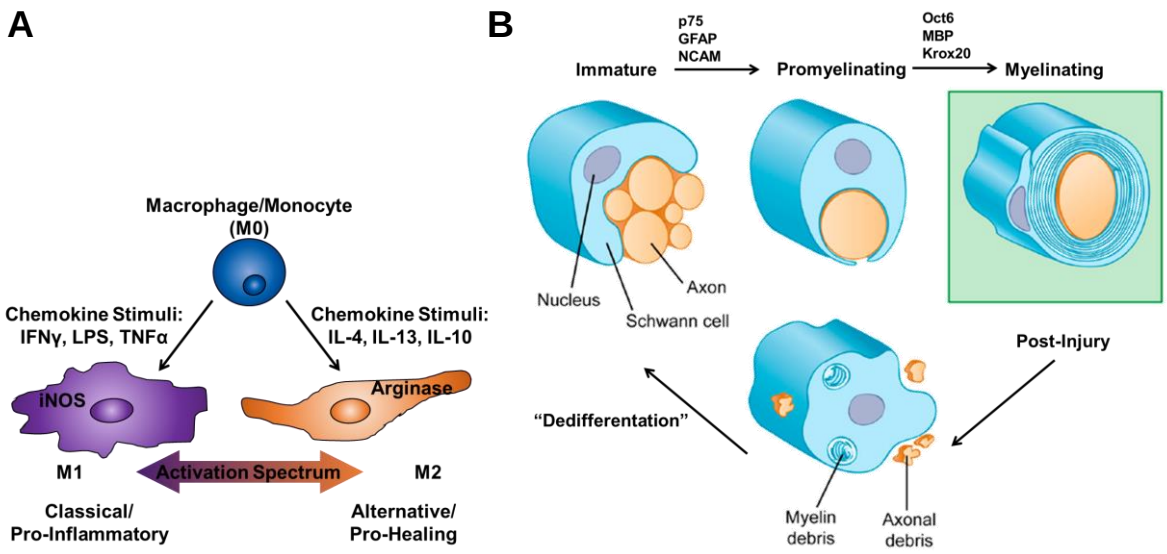

Figure 1-6. Macrophage and Schwann cell phenotypes

Following injury support cells in the microenvironment undergo phenotypical changes. **(A)** Macrophages can assume classical (M1) or alternative activation (M2). **(B)** Schwann cells undergo a "dedifferentiation" process where they assume a phenotype similar to immature cells.
(Part B has been freely adapted from © 2008 Salzer Rockefeller University Press under a Creative Commons Attribution license. DOI: 10.1083/jcb.200804136)

In recent years, many different tissues engineered systems have emerged to treat large nerve gaps. These strategies are routinely evaluated for their effects on neurons but not for their influence on macrophage and Schwann cell phenotype. Following nerve injury, activated macrophages can induce axon retraction. Therefore, approaches aimed at depleting the injury site of macrophages with anti-inflammatory drugs, such as clodronate and minocycline, have garnered attenion. An *in vitro* time lapse video study by Horn et al. concluded that the direct cell-cell contact of macrophages and neurons initiated axon retraction 100% of the time. However, axon retraction in response to the macrophages diminished when neurons were cultured on a growth-promoting laminin substrate. However, the authors did not comment on whether the substrate was affecting the intrinsic growth capacity of the neuron, or altering the activation state of the macrophages, or both. In this study, we offer some additional insight by testing the effects of a growth permissive

substrate, the porcine SCM, specifically on macrophage activation sate. Lastly, Horn et al. reported that only macrophages previously activated to M1, with interferon-y or lipopolysaccharide (LPS), induced significant axon retraction. This result supports the growing theory that macrophage activation state, and not their presence, is critical when considering nerve regeneration.

Macrophage activation is gaining great popularity for improving outcomes in the regeneration of many tissue types include cardiac, dermal, muscle, bone and neural.[76] Most studies, however, focus on shifting the macrophage phenotype towards M2 using established immunomodulatory cytokines such as IL-4, IL-13, M-CSF or exploratory drugs and compounds. Using biomaterials to control macrophage activation, however, eliminates the challenges of delivering these molecules in a clinical setting. Some of the groups who have recently begun testing biomaterials for their effects on macrophage activation are highlighted below.

In a 2013 study, Franz et al created “artificial ECM” (aECM) featuring collagen type I and highly sulfated HA, a type of GAG. The group found that their matrix possessed immunomodulating properties and dampened inflammatory activity of M1-polarized macrophages. The group suggested that their aECM is a promising coating for other biomaterial implants to modulate the healing response.[77] These results were very exciting for us because collagen and sulfated-GAGs are two primary constituents of our SCM. Furthermore, we test it as an adhesive coating on TCP and the HA fibers. Franz’s study indicated our potential for success.

Nanotopography can also affect macrophage activation which occurs most likely through the manipulation of cell shape and orientation.[78] Bartneck et al. found that 2D and 3D electrospun PLGA scaffolds conjugated with RGD (fibronectin derived peptide sequence) reduced macrophage inflammatory responses and directed cells towards M2.[79] Potas et al. covalently linked IL-10 (an M2 stimulating cytokine) to electrospun PCL scaffolds and the scaffolds were wrapped around intact rat sciatic nerves. The group found significantly increased expression of M2 macrophages at the scaffold and in the surrounding tissue evidenced by Arginase 1 and CD206 staining. IL-10 remained immobilized and bioactive for up to 120 days *in vivo*. The group concluded that

biofunctionalized nanofibers are useful for manipulating the peripheral nerve cellular environment and that these types of materials should be adapted for more therapeutic strategies.[80] We agree with these conclusions and aim to utilize topographical (aligned HA fibers) and adhesive biochemical cues (SCM and CSA) in our own scaffolds for directing PNI regeneration.

Biomaterials approaches to altering Schwann cell phenotype have garnered less interest than macrophage studies. However, a few groups having studied the effects of topography[81, 82], stiffness[83], soluble growth factors (e.g. neuregulin)[84], and ECM (e.g. collagen and laminin),[85] for regulating Schwann cell function, especially actin cytoskeletal dynamics, migration, myelination. There are also many groups working on differentiating stem cells from a variety of sources (e.g. human dental pulp, adipose tissue, and umbilical cord) towards a Schwann cell phenotype for treating PNI.[86, 87] These cells are often combined with a biomaterial scaffold. But very few studies are looking at the phenotypical transition, from dedifferentiated/immature to mature, in the Schwann cells as we do here. Cellular plasticity and a spectrum of activation has been demonstrated with macrophages. Schwann cell phenotype can also exist on a spectrum. We believe these two non-neuronal cell types undergo paralleled changes following injury that can be studied, modeled, and influenced similarly with biomaterials.

All of the studies reviewed here motivated the work in this thesis. However, these approaches to PNI repair have never previously come together into a single body of work. Our collective studies offer improved insight into the endogenous potential of the injured peripheral nerve and offer ways to incorporate intrinsic repair cues into a biomaterial system for treating large gaps.

Summary

In a recent review in Experimental Neurology, Webber and Zochodne argued that improving regenerative success [in peripheral nerves] requires "...models that prominently display the problem at hand and a means to locally influence the regenerative milieu."[88] Many current peripheral nerve repair strategies focus on delivering positive, growth promoting cues (e.g. extracellular

matrix, ECM) while eliminating negative, growth inhibiting cues (e.g. chondroitin sulfate proteoglycans, CSPGs) at the injury site. We hypothesized that recapitulating the positive and negative cues of the peripheral nerve injury microenvironment would improve regeneration. Moreover, other groups often fail to test the effects of their cues on cell types other than the neurons. We aim to provide appropriate substrates to facilitate Schwann cell and macrophage responses as well as axonal outgrowth.

In Chapter 2, we tested the effects of a characteristic CSPG, Chondroitin Sulfate A (CSA) on neurite dynamics of dissociated chick embryo dorsal root ganglion (DRG) neurons using time lapse video microscopy. DRG growth was recorded on different adhesive substrates, including a novel, porcine-derived spinal cord matrix (SCM). The SCM significantly increased frequency of neurite extension coordinated by a significant reduction in the neurites' time spent stalled. The SCM also mitigated inhibitory effects of CSA, producing longer neurites than the controls without CSA treatment. We also quantified neurite extension and retraction rates. Next we aimed to elucidate receptors involved in mediating the observed neurite behavior. We hypothesized that CSA mediates the upregulation of cell-surface binding receptors in the neurons and tested this using flow cytometry with fluorescently tagged antibodies for the neurons' surface molecules. Our results showed a significant increase in Syndecan-3 receptor expression in neurons treated with CSA. Syndecans would most likely bind to the sulfated glycosaminoglycans measured in our SCM. Together these results suggest that CSA plays an important role in priming cells to bind newly synthesized ECM during repair and our isolated SCM is a good mimic of native ECM.

In Chapter 3, we modify our CSA and SCM cues to be presented as part of a biomaterial scaffold. To immobilize the CSA, we methacrylate it to CSMA using an established protocol for creating methacrylated hyaluronic acid (MeHA). CSMA, SCM, and MeHA polymers were electrospun into scaffolds to deliver these adhesive molecules along with a topographical cue (aligned nanofibers). The ability of these scaffolds to promote neuron outgrowth was again tested with chick embryo DRGs. Our results showed significantly increased neurite outgrowth on electrospun

hyaluronic acid fibers with SCM and low levels of CSA. Higher incorporation of CSA maintained its inhibitory properties.

In Chapter 4, we evaluate the ability of our biomaterials cues from Chapters 2 and 3 to modulate the phenotypes of macrophages and Schwann cells (SCs). Specifically, we explored the effects of the CSA (soluble, chemical cue), SCM (adhesive cue), and aligned HA nanofibers (topographical cue). We hypothesized that one or more of our biomaterials cues would accelerate the macrophages return to a resting state, following classical activation (M1) with lipopolysaccharide (LPS) and/or direct the cells towards an alternative activation (M2) state. Analogously, we hypothesized our cues would accelerate the SCs transition to a mature/pro-myelinating state, following treatment with LPS, used here to mimic immaturity/injury. Cell phenotypes were functionally assessed 12, 24, and 48 hours following LPS stimulation. Quantified reverse transcription polymerase chain reaction (qRT-PCR), immunofluorescence (IF), and sandwich-ELISA based antibody arrays were used to measure changes in mRNA expression, morphology, and cytokine release, respectively.

Our results showed that the SCM and HA nanofibers suppressed the effects of LPS on the macrophages by reducing inducible nitric oxide synthase gene expression. The HA fibers also prevented LPS-induced morphological changes. Release of IL-1a, an M1 cytokine, was also reduced from cells cultured with these cues. Similarly, the SCM and HA fibers significantly influenced Schwann cell phenotype. Mature gene markers, Oct6 and Krox2, were significantly upregulated while immature markers such as GFAP were significantly downregulated. SCs on the fibers assumed a mature, bipolar morphology, significantly elongating in the fiber direction. Furthermore, these changes were observed in as little as 24 hours, much faster than previous studies.

In Chapter 5, we present the overall discussion and conclusions of this work and proposed future directions. We developed a method for measuring receptor expression in the neurons (Chapter 2) and we suggest expanding this flow cytometry effort to include other syndecans, other receptors (e.g. integrins), neurons cultured with our other biomaterials cues, and the other cell

types (macrophages and SCs). Based on the improved neurite outgrowth observed on our CSMA and MeHA, and SCM and MeHA, scaffolds (Chapter 3) we predict that coupling these cues will have synergistic effects on neurite outgrowth. We are especially interested in delivering the cues as opposing linear gradients. We ultimately aim to create a single, scaffold system that could be implanted inside existing NGCs during normal PNI surgeries and we discuss some methods for moving our biomaterials *in vivo.* In the future, we propose to test our biomaterials with co-cultures of the DRG neurons and non-neuronal cells (macrophages and SCs) based on the significant changes in these cells' morphology and cytokine release (Chapter 4).

Overall, we believe that we have provided a collection of approaches to understanding and utilizing the inherent regenerative potential of injured peripheral nerves. We believe the insight provided here can serve the design of other tissue engineered systems for large peripheral nerve gaps or be adapted to study the neurons, immune cells, and glia of the CNS. Moreover, we hope the specific biomaterials explored here will find widespread application in the nervous system.

CHAPTER 2: POSITIVE AND NEGATIVE CUES FOR MODULATING NEURITE DYNAMICS AND RECEPTOR EXPRESSION

Introduction

Chondroitin sulfate proteoglycans (CSPGs) are extracellular matrix (ECM) molecules of interest that may be overlooked during peripheral nerve repair. CSPGs are well-known for their inhibitory role in the central nervous system following spinal cord injury[89], but CSPGs are also deposited by endothelial, inflammatory, and Schwann cells following peripheral nerve injury (PNI). Despite increased CSPGs in the PNI microenvironment, only a few groups have explored the effect of CSPGs on peripheral neurons.[20, 26, 90] Rather, most neural tissue engineering research focuses on delivering only growth promoting factors to encourage neurite outgrowth. We hypothesize that recapitulating the injury microenvironment with both positive (growth permissive) and negative (growth inhibitory) cues can better promote nerve regeneration.

In this study, we investigated the ability of materials-based cues to modulate neurite behavior and receptor expression in peripheral neurons. Our first objective was to quantify the effects of a characteristic CSPG, Chondroitin Sulfate A (CSA), on neurite extension and retraction using time lapse video microscopy. Secondly, we investigated the ability of a novel biomaterial, derived from porcine spinal cord matrix (SCM), to improve neurite outgrowth in the presence of the inhibitory CSA. Lastly, we measured the ability of CSA to induce Syndecan-3 receptor expression in peripheral neurons using flow cytometry.

Axons in the PNI environment face obstacles to regeneration including inflammatory cells, inhibitory chemical cues, and physical barriers.[91] We have hypothesized that these obstacles induce axon retraction events leading to regeneration failure. Selective axon retraction, or pruning, is a normal part of healthy tissue development[17, 19], however, the role of axon retraction following PNI is less understood and less studied. Few studies have used live cell imaging techniques to examine neurite retraction behaviors. Even fewer studies have examined neurite retraction in response to a negative cue, such as CSPGs. Of over thirty studies reviewed that reported using

time lapse imaging to capture neurite retraction in response to cues such as force induction[92, 93], topographical barriers[72, 94], substrate mechanics[95, 96], chemical cues[50, 97], or other cells[98], only four quantified their observations. Therefore, the first objective in this study was to quantify the effects of soluble CSA (mimicking CSPGs liberated from healthy ECM following injury) on neurite extension and retraction in real-time.

It has previously been demonstrated that CSPG exposure can lead to increased membrane density of beta-1 integrins in peripheral neurons.[99] Furthermore, the effects of blocking antibodies against beta-1 integrins were dependent on the *in vitro* substratum, with especially permissive substrates able to overcome the effects of the block.[100] In addition to upregulating integrins, we hypothesized that CSA can also induce the upregulation of another class of surface receptors called syndecans. Syndecans perform diverse functions including participation in cell-matrix and cell-cell adhesion, migration, and proliferation.[101, 102] Syndecans can also bind a wide variety of ECM molecules and growth factors.[103] Syndecan-3 was the focus in this study because it is the most abundant syndecan in the nervous system.[104] Though typically studied as inhibitors to regeneration, we predict CSPGs can prime neurons for growth by inducing the upregulation of Syndecan-3.

Laminin has a long-established ability to promote neurite formation and extension[105, 106] and remains a popular adhesive substrate in neural tissue engineering, especially because it binds to integrins.[107] However, we hypothesized that our SCM would provide a more diverse and physiologically relevant substrate resulting in better neurite growth. Therefore, we tested SCM as an adhesive substrate for culturing neurons in the presence of soluble CSA.

The SCM significantly increased frequency of neurite extension coordinated by a significant reduction in the neurites' time spent stalled/unmoving. Furthermore, neurons grown on the SCM, even in the presence of CSA, had longer neurites than control substrates without CSA. Our results also showed a significant increase in syndecan-3 expression in DRG neurons treated with

CSA, compared to basal expression in untreated neurons. We expect that CSA-induced upregulation of syndecan-3, and the heterogeneous composition of the SCM, (especially presence of sulfated glycosaminoglycans) modulates neurite behavior via Syndecan-matrix binding.

Experimental

Materials

Reagents used for the spinal cord matrix (SCM) isolation include fresh-frozen porcine spinal cords (ECM Science), sodium acetate (Sigma), Ethylenediaminetetraacetic acid (EDTA; Calbiochem), acetic acid (EMD Millipore), and sodium chloride (Fisher BioReagents). Colorimetric assay reagents include Direct Red 80 (Alfa Aesar), and 1,9-dimethyl-methylene blue (DMMB), type I collagen from calfskin, and papain buffer all from Sigma. Serum free cell culture media (SFM) was composed of DMEM/Ham's F12 (GE Healthcare Life Sciences), 2mM L-glutamine (GE Healthcare Life Sciences), 50 U/mL Penicillin-Streptomycin (Sigma), 0.6% B-27 nutrient supplement (Gibco Life Technologies) and 50 ng/mL nerve growth factor (NGF; R&D Systems). Other culture materials include laminin (Calbiochem) and chondroitin sulfate A from bovine trachea (CSA; Sigma). Neurons were harvested from chick embryos; eggs purchased from Charles River (Roanoke, IL). Immunocytochemistry materials include primary anti-neurofilament 200 (Sigma), secondary AlexaFluor488 goat anti-mouse IgG (Invitrogen), 4',6-diamidino-2-phenylindole (DAPI; Fisher), paraformaldehyde (PF; Acros Organics), Triton-X (MP Biomedicals), bovine serum albumin (BSA; Fisher BioReagents), and goat serum (Sigma). Flow cytometry materials include Accutase (MP Biomedicals), primary anti-Syndecan-3 (Santa Cruz Biotechnology), secondary goat anti-rabbit IgG-FITC (Santa Cruz Biotechnology), primary anti-neurofilament 200 (Chemicon) and secondary AlexaFluor594 goat anti-rabbit IgG (Invitrogen).

Isolation and Characterization of Spinal Cord Matrix Proteins

Our adhesive substrate was derived by isolating protein components from frozen, closed herd porcine spinal cords. The cords were disinfected with 1% sodium hypochlorite, washed in cold phosphate buffered saline (PBS) to remove unbound material, and then immersed in PBS

containing 0.5M sodium acetate and 0.1M EDTA to remove exogenous protein. Cords were rinsed three times with PBS, blended into small pieces, and digested in 0.02M acetic acid for 4 days. Matrix proteins were then salt precipitated with increasing concentrations of sodium chloride (up to 2M), dialyzed against deionized water, and lyophilized for the final product.

The concentrations of sulfated glycosaminoglycans (sGAG) and collagen in the spinal cord matrix (SCM) were measured using absorbance spectrophotometry. sGAG content was quantified by DMMB binding according to a previously published protocol[108] while collagen content was measured using an adapted Sirius red-based colorimetric assay.[109] Lyophilized SCM specimens (n=8; dry weight=25 mg) were digested in either papain buffer or 0.1M acetic acid prior to measuring sGAG and collagen, respectively. CSA (0.2-2 µg/well) and collagen I (20-200 µg/well) were used to create standard curves for the DMMB and Sirius Red assays, respectively. Final values are reported as µg of sGAG, or collagen, per mg of dry weight of SCM.

Dissolution of the dried matrix proteins in 0.1M acetic acid was facilitated using an orbital shaker for 2 days. The solution was centrifuged at 3000 rpm for 10 minutes to pellet any insolubles, and the supernatant was collected and used as the experimental substrate for the following cell experiments.

Cell Culture

Chick embryo dorsal root ganglia (DRG; E9-11) were harvested, trypsinized, and mechanically dissociated according to a previously described protocol.[110] Dissociated neurons were plated (6000 cells/cm^2) in a 24-well tissue culture plastic plate coated with either spinal cord matrix (SCM, experimental condition), laminin (LAM) or left uncoated (denoted TCP). Wells were coated via adsorption by incubating in either the SCM or LAM solutions (5 µg/cm^2) for 4 hours and rinsing 3x with PBS (laminin manufacturer's protocol). Neurons were cultured for 2 days in serum free media (SFM) either with or without 10 µg/mL Chondroitin Sulfate A (CSA).

Microscopy and Image Analysis

Time Lapse Video

Dynamics of extending neurites were recorded using a Nikon Eclipse inverted microscope fitted with an incubation chamber maintained at 37C, 5% CO_2, and 90% humidity. Bright field images were captured every 10 minutes, for 12 hours, beginning 24 hours after seeding (to allow for sufficient cell attachment). The following parameters were measured from the video recordings: average neurite extension and retraction rates (μm/min) and extension, retraction and stalled time as a percentage of total neurite movements. Neurite length was measured as a straight line from the center of the neuron cell body to the neurite tip in every frame of the time lapse videos. The change in neurite length between frames was used to determine if the neurite was actively extending, retracting, or remaining unchanged/stalled for any given 10 minute interval. Changes in neurite length less than ± 5μm were considered negligible. The use of ±5 μm as the cut-off for eligibility of neurite extension or retraction was due to limitations in measurement and consistency. The three types of neurite movement (extension, retraction, or stalled) were then reported as percentages of a given neurite's total movements. For every change in neurite length, an extension or retraction rate was determined by dividing the respective change in neurite length by the time interval between frames and the average extension and average retraction rates were determined across all cells.

Figure 2-1 shows examples of the neurite length measurement technique and the types of neurite movements analyzed from the time lapse videos. Only neurites reaching a total length of greater than two times the cell body diameter were included. Neurites that contacted another neurite or another cell body, or that left the field of view, were excluded. For highly branched neurites, only the branch reaching the longest maximum length was traced, even if that branch did not remain the longest throughout the entire video (supplemental video 1).

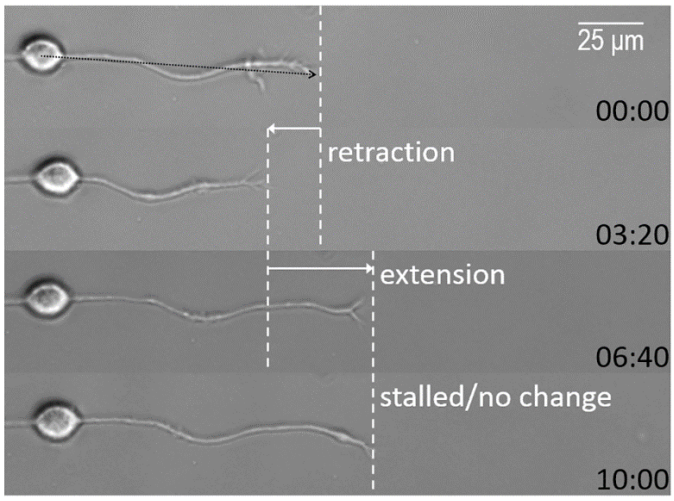

Figure 2-1. Types of neurite movements and measurement technique

Still images from a representative time lapse video illustrate the three types of neurite movements analyzed – retraction, extension, and stalled (change in length <± 5 µm). Neurite length was measured as a straight line from the center of the cell body to the neurite tip (black arrow) in each frame of the time lapse videos. Change in length between each frame was used to determine if the neurite was extending, retracting, or stalled/remaining unchanged. Time shown in hh:mm.

Immunofluorescence

After 48 hours of total culture time, cells were fixed (4% PF), blocked (1% goat serum), and stained with anti-neurofilament and DAPI to visual neurites and cell nuclei, respectively. Final neurite lengths were measured from fluorescent micrographs as described for measuring neurite length in the videos. 5 random positions were imaged for each replicate (n=3) of each condition. The experiment was repeated 4 times for a total of 60 images per condition. Images were captured using NIS Elements software (Nikon) and analyzed using ImageJ. The seeding density (6000 cells/cm^2) and total culture time (48 hours) were specifically selected because, when grown for longer periods, neurites began to contact one another and formed networks that made tracing individual neurites impossible. Finally, DRG neurons cultured for 48 hours, with or without CSA, were also stained with anti-Syndecan-3 to visually confirm receptor expression prior to quantification using flow cytometry.

Flow Cytometry

The ability of CSA to induce the upregulation of Syndecan-3 receptors was quantified using flow cytometry as previously described for measuring opioid receptor expression in murine DRG neurons with slight modifications.[111, 112] Chick embryo DRG neurons were harvested, dissociated, and seeded on TCP in SFM containing 10 µg/mL CSA as described above for the video experiments. After 48 hours, neurons were detached from the plate using Accutase and spun down at 2000 rpm for 3 minutes. The cell suspension was washed in PBS containing 1% BSA and 0.5% Triton-X (wash solution), fixed in 4% PF, blocked in 1% goat serum, and incubated in an amino-terminal (1-300) anti-Syndecan-3 receptor antibody for 30 minutes on ice (1 µg/500 mL wash solution). After a further wash and incubation for 30 minutes in the secondary antibody (goat anti-rabbit IgG-FITC, 1:100), a minimum of 20,000 neurons per sample were analyzed on an Attune Acoustic Focusing Cytometer (Blue/Violet System) using Attune Cytometric Software v2.1 for acquisition (Applied Biosystems).

Gating for the neuronal population was conducted using the following steps in each experiment. First, the population of interest was defined as region 1 (R1) by size (forward scatter, FSC-H) and granularity (side scatter, SSC-H). To confirm this gated population contained neurons, while excluding cellular debris and dying cells, samples were stained with primary neurofilament (1 µg/mL) and secondary antibodies for 30 minutes each on ice. DAPI staining (400 ng/mL; 5 minutes) was used to identify cellular debris, dead, and dying cells. The population of interest was thus confirmed to be neurons by staining positively for neurofilament and negatively for DAPI. **Figure 2-2** shows example density plots of the gating steps.

Neurons cultured in SFM without CSA treatment were used to determine basal expression levels of Syndecan-3. Treated and untreated cells without any antibody staining were used to control for background/autofluorescence. Nonspecific fluorescence, measured from cells stained with just the secondary antibody, was subtracted and the mean fluorescence intensity (MFI) was obtained for each sample.

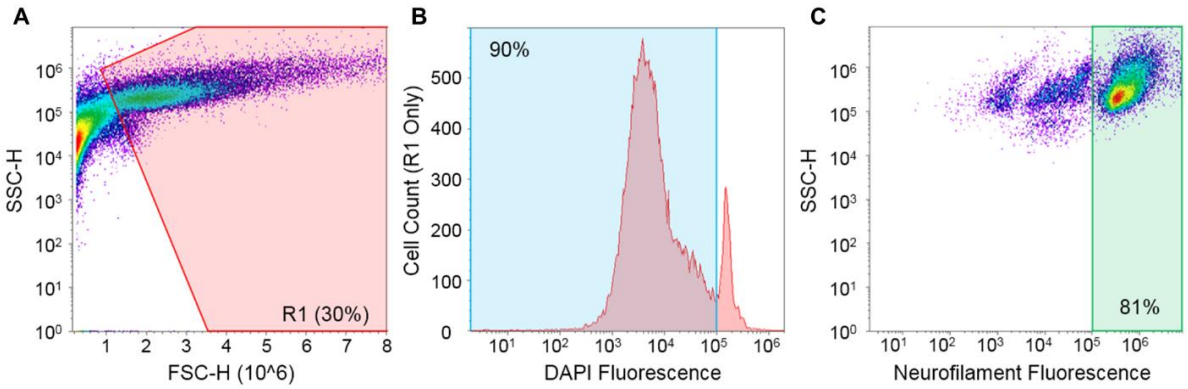

Figure 2-2. Flow cytometry gating steps

Flow cytometry was used to analyze Syndecan-3 expression in primary chick embryo DRG neurons detected by fluorescent antibodies to the receptor antigen. Samples were gated first by their characteristic forward (FSC) and side (SSC) scatter profiles **(A)**. Cells were gated as region 1 (R1), eliminating very small events such as cellular debris. For this representative example (total event count: 82,967), region 1 contained 30% of the events (24,893). DAPI was used as the live/dead discriminator **(B)**. DAPI negative events represent the fraction of viable cells within R1 (90%; 22,403). Finally, neurons were identified from a plot of neurofilament (NF) fluorescence against side-scatter **(C)**. The NF positive cells represent the fraction of R1 that is specifically neurons (81%; 20,163). This sequence of gating steps was used for each experiment in order to confirm that a minimum of 20,000 neurons were ultimately analyzed for Syndecan-3 expression.

Results

Spinal Cord Matrix Protein Quantification

Average collagen concentration of the SCM was 296.2 ± 25.2 µg collagen/mg dry weight, while average sulfated glycosaminoglycan concentration was 4.3 ± 0.4 µg sGAG/mg dry weight. 'Dry weight' describes the full starting weight of the SCM, however, a small fraction of the SCM was insoluble. Thus, collagen and sGAG content in our SCM coatings may be higher than reported here. Nevertheless, our results are comparable to a study by Medberry et al. that used similar assays to measure collagen and sGAG content of decellularized pig spinal cords.[113]

CSA Treatment and SCM Substrate Influence Neurite Outgrowth Parameters

In this study, we used time lapse video microscopy to record outgrowth parameters of peripheral neurons. We measured frequency and rate of neurite retraction, which are observed but not often quantified in the literature, especially in response to a 'negative' cue such as CSA.

Our results showed that neurites spent an average of 17.7 ± 2.8% of their "time" (meaning of the video frames) retracting for all culture conditions tested (one-way ANOVA; $F_{0.05\ (5,138)} = 1.42$; $p = 0.22$). CSA had no significant effect on the frequency with which neurites retract. Neurons cultured on the SCM substrate spent significantly more time extending compared to the laminin and plastic controls. Moreover, this increased extension on the SCM corresponded to a significant decrease in the time the neurites spent stalled/unmoving compared to both controls. This trend was maintained for conditions with and without the CSA, although only the latter was statistically significant. A complete summary of neurite movements for cells grown in each of the six culture conditions is presented in **Figure 2-3A**. For each condition, the three types of neurite movement — retraction, extension, and stalled — add to 100% of total movements. The frequencies of retraction, extension, and stalling occurred independent of whether the cell was in the early or later stages of culture.

Average neurite extension and retraction rates were also measured from the time lapse videos. Average extension rates were statistically similar between all six experimental conditions (one-way ANOVA; $F_{0.05\ (5,137)} = 1.53$; $p = 0.19$). Average retraction rates on the plastic and laminin, with or without CSA, were also statistically similar to one another. Interestingly, neurons grown on the SCM had significantly increased retraction rates compared to the two control substrates (**Figure 2-3B**). This result was surprising given that neurons grown on the SCM had the longest final neurite lengths overall (next section). However, this unexpected outcome reinforces that the SCM is indeed a permissive substrate for neurite outgrowth in spite of neurite retraction behaviors.

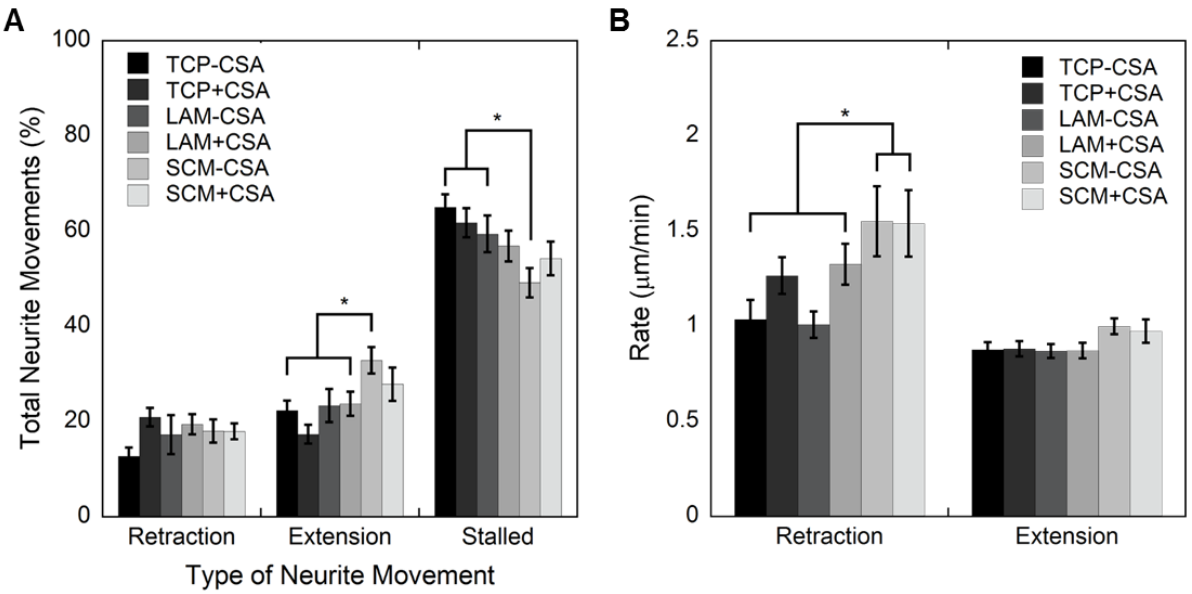

Figure 2-3. Quantified neurite behavior from the time lapse videos

(A) Average time spent extending, retracting, or stalled as a percentage of the neurites' total movements. Neurons on SCM spend significantly more time extending, and significantly less time stalled, than controls. **(B)** Average neurite extension and retraction rates. Extension rates are statistically similar for all conditions. The retraction rate of neurons cultured on the SCM are significantly greater then neurons cultured on TCP-CSA and LAM-CSA. * indicates $p<0.05$; 4 trials, 3 replicates per condition per trial, n>18 neurites measured per condition.

SCM Substrate Promotes Growth in the Presence of CSA

Following the time lapse recordings, the neurons were fixed and stained to analyze final neurite outgrowth using immunofluorescence microscopy. Example fluorescence micrographs of neurons grown on laminin (LAM) or spinal cord matrix (SCM) substrates with (+) or without (-) Chondroitin Sulfate A (CSA) are shown in **Figure 2-4A**. Final average neurite lengths were quantified from 4 independent experiments, each with 3 replicates of the 6 conditions. Greater than 95 total neurites were measured for each condition. Results, reported as mean ± standard error, are summarized in **Figure 2-4B.**

The results revealed significantly reduced growth in the presence of the CSA for neurons grown on all substrates. This result was not surprising as CSA has previously been demonstrated as an inhibitor of neurite outgrowth.[114, 115] However, neurons grown on the SCM had the longest

average neurite lengths overall. Neurons grown on the SCM without CSA had significantly longer neurites than all other conditions. Neurons grown on the SCM with CSA had significantly longer neurites than the neurons grown on TCP or LAM with CSA. Furthermore, cells cultured on the SCM with CSA had an average neurite length significantly longer than those cells on TCP *without* CSA treatment, suggesting that our matrix substrate promotes neurite growth even in the presence of the soluble inhibitor.

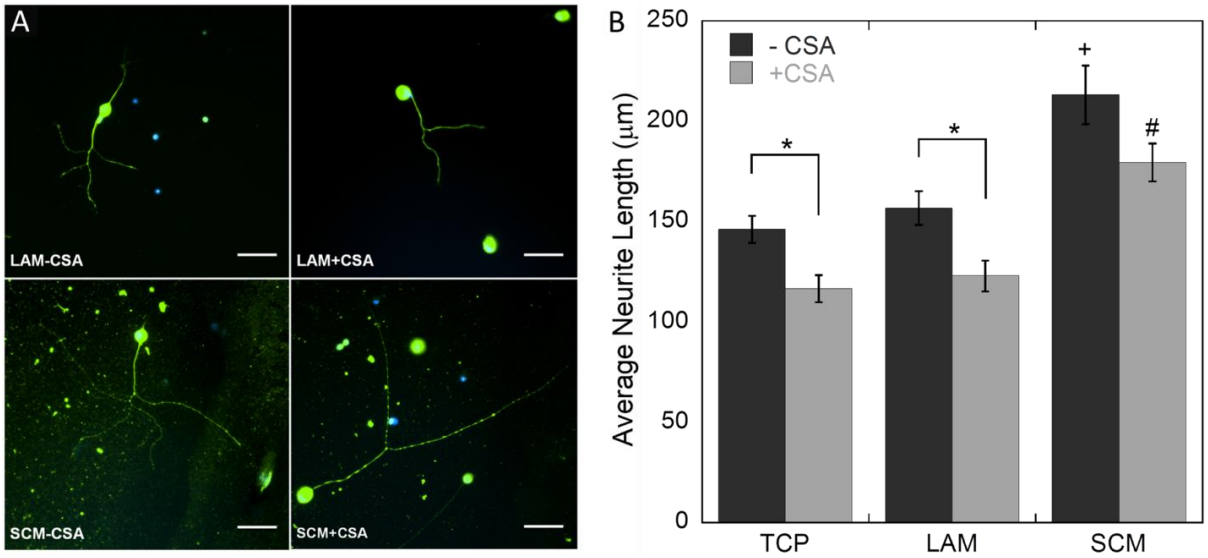

Figure 2-4. Quantified neurite outgrowth from the fluorescence micrographs

(A) Dorsal root ganglion neurons grown on laminin (LAM) or spinal cord matrix (SCM) coated plastic, treated with (+) or without (-) Chondroitin Sulfate A (CSA) stained with anti-neurofilament (green) and DAPI (blue) to visualize neurites and cell nuclei, respectively. Scale bars = 50 µm. **(B)** Quantification of neurite outgrowth after 48 hours. CSA significantly reduced neurite outgrowth in all conditions. Neurons grown on SCM without CSA were significantly longer than all other conditions, + $p<0.05$. Neurons grown on SCM with CSA were significantly longer then all conditions except LAM-CSA and SCM-CSA, # $p<0.05$. $n>95$ neurites measured per condition.

Final neurite lengths agreed with the video results for each culture condition. Using the 'SCM-CSA' neurons as an example, the video results showed these cells spent an average of 18% of the time retracting at an average rate of 1.55 µm/min, while they spent an average of 35% of the time extending at an average rate of 1.00 µm/min. Given that total culture time was 48

hours (2880 minutes), and the remaining 47% of the videos the neurites were stalled (0 μm/min), the expected final outgrowth would be

$$\left(\left(1.00\ \frac{\mu m}{min} \times 0.35\right) - \left(1.55\ \frac{\mu m}{min} \times 0.18\right) + \left(0\ \frac{\mu m}{min} \times 0.47\right)\right) \times 2880\ \text{mins} = 204.5\ \mu m$$

which is well within the range measured from our micrographs; final average neurite length on the SCM-CSA was 213.1 ± 14.6 μm.

Given that average neurite extension rates were similar among all groups, it is more likely that the increased extension frequency, and reduced neurite stalling, on the SCM led to the longest overall neurite outgrowth despite the increased retraction rates on the SCM. Moreover, these increased retraction rates may have to do with two different mechanisms of retraction (resorption vs. fragmentation) on the different substrates (more details in Discussion section).

CSA Treatment Increases Syndecan-3 Receptor Expression

Flow cytometry was used to determine the effect of Chondroitin Sulfate A on Syndecan-3 receptor expression in the DRG neurons. Expression was quantified using the median fluorescence intensity (MFI) normalized to cells that were not exposed to CSA. The results revealed a 21.5 ± 7.6% increase in Syndecan-3 expression for the neurons treated with CSA compared to the untreated control ($p < 0.05$; Student's t-test; $n = 6$ experiments). We also tested concentration dependency of the receptor upregulation on neurons using 1 mg/mL CSA. At the higher CSA concentration, the neurons were unable to be lifted from the dish in order to conduct flow cytometry. However, this observation supports our hypothesis that CSA increases cell-substrate binding. **Figure 2-5** contains a representative histogram (**2-5A**) of receptor expression (relative fluorescence) from the flow analysis as well as summarized MFI results (**2-5B**).

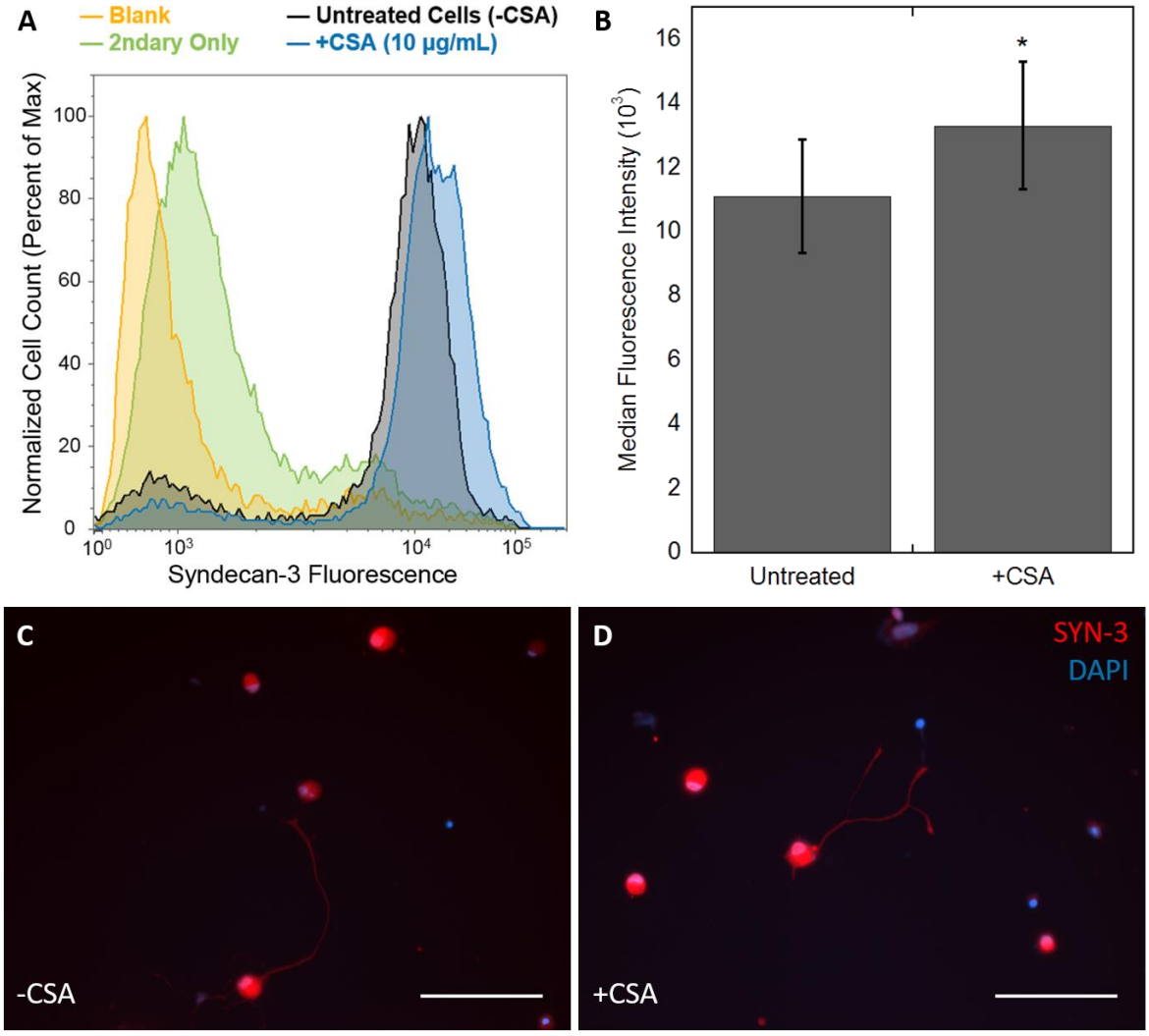

Figure 2-5. Syndecan-3 expression in DRG neurons

(A) Syndecan-3 expression increased in fluorescence intensity for CSA-treated neurons compared to the untreated control cells as evidenced by the peak shift. **(B)** Quantification of flow cytometric analysis reported as median fluorescence intensity (MFI). MFI statistically increased for CSA-treated cells compared to untreated controls. *p<0.05; Student's t-test (n=6). **(C)** and **(D)** Immunofluorescence micrographs reveal Syndecan-3 expression throughout the cell body, neurite, and growth cone of untreated (-CSA) and treated (+CSA) cells. Scale bars = 100 µm.

Syndecan-3 immunostaining was also performed on the CSA-treated DRG neurons to identify localized receptor expression. However, the fluorescence micrographs revealed that Syndecan-3 expression was present throughout the cell bodies and neurites. Furthermore, expression was clearly present in the control neurons (no CSA) as well as the CSA-treated ones (**Figure 2-5C** and **2-5D**). However, this result is not surprising given that we know Syndecan-3 is constitutively expressed in the nervous system and we know from the flow cytometry results that receptor expression was indeed increased with CSA treatment. Furthermore, previous studies have suggested that CSA can affect DRG neurons at both the growth cone and the cell soma.[116] It is worth noting that neurons in the micrographs were stained (antibody concentrations) and imaged (exposure times) using the exact same methods and the images have not been modified in any way.

Discussion

In this study, we have successfully recorded neurite outgrowth dynamics using live cell imaging. Our results provide previously unreported neurite retraction parameters, particularly in response to a negative cue (CSA). While published data on neurite retraction rates is inconsistent, studies have reported comparable neurite extension rates for chick embryo DRG neurons as reported here.[50, 117] Other studies have also reported that DRG neuron extension rates are not affected by their growth substrate. We measured significantly increased retraction rates for neurons grown on the SCM. This result was especially surprising given that these neurites were the longest overall. One possible explanation for this difference could be the mechanism of retraction on the SCM substrate vs. the controls.

Time lapse videos revealed that most neurites underwent simple retraction, or resorption, where the axonal cytoplasm is intact and all components (e.g. actin and microtubules) are returned to the cell soma (supplemental video 2). Simple retraction is a controlled process that requires time for protein depolymerization.[118] Neurons on the SCM, however, appeared to undergo fragmented retraction as opposed to simple retraction (supplemental video 3). Fragmented

retraction occurs when return of all the axonal proteins would not be energy efficient for the cell and therefore axon shedding occurs.[119] Neurite length provides one indicator of whether or not a neuron will undergo fragmentation, with a threshold for fragmented retraction of approximately 200 μm.[120] Because the SCM neurons were the only ones with an average length >200 μm, this may be one explanation for the faster retraction rates.

Despite the increased retraction rates, neurons grown on the SCM substrate were still the longest overall. This result may be attributed to these cells spending significantly more time extending than stalled compared to controls and regardless of CSA treatment. Increased extension and reduced stalling on the SCM may stem from the heterogeneity of the matrix. Laminin, for example, binds preferentially to integrins. CSPGs are also capable of binding to integrins at the same sites that would bind laminin.[115] We speculate that integrin binding becomes saturated on substrates such as laminin leading to increased neurite stalling. Our SCM, however, provides collagen sites for integrin binding as well as GAG binding sites for syndecan receptors, potentially making it an improved substrate over traditional adhesive cues.

Our study shows, for the first time, significantly increased expression of Syndecan-3 receptors in response to CSA treatment in neurons. This increase in Syndecan-3 receptors could lead to increased neuron interactions with the growth substrate and therefore increased neurite extension. The presence of these receptors elucidates one positive role for the chondroitin sulfate released following PNI. The increase in Syndecan-3 expression measured here was significant but modest; this result could be explained by the experimental timeline. For example, a study by Bao et al 2011 used flow cytometry to examine integrin receptor expression following spinal cord injury and saw the onset of increased expression was at 12 hours.[121] Thus syndecan expression may have peaked and declined by the time we analyzed the cells (48 hours of CSA treatment was chosen in order to match the total culture period of the microscopy data). Additionally, syndecans modulate cell-substrate binding, but flow cytometry required lifting the cells from the

dish. This step may have cleaved or otherwise degraded some receptors before analysis, therefore we were not measuring a maximal level of expression. Nevertheless, our results are appropriate for the cell type being tested and are comparable to previously published reports that have used flow cytometry to measure receptor expression in other neurons.[111, 112]

Syndecan receptor trafficking in neurons is not fully understood, so we can only speculate on the mechanism by which CSA induces Syndecan-3 expression. However, we know that CSA can lead to increased intracellular calcium in the growth cone[115], which plays a role in initiating many signaling cascades and may include syndecan synthesis. We have also speculated on mechanisms by which upregulated Syndecan-3 receptors could mediate the improved outgrowth observed on the SCM. First, we anticipate that upregulated syndecans would bind to the sulfated GAGs present in the SCM (especially heparan sulfate) allowing extending neurites to maintain strong adhesion to the substrate without saturating other key binding receptors (e.g. integrins). This binding would promote more continuous neurite extension with fewer stalling events. Secondly, the CSA-induced syndecans could act as co-receptors for the binding of certain integrin variants mediating improved focal adhesion formation and migration.[122] Additionally, both integrin and syndecan receptors provide interaction between ECM ligands and the actin cytoskeleton via their role in intracellular signaling machinery. These pathways may work together to inhibit phosphorylation of Rho which is known to mediate actin and myosin depolymerization leading to neurite contractility.[22] Finally, the increased syndecan receptors could work to stimulate neurite outgrowth by sequestering NGF in the media at the cells' surface.[103]

Many PNI repair strategies focus on counteracting inhibitory signaling of the CSPGs released at the injury site. Popular approaches to counteracting CSPGs include inhibiting their downstream signaling pathways with Rho/ROCK inhibitors[123, 124] or degrading the GAG side chains with bacterial enzyme Chondroitinase ABC.[125, 126] We suggest these treatments of PNI may be flawed. These drugs would alter the CSA-syndecan response reported here and ultimately may inhibit the cells ability to bind strongly to ECM during regeneration.

Despite a few conflicting studies[127, 128], the now leading hypothesis for how CSPGs interact, and therefore inhibit, neurite outgrowth is through the GAG side chains rather than the protein core. Thus, our study utilized chondroitin sulfate A (CSA) as the representative inhibitory component of injured nerve ECM. Chondroitin sulfate is the most abundant of the GAGs in the nervous system and other studies have used CSA specifically as an inhibitory molecule in the study of axon behavior.[129] We recognize that soluble CSA and immobilized CSA (or CS that is protein bound, CSPG) can interact with both the neurons and other substrate proteins in different ways.[26, 130] Given the flow cytometry results with soluble CSA (increased Syndecan-3), however, we hypothesized that low levels of immobilized CSA would be beneficial for neuron growth. Therefore, we needed a way to present the CS cue longer term, especially if it was to ultimately be part of an implantable PNI repair strategy. In the next Chapter, we present a method for immobilizing the CS cue within the hyaluronic acid nanofibers.

Conclusions

In this study, we have demonstrated that porcine spinal cord matrix (SCM) proteins are an especially permissive substrate for culturing peripheral neurons and mitigating inhibition of Chondroitin Sulfate A (CSA), using time resolved and quantified extension and retraction data. Additionally, this was the first look at the influence of a CSPG on syndecan receptor expression using flow cytometry with chick embryo neurons. The objective of this research is not only to identify positive and negative cues for promoting neuron growth but to ultimately utilize these cues as part of an implantable tissue engineered device.

Several nerve regeneration strategies aim to degrade or block CSPG effects pharmacologically. CSPGs have previously been explored for regeneration in cartilage[131], bone[132], and skin[133] but very few studies have explored the potential benefit of incorporating CSPGs into a tissue engineered scaffold for neural regeneration. We are interested in exploiting positive roles for CSPGs as part of a tissue engineered PNI repair strategy. Our long-term goal is to fabricate a biomaterial scaffold featuring ECM and CSPG cues that will provide support for, or even replace,

the Bands of Bungner and is expected to succeed in larger defects where current treatments fail. In the next Chapter, we explore combinations of our SCM and CSA cues and incorporation of these cues into an electrospun nanofibrous scaffold for promoting nerve outgrowth.

CHAPTER 3: NEURITE OUTGROWTH ON NANOFIBROUS SCAFFOLDS COMBINING ADHESIVE SCM AND IMMOBILIZED CSA CUES

Introduction

Following injury, dedifferentiated Schwann cells in the distal nerve stump, which have lost contact with the injured axons, begin to over express extracellular matrix molecules (ECM). The deposited ECM molecules, including laminin and chondroitin sulfate proteoglycans (CSPGs), provide a substrate for axonal elongation.[134] As regenerating axons enter the distal portion of the nerve, they are guided by this substratum. Once Schwann cells regain axonal contact, their expression of the matrix is suppressed. This creates a dynamic environment where the most active Schwann cells are located most distally in the nerve gap. These substrate-adsorbed factor help maintain the proper directionality of axonal regeneration.[134] In this Chapter, we aim to mimic the physical and adhesive guidance of native Schwann cells with a bioengineered scaffold featuring the cues studied in Chapter 2.

Following successful completion of the experiments in the preceding chapter, we aimed to incorporate the two cues (Chondroitin Sulfate A, CSA and the porcine spinal cord derived matrix proteins, SCM) into an electrospun nanofibrous scaffold to further improve neurite extension with the added benefit of a topographical cue. Our objectives for this work were to combine multiple factors for promoting nerve regeneration (topographically aligned nanofibers and permissive and inhibitory adhesion molecules) into one bioengineered scaffold, to characterize the scaffold, and to record the behavior of neurite outgrowth on the scaffold. To immobilize CSA, we modified it with methacrylate groups prior to blending it into an electrospun nanofibrous scaffold containing hyaluronic acid (HA) base polymer. HA has already been demonstrated as a beneficial polymer for neural tissue engineering[48, 135] and our lab uses a well-established protocol for spinning it into nanofibers.[136]

We previously studied the effects of SCM as an adhesive substrate for nerve outgrowth along with the effects of soluble CSA (study summarized in **Figure 3-1**). We then utilized these

cues in combination with an electrospun HA nanofibrous scaffold. We found significantly improved neurite growth on fibers blended with either the SCM or the CSA. These results show that, despite the general opinion that spinal cord has limited healing ability, our isolated material contains ECM components present in the healthy spinal cord capable of promoting neurite outgrowth. Furthermore, our results show potential utility in the CSPGs expressed following injury and we suggest that degrading or blocking these molecules completely may be a misguided approach to peripheral nerve repair. Ultimately, we aim to exploit SCM and CSA as part of a tissue engineered PNI repair strategy that mimics the positive and "negative" cues of the injury site with the long-term goal of better treating large nerve gap injuries in the clinic.

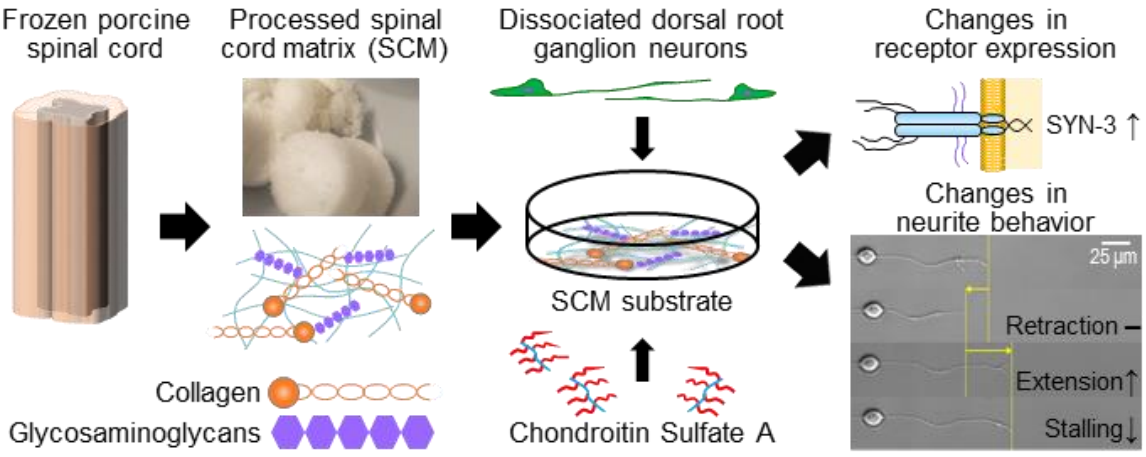

Figure 3-1. Visual summary of Chapter 2

This figure summarizes the methods and results from the experiments presented in Chapter 2. Changes in receptor expression and neurite behavior in response to CSA and SCM in these experiments motivated the use of these cues here.

Experimental

Materials

Macromer synthesis and electrospinning materials include sodium hyaluronate (HA; MW 40kDa; ECM Science), methacrylic anhydride (Sigma), sodium hydroxide (NaOH; Fisher Chemical), polyethylene oxide (PEO; MW 900 kDa; Sigma), Irgacure 2959 (BASF), and 3-(trimethyoxysilyl)propyl methacrylate (Sigma). For all other materials used for cell culture and immunocytochemistry, please refer to Chapter 2.

Macromer Synthesis

Hyaluronic acid (HA) and Chondroitin Sulfate A (CSA) were modified with methacrylate groups (30% substitution) based on previously described protocols.[137, 138] Briefly, 1% (w/v) HA and 2.5% (w/v) CSA solutions were prepared separately in deionized (DI) H_2O. Methacrylic anhydride in molar excess was added dropwise to each of the solutions. The pH of the reaction was adjusted to 8.0 with 5N NaOH. The reactions were carried out over 2 days with constant stirring and frequent pH adjustment. Mixtures were purified from unreacted reagents by dialysis (MWCO: 2,000; Spectrum Laboratories) against DI H_2O for 2 days with 6 water changes and lyophilized to recover the final products. In this study, 3g of HA in 300 mL of DI water was reacted with 6.66 mL methacrylic anhydride to produce methacrylated hyaluronic acid (MeHA) and 1g of CSA in 40 mL of DI water was reacted with 2 mL methacrylic anhydride to produce methacrylated chondroitin sulfate (CSMA).

Scaffold Fabrication

MeHA was selected as the base polymer for our scaffolds because it has previously been demonstrated as a suitable material for DRG neuron culture.[136] The base electrospinning solution and electrospinning parameters are described in detail elsewhere.[139] Briefly, 2wt% MeHA, 3wt% PEO (carrier polymer), and 0.05wt% Irgacure 2959 (photoinitiator) were combined in DI water. The solution was ejected at 1.2 mL/hr (using a programmable syringe pump, KD Scientific) through a 6 inch, 18-gauge blunt tip needle charged to 22 kV. Fibers were collected for 45 minutes

on a grounded, custom built rotating mandrel (2 inch diameter, ~4.5 m/s or ~1700 RPM) positioned 12 cm from the needle. Electrospinning on a rotating mandrel is used to create aligned fibers for topographical guidance. ~50 μm thick fiber scaffolds were collected on 12 mm round methacrylated coverslips (3-(trimethoxysilyl)propyl methacrylate according to manufacturer's protocol) affixed to the mandrel. After fiber collection, scaffolds were carefully removed from the mandrel and crosslinked with 10 mW/cm^2 UV light exposure in a nitrogen purged environment for 20 minutes. Scaffolds were rinsed in PBS for 24 hours to remove PEO before use.

Increasing concentrations of CSMA were incorporated into the fibers via blend electrospinning by varying the weight ratio of MeHA to CSMA in the electrospinning solution. Final polymer concentration in the solution remained 2wt%. The amount of CSMA incorporated into the fibers is indicated by the MeHA/CSMA ratio. For example, pure MeHA fibers are denoted (100/0), fibers spun from a solution of 1wt% MeHA and 1wt% CSMA (other component concentrations remain the same) are denoted (50/50), and pure CSMA fibers are denoted (0/100).

CSMA was immobilized into the fibers via the methacrylate sites which are used to attach photoreactive crosslinkers. The crosslinked material is no longer water soluble. Using polymers with 30% methacrylation, which has a tensile modulus of ~500 Pa, creates a soft substrate that is close to the native mechanics of neural tissue and is typically preferred by neurons.[140]

Blend electrospinning was also used to incorporate SCM into the fibers using the following spinning solution: 2wt% MeHA, 3wt% PEO, 0.05wt% I2959, in a mixture by volume of 80% DI H_2O and 20% SCM solution (dry SCM dissolved in 0.1M acetic acid).Voltage (22kV), flow rate (1.2 mL/hr), mandrel speed (4.5 m/s) and distance between the mandrel and needle tip (12 cm) remained the same during the spinning of all solutions described. Lastly, the SCM was also tested as an adhesive coating on the MeHA control fibers. 5 μg/cm^2 coatings were applied via adsorption for 4 hours and rinsed 3X with PBS, same as previously described for coating well-plates.

Fiber Characterization

Scanning electron microscopy (SEM) was used to analyze the surface morphology of the MeHA fibers. Samples were sputter-coated with gold at 200 Torr for 20 seconds. A JEOL field emission scanning electron microscope was used with an acceleration voltage of 15 kV. Average fiber diameter and fiber orientation were evaluated from three distinct images per sample using ImageJ software. Fiber alignment was determined by measuring individual fiber angles relative to the horizontal (0°). Each angle measurement was sorted into bins (15°/bin from -90° to 90°). The mean and median values of the measured angles (n = 15 fibers per image) were calculated. Percent alignment was defined as the fraction of fibers falling into the bin that also contained the calculated mean and median angles (adapted from Li 2007).[141] These results were corroborated using measurements collected from the ImageJ plugin OrientationJ.

Cell Culture, Immunofluorescence Microscopy, and Neurite Outgrowth Analysis

Dissociated chick embryo dorsal root ganglia (DRG) neurons were cultured on the scaffolds, fixed, stained and analyzed using identical methods to those described in Chapter 2 Methods. The influence of fiber alignment on individual neurite length was confirmed and the directionality of the neurite outgrowth was measured relative to the fiber direction. A straight line was drawn from the center of the cell body to the neurite tip. Angles were measured between this line and the fiber direction (horizontal/0^{o}).

Statistical Analysis

Sample means were compared using a one-way analysis of variance (ANOVA) test and Fisher's LSD post hoc analysis. All data is reported as mean ± standard error and any differences indicate statistical significance ($p<0.05$), unless otherwise noted.

Results

CSMA Nanofibers

In this study, we successfully modified CSA with methacrylic anhydride to produce CSMA. The CSMA was then electrospun into nanofiber blends with methacrylated hyaluronic acid (MeHA) without any modifications to the base MeHA electrospinning parameters. The concentration density of CS incorporated into the blended fiber scaffolds was estimated by dividing the mass of the dry CSMA incorporated into each electrospinning solution (4.25, 8.5, 12.75 or 17mg) by the total surface area of our collection mandrel (340 cm^2). Fiber scaffolds were collected on 1 cm^2 round coverslips attached to the mandrel. Therefore, the 25, 50, 75, and 100% CSMA fiber scaffolds contained approximately 12.5, 25, 37.5 and 50 µg CS/cm^2, respectively. Individual scaffolds were placed in each well of a 24-well plate for cell experiments. Interestingly, the concentration in the 25% CSMA scaffolds (12.5 µg/cm2) is very close to that used in the soluble CSA studies (10 µg/cm^2).

DRG neurons were cultured for 2 days on fibers containing increasing concentrations of CSMA. Final neurite lengths were measured from fluorescence micrographs and we found that at low levels of CSMA incorporation (25%), neurites were significantly longer than the MeHA control fibers. This result might be attributed to the CSMA retaining its ability to influence syndecan receptor expression (results from Chapter 2). Furthermore, this result agrees with other studies that have shown low levels of immobilized CSPG do not impede neurite outgrowth[142] and can even increase growth cone movement.[99] As the concentration of CSMA in the fibers increased beyond 25%, average neurite lengths decreased. Neurons grown on the pure CSMA fibers had significantly shorter neurite lengths than the MeHA controls, indicating some level of inhibition was still retained in the CS cue following its chemical modification. Nevertheless, neurons were still able to attach and grow on the purely CSMA fibers. This result is not surprising because CSPGs are a normal part of healthy ECM. Despite their overexpression following injury, CSPGs

are still capable of being bound by syndecans, integrins, and other receptors on the neurons. Complete neurite length results are reported in **Figure 3-2.**

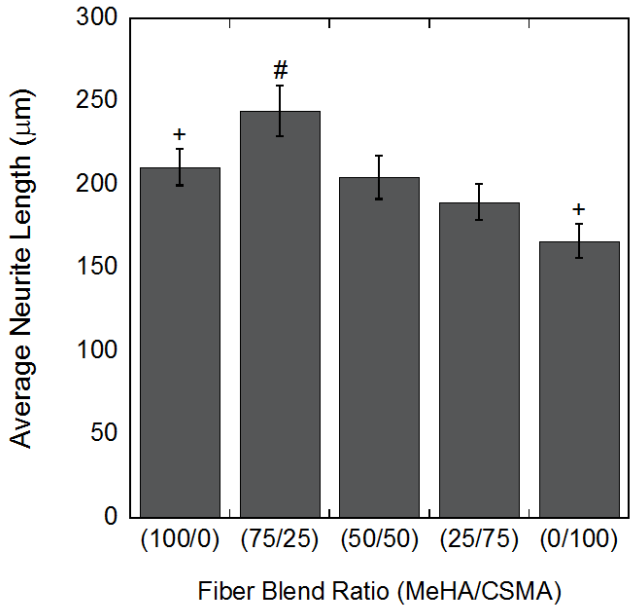

Figure 3-2. Quantified neurite outgrowth on MeHA/CSMA blended fibers

The effect of increasing CSMA concentration in MeHA and CSMA blended fibers on average neurite length from DRGs cultured on nanofiber scaffolds for 2 days. Neurons grown on MeHA/CSMA fibers in a 75/25 ratio were significantly longer than all other conditions, # $p<0.05$. Neurons grown on pure CSMA fibers (0/100) were also significantly shorter than pure MeHA control fibers (100/0), + $p<0.05$. $n \geq 49$ neurites measured per condition.

SCM Nanofibers

In addition to incorporating CSMA into the MeHA nanofibers, we also wanted to create nanofibers that incorporated the SCM cue. This was accomplished in two ways, as an adsorbed coating on the MeHA fibers, and blended into the polymer solution prior to electrospinning. The effects of incorporating SCM into the fibers on final neurite outgrowth from the DRG neurons is reported in **Figure 3-3.** Both methods of incorporation had significantly improved neurite outgrowth over the MeHA only controls. Example fluorescence micrographs of the DRG neurons grown on the different scaffolds as well as scanning electron micrographs of the fibers are shown

in **Figure 3-4.** Fibril proteins of native extracellular matrix provide guiding structures in the nanometer range (50-500nm). The nanofibers produced here had an average diameter of 250 ± 78 nm. The addition of the CSMA and SCM cues had no statistically significant influence on average fiber diameter or alignment.

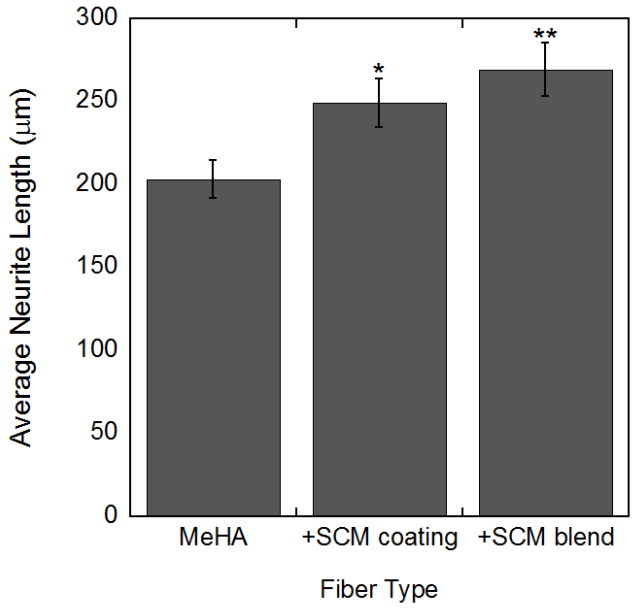

Figure 3-3. Quantified neurite outgrowth on SCM incorporated fibers

The effect of incorporating SCM into nanofibrous scaffolds on average neurite length from DRGs neurons grown on the scaffolds for 2 days. Neurons grown on MeHA fibers coated with 5 μg/cm^2 SCM solution ('+SCM coating') had significantly longer neurites than cells on the MeHA only control fibers, *p<0.05. Neurons grown on MeHA and SCM blended fibers ('+SCM blend') were also significantly longer than the controls and produced the longest neurites overall, **p<0.01. n≥58 neurites measured per condition.

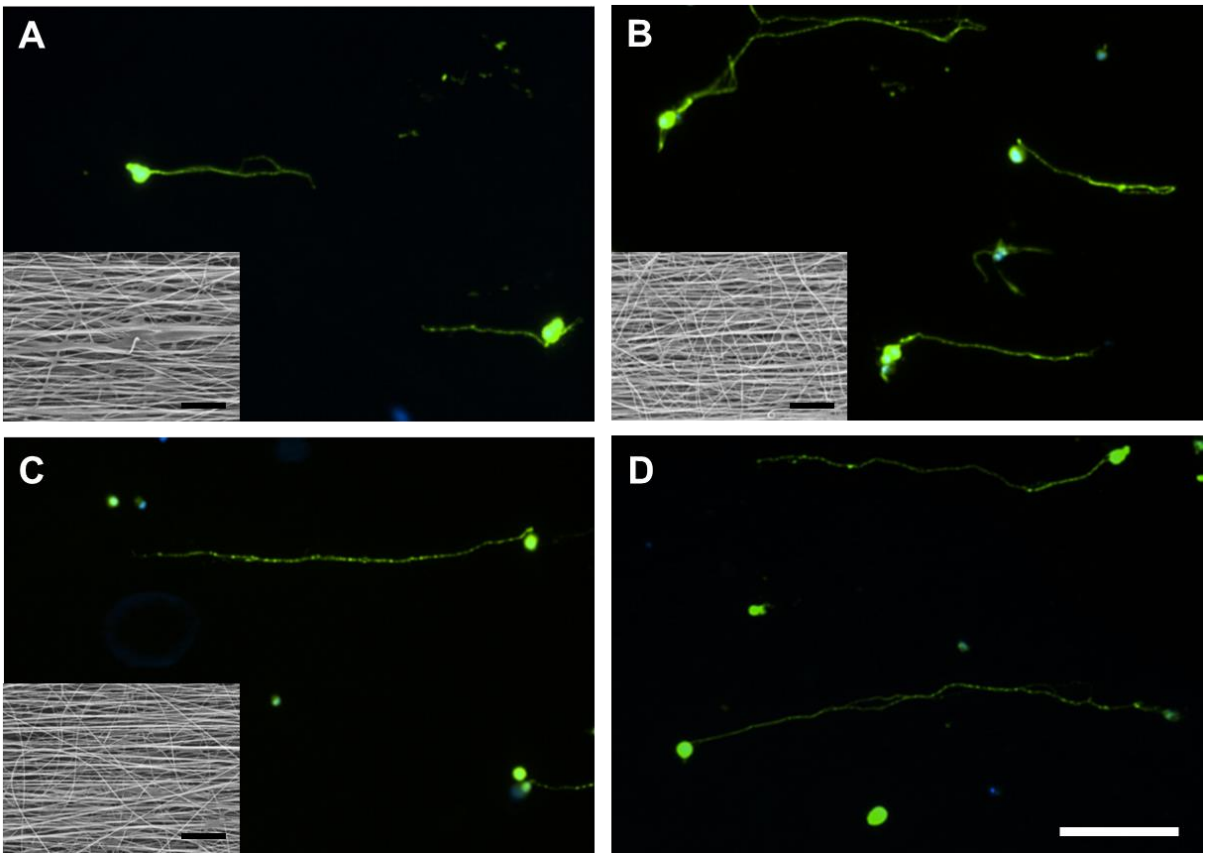

Figure 3-4. **Fluorescence micrographs of neurite growth on the blended fibers scaffolds**

Fluorescence micrographs of DRG neurons grown on blended nanofiber scaffolds for two days then stained with anti-neurofilament and DAPI. CSMA and SCM cues improve neurite outgrowth over MeHA only control fibers. Conditions are **(A)** MeHA control, **(B)** MeHA/CSMA (75/25) blended fibers, **(C)** MeHA + SCM blended fibers, **(D)** MeHA fibers + SCM coating. The insets show scanning electron micrographs (SEM) of fiber morphology. The SCM coating procedure (D) involves soaking the MeHA only scaffolds (A) in the SCM solution but SEM was not available for hydrated samples. Scale bars = 100 μm for FM and 10 μm for SEM.

Discussion

Following peripheral nerve injury (PNI), regenerating axons encounter CSPGs in both soluble and adhered forms. Soluble CSA and immobilized CSA (or CS that is protein bound, CSPG) can interact with regenerating neurons, and other substrate proteins in different ways.[130] Therefore, we immobilized our CS cue within the MeHA nanofibers. Given the flow cytometry results with soluble CSA (increased Syndecan-3), we hypothesized that low levels of immobilized CSA may also be beneficial for neuron growth. Therefore, we needed a way to present the CS cue longer term, especially if it was to ultimately be part of an implantable PNI repair strategy. We utilized the same reaction we already had experience with for methacrylating the HA. We found that our hypothesis was confirmed with our MeHA/CSMA (75/25) fiber results. Neurons grown on these scaffolds were an average of 35 μm longer than on the control fibers. Therefore, we planned to move forward with this particular blend in future experiments.

Hyaluronic acid is a popular polymer for neural tissue engineered regeneration strategies because it is naturally-derived, enzymatically degraded (via hyaluronidases in the body), and easily modified.[135] Another reason for selecting HA as our base polymer is that we can spin it out of water as opposed to harsh, volatile solvents. Water should better preserve the bioactivity of chemical cues such as the SCM and CSMA. Methacrylated chondroitin sulfate A (CSMA) and methacrylated hyaluronic acid (MeHA) have been combined previously in hydrogel form for tissue engineering.[143, 144] Additionally, decellularized porcine spinal cords have been explored for nerve regeneration strategies and have also been fabricated primarily into hydrogels.[113, 145] CSMA has previously been electrospun into nanofibrous scaffolds[146] but not uniquely in combination with MeHA. Similarly, decellularized matrix, including from spinal cord, has also been electrospun before, but is most often blended into gelatin or PLGA fibers.[147, 148] Our combination of the SCM with MeHA is a unique biomaterial and its use for nerve regeneration is a unique application of these two materials together.

With an average neurite length of nearly 270μm in 48 hours, the SCM blended fibers produced the longest outgrowth in this study. Interestingly, the increase in neurite length on the SCM blended fibers over the MeHA controls (269.4 – 203.5 μm = ~66 μm increase) was very similar to the increase seen on the SCM substrate compared to the plastic controls (213.1 – 146.2 μm = ~67 μm increase) from our previous work (Chapter 2 Results). This result helps verify the growth promoting effects of the SCM and suggests that its activity was not diminished during the electrospinning process.

The overall average neurite lengths were longer on the SCM blended scaffolds than the SCM coated plates (results of Chapter 2) because of the added benefit of the topographical guidance provided by the aligned nanofibers. Only aligned nanofibers were evaluated here because of their known ability to accelerate neurite growth.[47] However, we have previously confirmed this by testing DRG outgrowth on aligned and non-aligned electrospun MeHA. Additionally, we confirmed that neurites grow in the direction of alignment.

Aligned MeHA nanofibers induced significantly longer neurites than the non-aligned scaffolds, confirming the ability to accelerate outgrowth. Furthermore, the aligned fibers also directed neurite growth with >50% of neurites extending within ±15 degrees of the fiber direction. The neurite angle distribution on non-aligned scaffolds was much more random. Full results summarized in **Figure 3-5.**

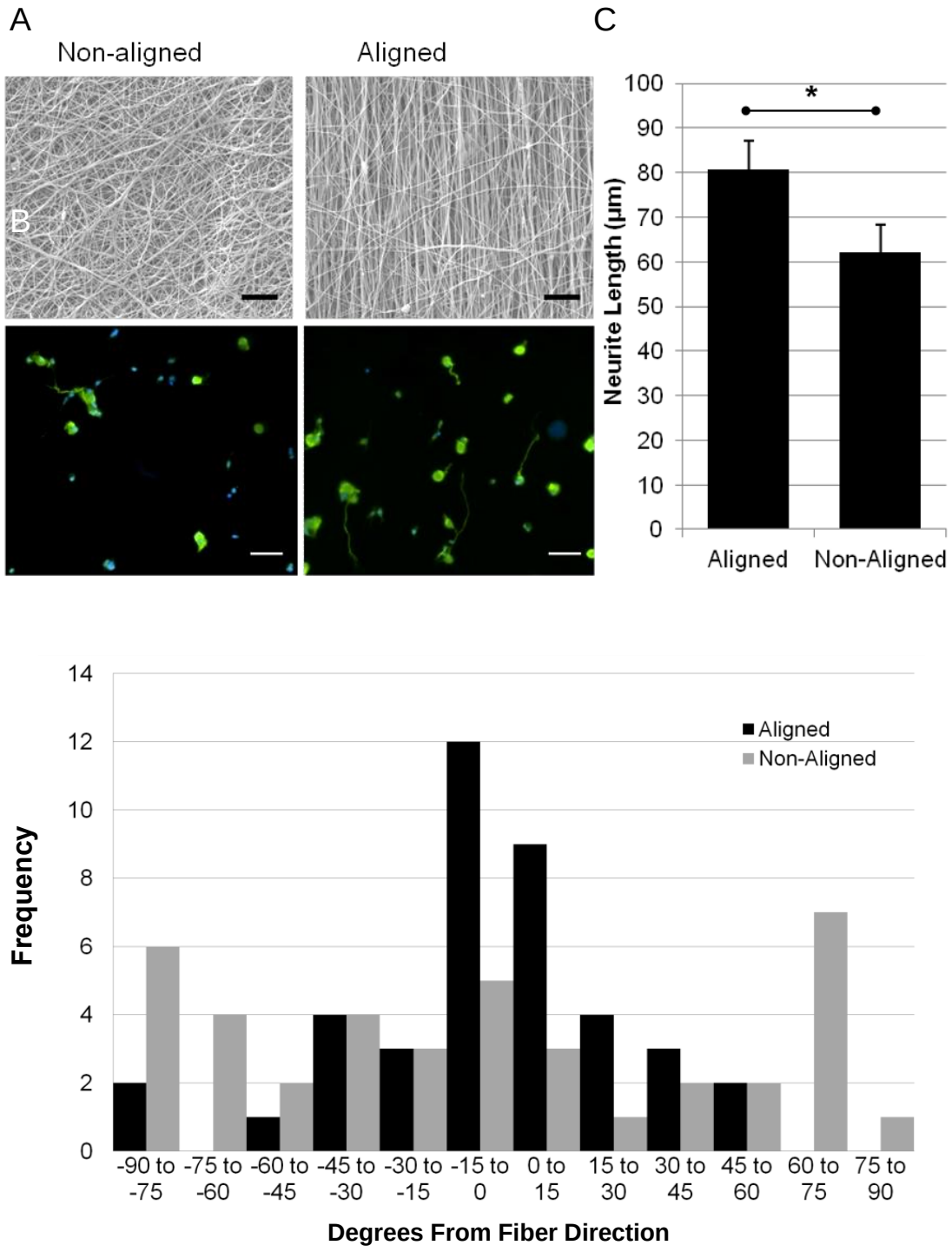

Figure 3-5. Characterization of aligned fiber scaffolds and their effect on neurite growth

A) SEM images of non-aligned (700 rpm) and aligned (2500 rpm) MeHA nanofibers. Scale 10 µm. **B)** Dissociated DRGs grown for 24 hours on nanofibers. Stained with DAPI and Anti-neurofilament. Scale 100 µm. **C)** Quantification of neurite outgrowth revealing accelerated growth on aligned vs. non-aligned fibers. * $p < 0.01$, Mann-Whitney ranked-sum test. **D)** Distribution of neurite angles relative to the fiber direction for aligned scaffolds and to an arbitrary reference angle for non-aligned. n = 45 neurons measured per condition.

It has previously been suggested that a ratio of growth-promoting to growth-inhibiting cues in a substratum is key to success following nerve injury.[130] Therefore, we were interested in testing the combined effects of SCM, CSMA and MeHA to see if they could work synergistically to promote neuron growth. We created two scaffold combinations and cultured the DRG neurons on them as described previously (full methods in Chapter 2). Specifically, we tested 75/25 MeHA/CSMA blended fibers with a SCM coating (5μg/cm^2) and created tri-blended fibers of all three polymers (75/25 MeHA/CSMA where DI H_2O was replaced by the dissolved SCM solution; see SCM blended fiber method above). Unfortunately, we did not see statistically improved neurite outgrowth with either of these combinations (data not shown). We predict that the SCM coating may have masked the influence of the CSMA. Furthermore, the tri-blended fibers may not have an optimized combination of the two chemical cues.

In the future, we plan to combine these cues in a variety of different concentrations and different presentation styles to systematically identify a potentially useful combination. We are particularly interested in delivering the cues as patterned spots or gradients because of the known benefits of physical and chemical gradients for directing and accelerating neuronal growth and migration.[62] We hypothesize that normally inhibitory CSA, can be exploited for directing axon regeneration especially when co-delivered with the growth-permissive SCM. We predict that opposing linear gradients of the two adhesive cues within the fibers would promote the most robust and direct neurite outgrowth in the direction of increasing SCM and decreasing CSA. Our preliminary work on electrospun gradient formation, with RGD peptide conjugated MeHA, is provided in Appendix A. In the future, we hope to adapt/expand this work to incorporate the CS and SCM cues.

Finally, in this study we aimed to analyze neurite extension and retraction behavior on the fibers using time lapse video. The cells were harvested, trypsinized, and mechanically dissociated using the same methods as described in Chapter 2. To visualize the neurites, which have similar diameter to the individual nanofibers, time lapse imaging must be conducted under a fluorescence filter and not under bright field as was done previously.

Prior to time lapse imaging, the neurons were made to fluoresce in one of the following ways: transfected with green fluorescent plasmid (GFP) using Amaxa® Chicken Neuron Nucleofector® Kits (Lonza), incubated with Vybrant Green DiO dye or CellTracker Red CMPTX dye (both Molecular Probes, Life Technologies), or transfected with CellLight Actin-GFP BacMam 2.0 (Molecular Probes, Life Technologies). All transfection and/or dying was carried out per the manufacturers' protocols.

Our dissociated DRGs were successfully labeled using all of the methods. However, several issues arose when trying to capture the neurite outgrowth in real time. First, all the fluorescent markers were susceptible to bleaching over the course of the time lapse period (12 hours). Even with images captured only once every 10 minutes, cells were often too dim to see anymore after the first few images. Secondly, most of the markers led to increased apoptosis in the neurons, suggesting that the cells were under stress. Therefore, any outgrowth captured from these cells likely would not reflect "normal" neurite behavior. Full outcomes are summarized in **Table 3-1.**

Product Name	**Labeling Mechanism**	**Cell Staining Conditions**	**Methods (Concentrations; Incubation times) Attempted**	**Outcomes**
Amaxa® Chicken Neuron Nucleofector® Kit with GFP	Electroporation	Suspension	2µg GFP Vector per 100µL cell suspension	Transfection rates <30%; required >2 million cells for each attempt
Vybrant Green DiO	Lipophilic dye stains cell membrane	Both	5µL dye per 1mL culture media; 2-30 minutes	Stained cell bodies but not the neurites; severe photobleaching
CellTracker Red CMPTX	Membrane permeable, cytoplasmic stain	Both	0.25-5µM dye in media; 15-45 minutes	Increased apoptosis/cell death
CellLight Actin-GFP BacMam 2.0	Viral transfection	Plated	10-50 particles per cell; 12-24 hours	Increased apoptosis/cell death

Table 3-1. Fluorescence labeling techniques attempted for live cell imaging on the fibers

Conclusions

In this study, we successfully incorporated the SCM and methacrylated CSA into electrospun HA scaffolds. These added adhesive cues provide improved neurite outgrowth over HA nanofibers alone. The objective of this research is not only to identify positive and negative cues for promoting neuron growth but to ultimately utilize these cues as part of an implantable tissue engineered device. Our long-term goal is to improve treatments for large peripheral nerve gaps where normal repair processes can be delayed or deficient and current treatments are insufficient to achieve full recovery. In the next chapter, we test the effects of the CSA, SCM, and HA nanofibers on macrophage and Schwann cell phenotype as these cells are critical to successful peripheral nerve repair.

CHAPTER 4: A BIOMATERIALS-BASED APPROACH FOR ACCELERATING MACROPHAGE AND SCHWANN CELL PHENOTYPE TRANSITION AFTER PNI

Introduction

Many tissue engineering approaches to treating peripheral nerve injury (PNI) show great promise *in vitro* but test poorly in animal models compared to autografts.[7, 43] These poor outcomes may result from failure to study the response of other cell types present in the PNI microenvironment prior to *in vivo* studies. The purpose of this study was to evaluate the ability of our biomaterials cues, previously demonstrated to have growth promoting effects on dorsal root ganglia (DRG) neurons[149], to modulate the phenotypes of macrophages and Schwann cells (SCs). Specifically, we explored the effects of Chondroitin sulfate A (CSA; soluble cue), porcine spinal cord extracellular matrix (SCM; adhesive cue), and aligned hyaluronic acid (HA) nanofibers (topographical cue). Our primary objective was to direct and accelerate the macrophages transition from a classically activated/pro-inflammatory state to an alternatively activated/pro-healing state using one or more of these cues. Similarly, we aimed to use the biomaterials cues to direct and accelerate the transition of Schwann cells from an immature state following injury to a mature and pro-myelinating one.

The Bellamkonda group was one of the first to study the effect of modulating macrophage phenotype for peripheral nerve repair. Over the past two decades, Bellamkonda and colleagues have studied several enhancements to basic nerve guide conduits for treating large peripheral nerve gaps. Some of the chemical and physical cues they've explored include material stiffness[150], channels[151], fiber alignment[45], fibronectin[152], laminin and nerve growth factor,[153] and different combinations of these cues just to name a few. In a 2012 study, the group successfully used interferon-y and IL-4 to polarize macrophages towards an M1 or M2 phenotype, respectively. Cytokines were delivered *in vitro* or released from an agarose hydrogel in an *in vivo* rat sciatic nerve injury model. Polarization to the M2 phenotype enhanced Schwann cell infiltration and axonal extensions into the nerve gap.[154] Furthermore, in the IL-4 (induces M2) scaffolds, axonal

growth rate, defined as axon length into the nerve gap as a function of time, was faster by a factor of 2 compared to their previous studies with other types of growth enhancing cues. The group concluded that regulating macrophage phenotype minimizes the need for other more sophisticated NGC modifications and might alone be sufficient to influence long-term regenerative outcomes without the need to modulate any other inhibitory factors present in the PNI environment. CSGPs are one such inhibitory factor present following PNI. In Chapters 2 and 3, we demonstrated that soluble and adhesive CS cues, while typically inhibitory, can positively influence neuron growth and receptor expression.[149] Therefore, we wanted to explore the effect of CSA on macrophage and Schwann cell phenotypes. Ideally, the CSA would not exacerbate the cells inflammatory responses. The Bellamkonda study was especially motivating to the work in this Chapter. The ability to regulate macrophage phenotype with biomaterials would be a great advantage to promoting nerve repair even over the use of immunomodulatory cytokines.

The effect of topography on macrophage activation state has gained popularity in recent years. Early work focused on altering the surface roughness of orthopedic implants to improve wound healing[155] and modification of titanium surfaces remains a key focus in the field.[156, 157] More recently, macrophage activation has also been studied in response to smooth and sand-blasted/acid etched epoxy[158], nanogrooved silicon wafers[159], convex and concave micro-structured silicone[160], and electrospun poly-lactic acid *micro*fibers[161] to name a few examples. Most groups have found that topographical cues minimize inflammatory responses in the cells when compared to smooth controls. More groups have reported a reduction in pro-inflammatory cytokines than changes in gene expression or morphology. However, it has been shown that both minimized inflammatory response and peak cell alignment tend to occur on features approximately 400-500nm in width.[157, 162] Despite these promising results, very few studies have looked at both aligned *nano*fibers, especially of a natural polymer (e.g. HA), and ECM molecules (e.g. CSA and SCM) to modulate the progression of macrophage phenotype over multiple time points.

Additionally, no macrophages studies could be found that also evaluated the effects of their materials on Schwann cell phenotype.

A pioneering study by Chew et al. in 2008, tested the ability of aligned and non-aligned electrospun poly-ε-caprolactone (PCL) fibers to encourage human Schwann cell maturation.[81] Their real-time-PCR analyses revealed an upregulation of early myelination marker, P0, and downregulation of immature marker, NCAM-1, for cells grown on PCL fibers compared to PCL films. The authors hypothesized that functional changes in the cells may be a result of morphological changes induced by the alignment of the fibers. In this study, we test not only the effects of nanofibers and SCM on the cells gene expression but also on the cells morphology and cytokine release. Chew et al. demonstrated what promise electrospun fibers hold for enhancing Schwann cell maturation and recommended such scaffolds be used as a platform for transplantation of 'primed' cells for improving peripheral nerve regeneration. However, no follow up studies from the group could be found.

In this study, we hypothesized that one or more of our biomaterials cues would accelerate the macrophages return to a resting state, following classical activation (M1) with lipopolysaccharide (LPS) and/or direct the cells towards an alternative activation (M2) state. Analogously, we hypothesized our cues would accelerate the SCs transition to a mature/pro-myelinating state, following treatment with LPS, used here to mimic immaturity/injury. Peak inflammatory and neuroinflammatory response of the macrophages and SCs occurs around day 4 following PNI.[163] However, by introducing hyaluronic acid nanofibers (used here to mimic aligned SCs of the Bands of Bungner), it is predicted that we can accelerate (48 hours or less) a switch in the Schwann cells to a pro-myelinating state. Schwann cells are also responsible for laying down newly synthesized extracellular matrix proteins. The delivery of our novel SCM substrate is hypothesized to accelerate the cells towards maturity as these ECM cues would already be in place. To test our hypotheses, cell phenotypes were functionally assessed at three time points following LPS stimulation. Quantified reverse transcription polymerase chain reaction (qRT-PCR), immunofluorescence (IF),

and sandwich-ELISA based antibody arrays were used to measure changes in mRNA expression, morphology, and cytokine release, respectively.

Experimental

Methods for the spinal cord matrix (SCM) isolation and coating procedure and for electro-spinning the hyaluronic acid scaffolds are provided in Chapters 2 and 3, respectively.

Cell Culture

Macrophages

RAW 264.7 murine blood-derived macrophages (generously provide by Dr. Olivia Merkel) were cultured on tissue culture plastic (TCP) in Dulbecco's modified eagle medium (DMEM, Fisher) supplemented with 10% fetal bovine serum (FBS, Atlanta Biologics), 1% glutamine and 1% Penstrep. Cells were maintained at 37C in a humidified environment with 5% CO_2. Cells were split every 2-3 days using Accutase (MP Biomedicals) until ready for use (passages 8-13). Macrophages were induced to a classically activated state using 1 μg/mL lipopolysaccharide (LPS, Sigma) delivered in the media. To test the ability of our chemical and topographical cues to mitigate M1 activation, and/or induce M2 activation, LPS-stimulated macrophages were seeded (40,000 cells/cm^2) on TCP (positive/M1 phenotype control), SCM coating (10μg/cm^2), HA electro-spun nanofibers, or TCP with 10μg/mL of CSA in the media. Cells cultured on TCP without any LPS stimulation served as the negative control.

Schwann Cells

S16 Schwann cells, derived from rat sciatic nerve, were purchased from the American Type Culture Collection (ATCC; CRL-2941). The SCs were maintained using the same conditions and media formulation as the macrophages (see above). The cells were used during the same number of passages. LPS stimulation and culture with our chemical and topographical cues was also conducted using the same methods. The only difference from macrophage conditions was that during maintenance of the SC cultures (not during experimentation), TCP was treated with

1.5 μg/cm^2 poly-L-lysine (PLL; Sigma P-9155) per ATCC guidelines. PLL was used to maintain expansion of the SCs.

mRNA Expression (qRT-PCR)

At 12, 24, and 48 hours after cell seeding, RNA was isolated from the cells using a GeneJET RNA purification kit (K0761; ThermoFisher). cDNA (200 ng/sample, measured with a Qubit 2.0 Fluorometer, Q32866, Life Technologies) was prepared using a Taqman Reverse Transcription kit (N8080234, Applied Biosystems) and a thermocycler (2720; Applied Biosystems). Samples were run for 10 minutes at 25C, 30 minutes at 48C, and finally held at 4C until further analysis. Samples (2μL) were combined with forward and reverse primers (0.2μL), RNase-free water (7.6μL), and Power SYBR Green PCR Master Mix (10μL; Thermo) in wells of a MicroAmp Fast Optical 96-well reaction plate. Quantitative real time polymerase chain reaction (qRT-PCR) was conducted using a StepOnePlus™ Real-Time PCR Instrument (4376600; Applied Biosystems) with the accompanying StepOne PCR software (v 2.2.2; Applied Biosystems). Fold changes were quantified using the comparative $2^{-\Delta\Delta Ct}$ method[164] and standardized between three biological replicates as described by Willems et al 2008.[165] Fold changes are reported relative to cells without LPS treatment and normalized to an endogenous housekeeping gene. All reactions were conducted in triplicate. Primer sets were selected from the Harvard Medical School PrimerBank[166] and were ordered from Invitrogen Custom DNA Oligos. Complete primer list provided in **Table 4-1.**

Cell Type	Gene Name	Accession #	Primer Sequence (5' → 3')	Description
RAW 264.7 Macrophages	Glyceraldehyde 3-phosphate dehydrogenase (GAPDH)	NM_008084	F: AGGTCGGTGTGAACGGATTTG R: GGGGTCGTTGATGGCAACA	Housekeeping
	Inducible Nitric Oxide Synthase (iNOS)	NM_010927	F: GGAGTGACGGCAAACATGACT R: TCGATGCACAACTGGGTGAAC	M1 (Classic Activation)
	Arginase 1 (Arg1)	NM_007482	F: CTCCAAGCCAAAGTCCTTAGAG R: GGAGCTGTCATTAGGGACATCA	M2 (Alternative Activation)
S16 Schwann Cells	Beta-actin	NM_031144	F: CCTCTATGCCAACACAGT R: AGCCACCAATCCACACAG	Housekeeping
	Glial Fibrillary Acidic Protein (GFAP)	NM_017009	F: TCCTGGAACAGCAAAACAAG R: CAGCCTCAGGTTGGTTTCAT	Immature Markers
	Neural Cell Adhesion Molecule (NCAM)	NM_031521	F: GGGAGGATGCTGTGATTGTCT R: GCAGGTAGTTGTTGGACAGGAC	
	Nerve Growth Factor Receptor (p75)	NM_012610	F: GGTGATGGCAACCTCTACAGT R: CCTCGTGGGTAAAGGAGTCTA	
	Myelin Basic Protein (MBP)	NM_017026	F: AGAGTCCGACGAGCTTCAGA R: CAGGTACTTGGATCGCTGTG	Pro-myelinating/ Mature Markers
	Octamer Transcriptin Factor (Oct6)	NM_138838	F: CTCCTGGGGTCCTTCTAACT R: TTATACACAGATGCGGCTCTC	
	Early Growth Response 2 (Krox20)	NM_053633	F: GCCCCTTTGACCAGATGAAC R: GGAGAATTTGCCCATGTAAGTG	

Table 4-1. List of gene names, functions, and primer sequences used for PCR

Morphological Analysis

Following culture as outlined above, cells were fixed (4% paraformaldehyde for 30 minutes) and stained with DAPI and FITC-Phalloidin (Cytoskeleton Inc.) to visualize cell nuclei and F-actin filaments of the cytoskeleton, respectively. Images were taken on a Nikon Eclipse inverted fluorescent microscope. Five random positions were imaged in each of three replicates of each test condition, in three independent experiments, for a total of 45 images. A minimum of 100 cells were measured from the images and the following were quantified using NIS Elements automatic measurement feature: cell area (μm^2), cell elongation, and cell circularity (form factor). The thresholding tool was used to outline each object/cell. Cells that were on top of one another or that were at the edge of the field of view were manually excluded.

Proliferation

AlamarBlue reagent (Invitrogen was used to evaluate macrophage and Schwann cell proliferation in response to the same culture conditions outlined above. AlamarBlue was selected because it is a non-toxic, aqueous dye that can be used to assess net cell numbers over several time points within the same culture. Cell proliferation was measured by adding 10% (by volume) AlamarBlue to each well and incubating for 3.5h (S16) or 5h (RAW 264.7) at 37C. Incubation times were determined empirically by finding a length of incubation that produced linear correlation between cell count and AlamarBlue absorbance ($R^2 > 0.96$ for both cell lines), verifying the validity of the assay. After incubation, 100 µL media samples were moved to a 96-well plate in triplicate. Absorbance was read at 570 and 600 nm in a MultiskanGO spectrophotometer. Percent AlamarBlue reduction was calculated using the correction factor method as described in the manufacturer's instructions. Data represent mean ± standard error from three independent experiments.

Cytokine Release

G-Series Mouse Cytokine Array 1 (macrophages) and Rat Cytokine Array 2 (Schwann cells) were purchased from RayBiotech (Norcross, GA) and performed according to the manufacturer's instructions. The array was incubated with undiluted cell culture supernatant overnight. Supernatants were produced from 1 x 10^5 cells/cm^2 in 1mL of culture medium. Supernatants were collected 12, 24, and 48 hours after seeding and centrifuged for 2 minutes at 8,000 rpm to remove any debris. DMEM supplemented with 10% FBS was used to determine and remove background signal contributed by cytokines in the media. Signal intensity readings obtained for each cytokine were normalized to the positive control contained within the array (maximum possible signal intensity). Cytokine release is presented as median fluorescence intensity (from 4 replicates) of each of the tested conditions and was adjusted for relative cell number using results from the proliferation assay. Laser scanning and data extraction were performed by RayBiotech, Inc. Data analysis was conducted in Microsoft Excel and ImageJ.

Statistical Analyses

Sample means were compared using a one-way analysis of variance (ANOVA) test and Fisher's LSD post hoc analysis. All data is reported as mean ± standard error and any differences indicate at least statistical significance ($p<0.05$), unless otherwise noted.

Results

Changes in Macrophage Activation

RAW 264.7 macrophages were stimulated with 1 μg/mL of LPS to mimic the cells' pro-inflammatory response following injury, also referred to as classical activation (or M1). This initial response is often characterized by increased expression of inducible nitric oxide synthase (iNOS) as well as morphological changes in the macrophages to make them more capable of clearing cellular and tissue debris at the injury site. Cells also release pro-inflammatory cytokines including tumor necrosis factor alpha (TNF-α) and the following interleukins (IL-1, IL-6, IL-12).[167] Macrophages can transition to a pro-healing state, or alternative activation (M2), at later stages of repair and this transition can be facilitated with chemical cues (e.g. IL-4, IL-13, TGF-b). Here we have explored the ability of our adhesive and topographical cues, previously studied for their effects on neurons, on macrophage mRNA expression, morphology, proliferation, and cytokine release.

mRNA Expression

Expression of iNOS (M1) and Arginase 1 (M2) in the RAW 264.7 macrophages was measured by qRT-PCR at three time points following LPS stimulation. Results are reported as fold changes relative to unstimulated cells and normalized to the endogenous control gene, glyceraldehyde 3-phosphate dehydrogenase (GAPDH). As expected, LPS stimulation resulted in a strong upregulation of iNOS compared to the untreated controls. At 12 hours, iNOS expression was statistical similar between LPS-stimulated cells cultured with the CSA, SCM, and HA fiber cues and LPS-stimulated cells on plastic. However, some of our cues mitigated this upregulation at longer time points. 24 hours after stimulation, cells cultured on the HA nanofibers with LPS had significantly lower iNOS expression than cells on plastic with LPS ($p<0.05$; $n=3$). This significant

decrease was maintained through 48 hours ($p<0.01$; $n=3$). Furthermore, by 48 hours the cells cultured on the SCM coating with LPS also had significantly reduced iNOS expression ($p<0.05$; $n=3$). These results suggest that the SCM and HA nanofibers can suppress the effects of the LPS in as little as 48 hours when normal macrophage transition from M1 (following injury) towards M2 can take much longer. These results support our hypothesis that our cues would accelerate the return of the macrophages to a resting state.

Despite having the known effect of skewing macrophages towards the M1 phenotype, LPS treatment also produced a modest increase (~10-fold) in expression of the M2 gene, Arg1. This result was observed with all of our experimental cues and has also been observed in literature.[158] While none of the cues induced a statistically significant increase in Arg1, the cues appear to have no net negative effects on the cells, such as decreasing Arg1 expression.

Both iNOS and Arg1 were expressed in an oscillating pattern with a dip in expression levels at 24 hours compared to the other two time points. This pattern of expression has been observed previously in the literature and is described in more detail in the Discussion section. Complete results are summarized in **Figure 4-1**.

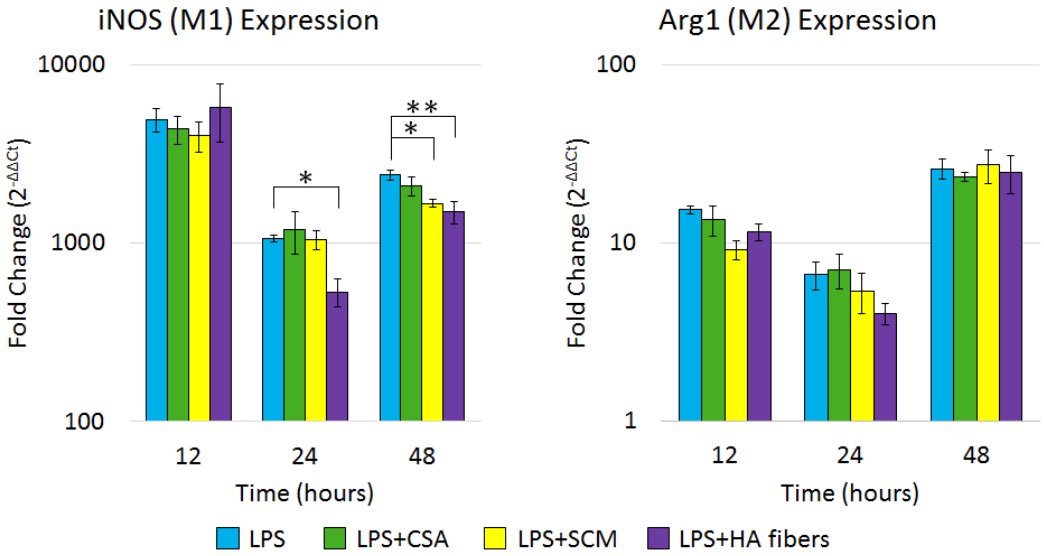

Figure 4-1. Summarized changes in macrophage gene expression measured with PCR

Changes in iNOS **(A)** and Arg1 **(B)** gene expression in RAW 264.7 macrophages. Cells cultured with the cues for 12, 24, or 48 hours following LPS treatment. Fold change relative to untreated (-LPS) cells. Internal control gene = GAPDH. Means ± SEM. n = 3 biological replicates (each run in triplicate). *p<0.05; **p<0.01; one-way ANOVA + Fisher's LSD post hoc.

Morphology

Changes in cell shape have long been associated with changes in cell function. Therefore, macrophage morphology has previously been studied as an indicator of M1 and M2 activation states.[78] Macrophage morphology, and its effects on activation state, have been studied in response to physical cues such as topography[157] and stiffness[168, 169] as well as many soluble factors. M1 activation is broadly defined by large, flattened cellular morphology while M2-polarized cells tend to assume a more elongated and spindle-like shape.[78]

In this study, the most significant changes in mRNA expression induced by our cues were observed after 48 hours of culture, therefore we selected 48 hours as the time point to conduct our morphological analysis. Cells were fixed and stained with FITC-phalloidin and DAPI to visual actin filaments and cell nuclei, respectively. Fluorescence micrographs of the cells grown in each of the culture conditions are shown in **Figure 4-2**. NIS elements software was used to measure

the average cell area, elongation factor, and form factor/circularity of the macrophages as defined in **Figure 4-3A.**

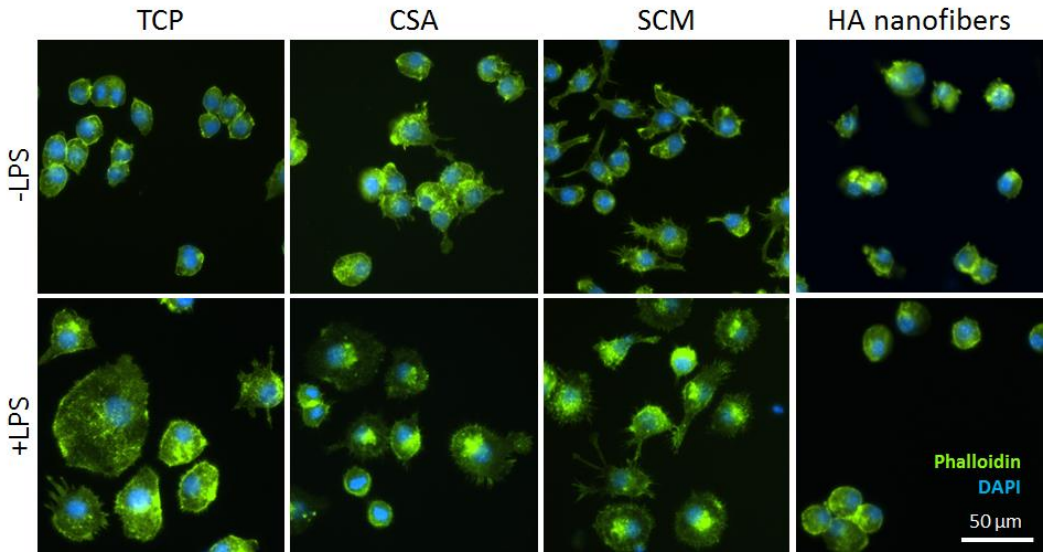

Figure 4-2. Fluorescence micrographs of RAW 264.7 macrophage morphologies

Fluorescence microscopy images of RAW 264.7 macrophages grown for 48 hours in the culture conditions indicated. Phalloidin and DAPI stain actin filaments and cell nuclei, respectively. Scale bar 50 µm for all images.

LPS treatment caused the macrophages to become large, flattened, and stellated, all characteristics of M1 activation. LPS significantly increased cell area for all conditions except the cells grown on the nanofibers. Cells grown on the nanofibers had statistically similar cell area with or without LPS treatment, suggesting possible suppression of the effects of LPS. However, cell area on the fibers was still slightly larger (439 ± 21 μm^2) than the TCP controls (221 ± 4 μm^2). Cells were also slightly larger in area in the presence of CSA (370 ± 11 μm^2). Cells grown on the SCM coating had statistically similar area to the TCP controls without LPS treatment.

An elongation factor of 1 indicates a perfectly circular cell. Our control macrophages (TCP-LPS) assumed a primarily oval shape (1.36 ± 0.03). The LPS treatment had no significant effect on cell elongation. However, cells grown on the SCM coating (-LPS: 1.50 ± 0.02; +LPS: 1.47 ±

0.03) had significantly increased cell elongation ($p<0.05$) compared to the TCP controls suggesting a possible benefit to the cells. Elongated and spindle-shaped morphology can be indicative of M2 activation in macrophages.[78] This result supports our hypothesis that at least one of the biomaterials cues would direct cells towards an M2 phenotype and this is an earlier marker of that. We predict that at longer culture times, or at higher SCM concentrations, this result may be more pronounced.

Form factor indicates the circularity and compactness of a cell, with 1 indicating perfectly round and 0 indicating a perfectly "star-shaped" cell. LPS treatment significantly reduced cell circularity for all conditions except the cells grown on the nanofibers. Cells grown on the HA nanofibers were very rounded and maintained a statistically similar form factor to the TCP condition with or without LPS treatment. This result again suggests possible mitigation of LPS effects by the fibers. Cells on the SCM also had reduced circularity compared to the TCP control (n.s.) but this is most likely a "side effect" of the increased elongation of these cells rather than a true indicator of M1 morphology (i.e. stellation produced by LPS). Complete, quantified morphological measurements for the macrophages are summarized in **Figure 4-3**.

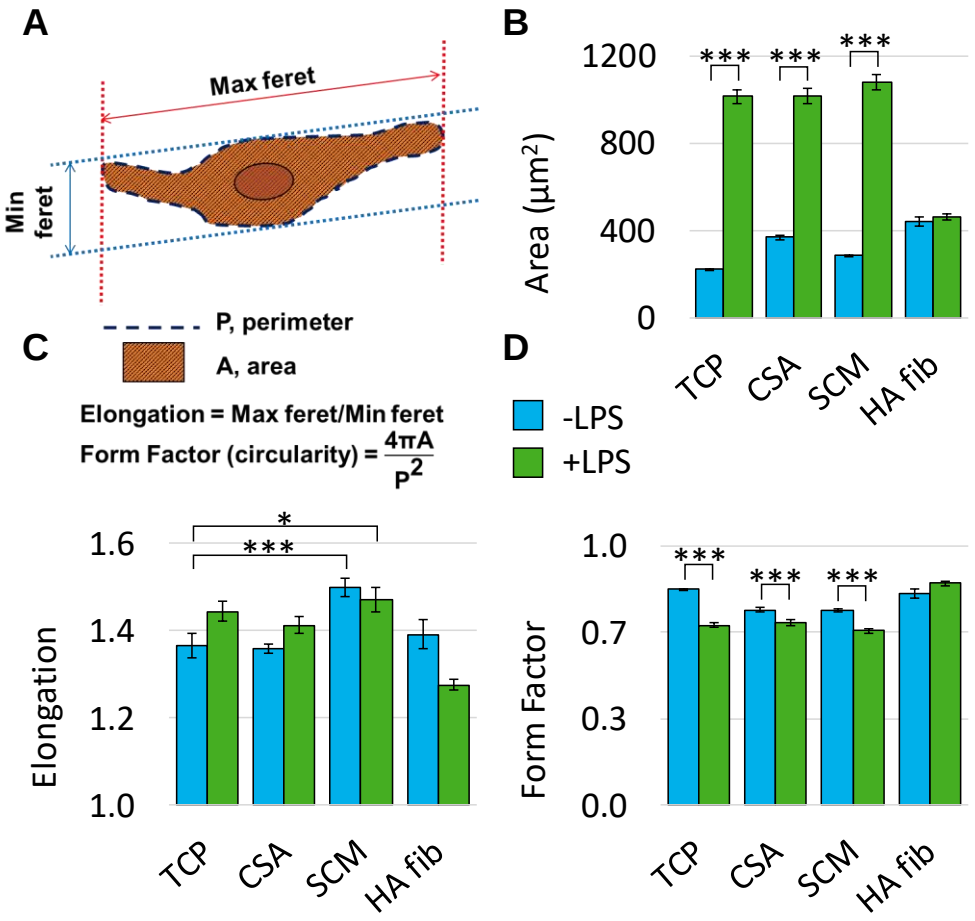

Figure 4-3. Quantified morphological features of RAW 264.7 macrophages

(A) Measurement parameters used to conduct morphological analysis. Graphs of **(B)** average cell area, **(C)** average cell elongation factor, and **(D)** average cell circularity/form factor for the RAW 264.7 macrophages grown for 48 hours in the indicated culture conditions. All data reported as mean ± SEM. n > 45 cells measured per condition. *p<0.05; ***p<0.001 one-way ANOVA with Tukey's HSD post hoc.

Proliferation

The effect of the different biomaterials cues on macrophage proliferation was evaluated using an AlamarBlue assay. Results are provided in **Figure 4-4**.

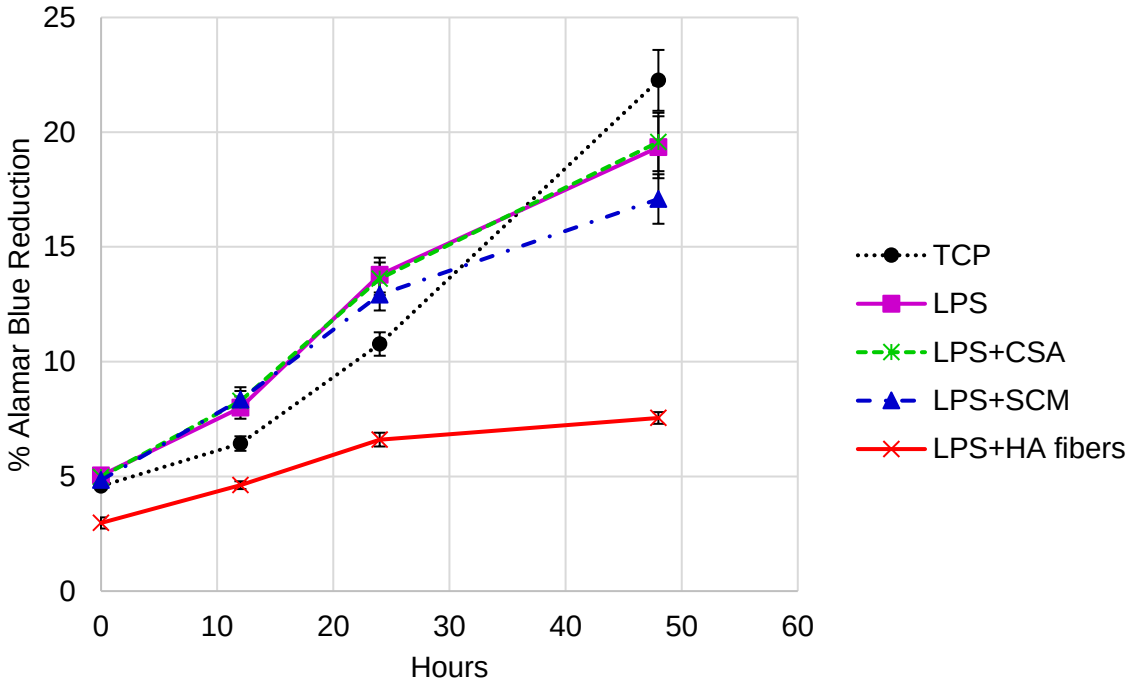

Figure 4-4. RAW 264.7 proliferation results

Cell numbers are increasing near linearly for all conditions. Fewer cells are attached to the HA fibers than in the other conditions and these cells are proliferating more slowly. Excluding the HA fiber condition, the LPS-treated cells have increased proliferation compared to untreated control cells through 24 hours. Between 24 and 48 hours proliferation slows for LPS-treated cells most likely due to limited space while the TCP condition has further increased proliferation.

Percent AlamarBlue reduction was correlated to actual cell numbers using a previously determined standard curve for the RAW 264.7 line (data not shown). There was a linear correlation between cell count and AlamarBlue absorbance ($R^2 > 0.96$). 50,000 cells were seeded in each well (100,000 for the HA fiber condition). After a 1 hour attachment time, scaffolds were moved to new wells and the media was refreshed in all wells. The first measurement at time 0 represents this point right after attachment. The results indicate that closer to 30,000 cells are adhered to the fibers following the well transfer as opposed to the intended 50,000.

Excluding the HA fiber condition, the LPS-treated cells had a greater proliferation rate compared to the untreated TCP control cells through the first 24 hours. This result was expected because macrophage proliferation is known to strongly increase in response to an inflammatory challenge [170]. However, the untreated cells appear to have increased proliferation between 24 and 48 hours while proliferation in the LPS-treated conditions is slowing. This result is likely due to space constraints in the wells. Our morphology results showed that the LPS-treated cells had an average cell area 4 times greater than the untreated cells. Thus, these cells may be approaching confluency which would slow their proliferation.

~40% fewer cells were attached to the HA fibers than the other conditions following the initial attachment period and moving of the scaffolds. Cells on the HA fibers were also proliferating linearly but at a slower rate. Cell numbers increased from ~30,000 to 75,000 on the fibers. Therefore, by 48 hours there were ~3 times as many cells on the TCP control than the fibers. Reduced proliferation could be linked to differences in the cells morphology on the fibers as well as their reduction in iNOS expression. Slowed proliferation could also indicate a reduced response to the LPS. Mitigating inflammatory effects of LPS is one of our goals for these biomaterials.

Cytokine Release

To provide additional insight into the activation state of the macrophages in response to our cues, we used a cytokine antibody array to screen for changes in the release of 20 different inflammatory factors. 8 of the 20 cytokines were not measured at levels above the media only (no cells) reference array. These cytokines, which are excluded from the results include: interferon-gamma (IFN-y), interleukins 1b, 3, 4, 5, 13 and 17, and KC (also known as CXCL1 or neutrophil activating protein 3). **Figure 4-5** contains full, semi-quantitative results from the array reported as median fluorescence intensity (MFI) measured from the supernatants of the macrophages seeded with the different materials cues and normalized to their respective cell numbers form the proliferation assay.

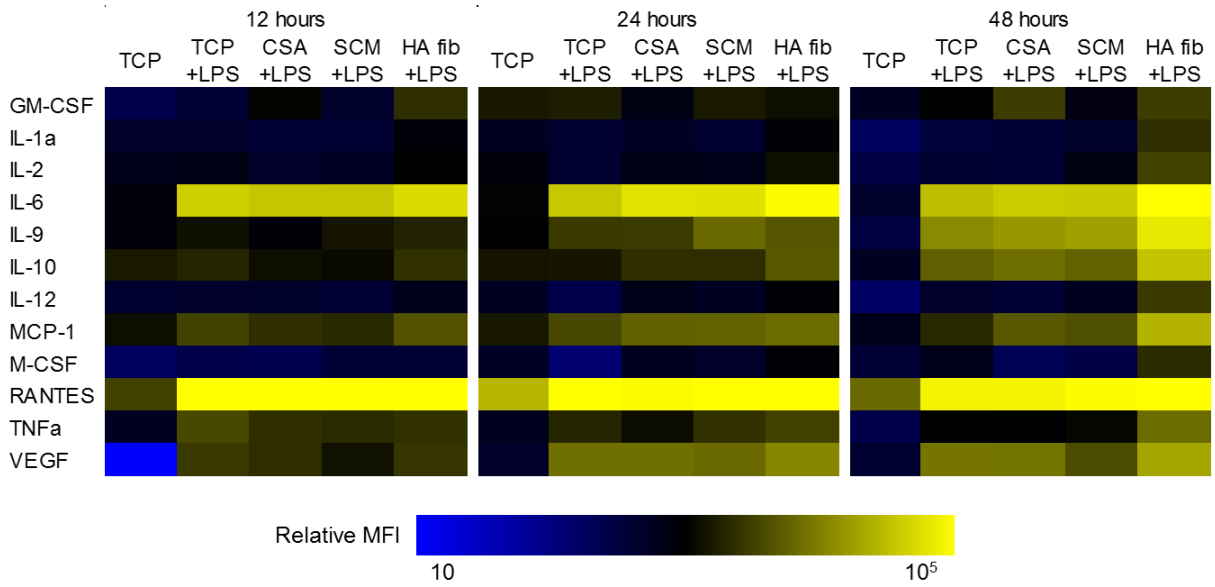

Figure 4-5. Cytokine release from RAW 264.7 macrophages

Normalized array data of the 12 cytokines that were measured above the DMEM only control are shown in a "heatmap." Heatmaps are of median fluorescence intensity (MFI) measured for each cytokine in each condition/sub-array and adjusted for cell number relative to TCP at each time point. MFI is already normalized to an internal positive control on the array and background fluorescence from the media is removed.

Overall, the heatmaps show a general pattern of cytokine accumulation over time as indicated by increased MFIs at 48 hours (yellow color indicates a higher concentration of cytokine compared to blue/black). However, this pattern was not maintained for tumor necrosis factor alpha (TNFa). Production of TNFa from the untreated macrophages (TCP control) remained constant while TNFa release from the LPS-treated cells peaked at 12 hours and decreased over time for the CSA and SCM conditions. This result is promising as TNFa is a cytokine associated with classical (M1) activation[171, 172] and our goal is to direct the cells towards alternative activation.

As expected, the release of several pro-inflammatory cytokines was strongly increased in response to LPS treatment, especially IL-6 and RANTES. While our biomaterials cues were unable to mitigate the effect of LPS on IL-6 and RANTES production, the cues did not exacerbate the

release of these M1 cytokines. Interestingly, cells cultured with the SCM or HA fibers had increased production of IL-2 compared to the TCP and TCP+LPS conditions. IL-2 is an anti-inflammatory cytokine with the ability to interfere with IL-6 dependent signaling.[173] The ability of these materials to increase IL-2 production is a potentially exciting result as we aim to reduce classical activation.

LPS treatment also induced the release of vascular endothelial growth factor (VEGF) from the macrophages. However, levels of VEGF released from the cells cultured on the SCM+LPS were reduced compared to TCP+LPS at all time points. VEGF is important for angiogenesis which must accompany axon regeneration[172], however, it has been shown that very high levels of LPS-induced VEGF can lead to pathological conditions and damaging angiogenesis. Suppressing this effect, as shown here, could be important for regeneration.[174]

The LPS-treated macrophages cultured on the HA nanofibers had increased release of most cytokines measured compared to both the TCP and TCP+LPS conditions at all time points. Increased production of IL-10 and M-CSF is especially promising as these cytokines are associated with alternative macrophage activation. M-CSF is often studied as an exogenous stimulating factor for directing monocytes towards M2.[175-177] Therefore, M-CSF release could potentially work in a positive feedback loop to continually direct the cells towards a pro-regenerative phenotype.

The most important outcome of these arrays is determining which cytokines to evaluate with quantitative ELISAs in the future. TNFa, IL-2, VEGF, IL-10, and M-CSF are some of the most interesting targets for future study with the macrophages and our biomaterials.

Changes in Schwann Cell Maturation

S16 Schwann cells were stimulated with 1 μg/mL of LPS (same as RAW 264.7 macrophages) to induce “dedifferentiation” and inflammatory response in the cells, mimicking injury. Gene expression and morphology of the SCs were evaluated to determine the effects of LPS. We hypothesized that LPS would induce significant increases in immature genes (GFAP, NCAM,

p75) and significant decreases in mature genes (MBP, Oct6, Krox20). We hypothesized that our cues (CSA, SCM, and HA fibers) would suppress or even reverse these effects of LPS.

Changes in gene expression over the three time points followed a similar, oscillating pattern to the RAW macrophage activation with LPS for every gene except for MBP. However, fold changes were not significantly different than the untreated control cells. Accordingly, the LPS also had no significant effects on SC morphology compared to untreated controls. Cells grown on the PLL coating were large and stellated with significantly increased cell area and significantly reduced form factor compared to TCP. This unipolarized morphology is indicative of immaturity[178], which is ideal for continued proliferation of the line, but not for our intended purpose of SC maturation and pro-myelination. PLL also caused significantly reduced Krox20 expression at 48 hours. Because of these findings we did not move forward using the LPS in combination with our cues but rather tested them on their own. Additionally, PLL was only used during maintenance of the SC cultures and was not used in combination with any of our test conditions. Untreated TCP served as the control for all remaining SC experiments. Appendix B contains full PCR and morphological data for the Schwann cell responses to LPS and PLL.

mRNA Expression

qRT-PCR was used to determine the effect of the CSA, SCM, and HA nanofibers on transcription of several key proteins related to maturation in the S16 Schwan cells. GFAP is an intermediate filament protein important for SC proliferation. NCAM is a cell surface glycoprotein important for cell-cell binding and alignment during the formation of the Bands of Bungner. p75 is a low-affinity nerve growth factor receptor. MBP is a protein responsible for maintaining proper myelin structure. Oct6 is a key transcription factor in the early myelination process. Lastly, Krox20 is a zinc finger transcription factor critical for myelination.[179] These markers are broadly characterized as immature (GFAP, NCAM, p75) or mature (MBP, Oct6, Krox20) but changes in transcription of these markers can have many different downstream effects. Changes in expression were considered significant at $p<0.05$ when compared to cells cultured on TCP control.

Treatment of the SCs with soluble CSA had net neutral effects by 48 hours (no significant change in any of the genes). Cells grown on the SCM had no significant changes in any of the immature markers by 48 hours. This is a very promising result as our goal is to utilize these cues to accelerate maturation and myelination following injury. Cells on the SCM had significantly reduced MBP expression, reduced Oct6 expression, and increased Krox20 expression by 48 hours. This combination of increased and decreased mature markers may also suggest net neutral effects of SCM on the SC phenotype.

SCs cultured on the HA fibers had no significant changes in NCAM expression at any time point. These cells had increased p75 expression at 12 and 24 hours but expression returned to control levels by 48 hours. Interestingly, cells cultured on the HA nanofibers had significantly decreased GFAP expression at 24 and 48 hours suggesting a possible shift away from an immature cellular phenotype.

SCs cultured on the HA fibers had no significant changes in MBP expression. These cells had significantly increased levels of Oct6 and Krox20 at 24 hours. By 48 hours, expression of these markers was still increased over the controls, but the changes were no longer statistically significant (Oct6 $p=0.15$; Krox20 $p=0.18$). Interestingly, Krox20 expression steadily increased over time for the cells grown on the nanofibers. This is a promising result suggesting that HA nanofibers may induce lasting decreases in GFAP and lasting increases in Krox20, ultimately leading to a more mature phenotype in the cells.

Some genes exhibited an oscillating expression pattern, similar to what was observed with the macrophages, but the pattern was less pronounced. **Figure 4-6** summarizes the Schwann cell PCR results. Complete numeric results are provided as bar graphs (mean fold change ± SEM) in Appendix B.

	CSA			SCM			HA nanofibers		
	12 hr	24 hr	48 hr	12 hr	24 hr	48 hr	12 hr	24 hr	48 hr
GFAP	**↑↑**	↓	–	**↑↑**	↓	–	↓	**↓↓**	**↓**
NCAM	–	–	–	↓	↓	–	–	–	–
P75	**↑**	–	↑	–	**↓**	–	**↑↑↑**	**↑↑↑**	↑
MBP	–	–	–	↓	**↓↓**	**↓↓**	↓↓	↓	–
Oct6	↓	↓↓	–	–	↓↓	↓↓	–	**↑↑**	↑↑
Krox20	↑	–	–	↑	–	↑↑	–	**↑**	↑↑

Figure 4-6. Summarized PCR results/changes in gene expression in the S16 Schwann cells

↑ upregulation; − no change; ↓ downregulation; Purple = Immature markers; Green = Mature markers. The number of arrows indicates strength of change. **Bolded** arrows indicate $p<0.05$ (one-way ANOVA with Fisher's LSD post hoc). Changes were calculated relative to TCP control and normalized to beta-actin (housekeeping gene).

Morphology

Like the study of cell shape for macrophage activation, cellular morphology has also been explored for its role in Schwann cell activity.[180] Following injury, hyper-proliferating Schwann cells form into aligned columns called the Bands of Bungner. This elongation of the cells' cytoskeleton likely induces other changes in cellular activity including the release of mitogens for macrophage activation and growth factors for axon regeneration.[181] Schwann cell morphology has been studied in response to topography[82, 182], stiffness[183, 184], and soluble factors[185]. Generally, immature Schwann cells are characterized by unipolarized morphology while migratory, and pro-regenerative SCs feature bipolar morphology.[178]

Only the HA nanofibers produced statistically significant differences in SC morphology. Changes include reduced cell area and form factor and increased elongation, all indicative of the bipolar phenotype. The SCs elongated in the direction of fiber alignment, putting out one or more thin extensions to bind the fibers. This rearrangement of the cells' cytoskeleton and/or enhanced binding at the ends of the cell tips, may have contributed to the observed differences in gene

expression on the fibers. Example fluorescence micrographs and quantified morphological parameters are presented in **Figure 4-7.**

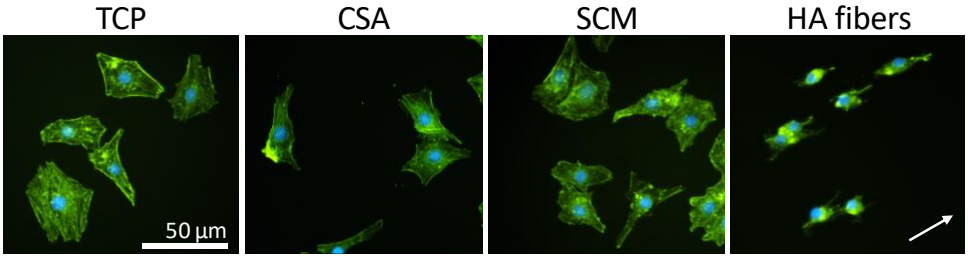

	TCP	CSA	SCM	HA fibers
Cell Area (μm^2)	2618 ± 109	2507 ± 94	2468 ± 92	780 ± 24 *
Elongation	1.71 ± 0.04	1.78 ± 0.05	1.79 ± 0.04	2.32 ± 0.07 *
Form Factor/ Circularity	0.55 ± 0.01	0.53 ± 0.01	0.54 ± 0.01	0.42 ± 0.01 *

Figure 4-7. Summarized morphological analysis of S16 Schwann cells

Fluorescence microscopy images of S16 Schwann cells grown for 12 hours stained with Phalloidin (green) and DAPI (blue) and quantified morphological parameters (mean ± SEM; n >120 cells per condition). *p<0.05 one-way ANOVA + Fisher's LSD post hoc. Arrow indicates direction of fiber alignment.

Proliferation

The effect of the different biomaterials cues on Schwann cell proliferation was evaluated using an AlamarBlue assay. Percent AlamarBlue reduction was correlated to actual cell numbers using a previously determined standard curve for the S16 line (data not shown). There was a linear correlation between cell count and AlamarBlue absorbance ($R^2 > 0.98$), verifying the validity of the assay for measuring proliferation. AlamarBlue assay results are provided in **Figure 4-8.**

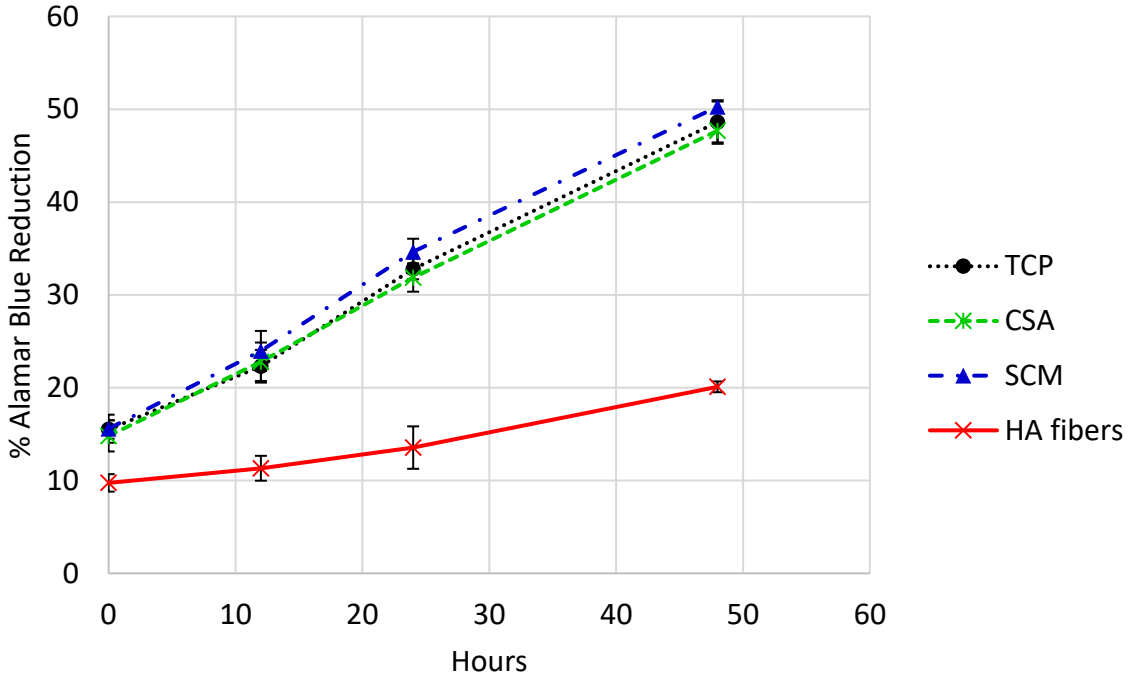

Figure 4-8. Schwann cell proliferation results

The effects of the different biomaterials cues on S16 proliferation were evaluated using an Alamar Blue assay. Cell numbers increase linearly for all conditions but proliferation rate is slower for cells grown on the HA nanofibers.

50,000 cells were seeded in each well (100,000 for HA fiber condition). The S16 cells required 12 hours to fully attach to the HA fibers. After this attachment period, scaffolds were moved to a fresh well of the plate, leaving behind any cells that may have settled under the scaffold, and media was refreshed on all the tested conditions. Note that proliferation and cytokine production (next section) were measured at 12, 24 and 48 hours after this media change but at 24, 36, and 60 hours after the SCs were initially seeded, which differs slightly from the macrophage data.

Cell numbers are increasing linearly for SCs grown on TCP (control), SCM-coated TCP, and TCP+soluble CSA. Cell numbers are increasing from the 50,000 seeded at the zero time point to ~150,000 cells at 48 hours. ~40% fewer cells are attached to the HA fibers than the other conditions following the initial attachment period and moving of the scaffolds. Cells on the HA

fibers are also proliferating linearly but at a slower rate. Cell numbers are doubling from ~30,000 to 60,000 on the fibers. Therefore, by 48 hours there are ~2.5 times as many cells on the TCP control than the fibers. Results of the proliferation assay were used to normalize the following cytokine release data to cell number.

Cytokine Release

The ability of CSA, SCM, and the HA fibers to affect cytokine release from the S16 Schwann cells was evaluated by measuring the secretion of 34 cytokines using the RayBiotech Rat Cytokine Antibody Array 2. Array scanning and data extraction were provided by RayBiotech. We analyzed the raw fluorescence intensity data using ImageJ and Excel. 17 of the 34 cytokines were not expressed at levels above the media only (no cells) reference array. These cytokines, which are excluded from the results include: CINC-1, CINC-2alpha, CINC-3, Fas ligand, Fractalkine, IL-1a, IL-1b, IL-1 R6, IL-10, Leptin, LIX, L-selectin, MIP-3alpha, MMP-8, Prolactin, RAGE, and Thymus chemokine. **Figure 4-9** contains full, semi-quantitative results from the array presented as a heatmap of median fluorescence intensity (MFI) measured from supernatants of the cells seeded with the different materials cues and normalized to adjusted for differences in proliferation.

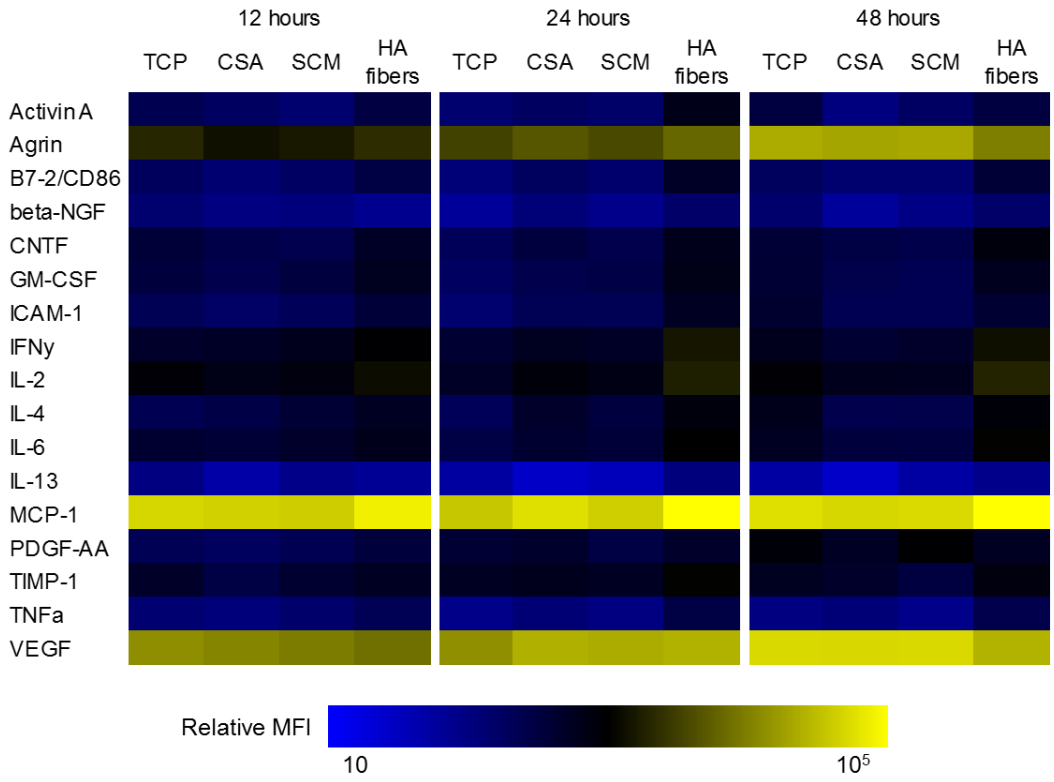

Figure 4-9. Cytokine release from S16 Schwann cells

Cytokine production from Schwann cells cultured with the biomaterials cues presented as a heatmap of median fluorescence intensity (MFI) adjusted for cell number relative to TCP at each time point. MFI is already normalized to an internal positive control on the array and background fluorescence from the media is removed.

The first observation to be drawn from Figure 4-9 is that cytokine concentrations in the supernatants collected from the SCs were much lower overall compared to cytokine concentrations in supernatant collected from the macrophages as evidenced by the primarily blue color. Only MCP-1 and VEGF were measured at high levels across all time points and for all conditions. Interestingly, the release of Agrin from the SCs is increasing over time. Agrin is a proteoglycan that plays an important role in the formation of neuromuscular junctions. It is generally produced by adult SCs and is not necessarily associated with nerve injury.[186] However, studies of increased Agrin at the distal stump show that it is useful for preservation of the end organ.[181]

SCs cultured with the CSA and SCM showed slightly reduced release of GM-CSF, IL-6, and INF-y at 48 hours compared to the TCP control. This is a potentially promising result as these cytokines can serve as both recruitment factors, and M1 stimuli, for macrophages. Alternatively, the SCs cultured on the HA nanofibers had slightly increased release of several cytokines compared to the TCP control including ciliary neurotrophic factor (CNTF), IL-2, and tissue inhibitor of metalloproteinases (TIMP)-1. Increased release of CNTF could be an exciting effect of the fibers as CNTF promotes neuron survival and axon growth following injury.[187] Furthermore, overexpression of CNTF can increase the expression of myelin proteins and direct differentiation in SCs.[188] TIMP-1 complexes with matrix metalloproteinases to prevent their access to bind protein substrates. TIMP-1 has a key role in controlling SC maturation and myelination following injury [189] and has also been shown to regulate maturation of oligodendrocytes in the CNS.[190] Agrin, IL-2, CNTF, and TIMP-1 are all interesting cytokines to explore with quantitative ELISAs in the future.

Discussion

The primary objective of this study was to evaluate the ability of three specific biomaterials cues, with established benefits for culturing DRG neurons *in vitro* [149], on two other key cell types of the PNI microenvironment. Here we tested 1) chondroitin sulfate A (CSA) as a soluble, chemical cue, 2) processed porcine spinal cord extracellular matrix (SCM) as an adhesive substrate, and 3) aligned hyaluronic acid (HA) electrospun nanofibers as a topographical cue for their ability to create fast and/or lasting changes in macrophage and Schwann cell phenotypes. Chondroitin sulfate proteoglycans, extracellular matrix, and the Bands of Bungner (these are aligned columns of immature Schwann cells mimicked here by nanofibers) are endogenous biological cues present following PNI that initiate repair programs. By providing these cues as a part of a scaffold, it could be possible to accelerate these repair programs and recovery. The presence of the nanofibers specifically could replace the need, to an extent, for SCs to align into a physical guide for regen-

erating axons. Consequently, the cells might begin their myelinating cascades sooner. An implantable scaffold, combining one or more of our cues, is the long-term goal of this research. Here we've conducted an *in vitro* analysis of cell phenotype in response to each cue individually. We found that the SCM and HA nanofibers direct both cell types towards regenerative phenotypes.

RAW 264.7 murine blood-derived macrophages were chosen as a representative macrophage cell line because their response to LPS is well-characterized in the literature [191, 192] making them a predictable model for testing the effects of our cues. Additionally, the RAW 264.7 line has long been established as a valid candidate for studying macrophage activation and function.[193] Changes in the macrophages' morphology, cytokine release, and gene expression in response to our cues were measured at 12, 24, and 48 hours following LPS activation. Here we aimed to capture both an early cellular response (12 hours) and also to evaluate the ability of our cues to successfully modulate cell phenotype in less than 48 hours before peak inflammation would occur.

iNOS and Arg1 fold changes, in all conditions tested, peaked at 12 hours, dropped by ~50% at 24 hours, and increased again at 48 hours. This oscillating and dampening pattern matches a previous study showing that macrophages have an intrinsic "clock" that regulates rhythmic gene expression and cytokine secretion upon LPS stimulation independent of systemic cortisol.[194] The SCM and HA fiber cues successfully reduced iNOS expression in LPS-treated cells at 24 and 48 hours compared to LPS-treated cells on the TCP control. We predict that longer time points would show a similar oscillating gene expression pattern with the SCM and HA fiber cues further accelerating the macrophages return to a resting state.

The HA nanofibers also had the most significant effects on macrophage morphology and were the only condition to suppress the typical LPS induced changes of increased cell area and reduced cell circularity. However, the very rounded morphology of the cells on the HA nanofibers was unexpected and spreading/elongation of the cells in the direction of fiber alignment would be preferred. Hyaluronic acid is not an especially adhesive polymer. We predict that at longer time points, as the cells lay down their own matrix proteins, the cells would begin to spread and align.

Additionally, combining the fibers with the adhesive SCM (as we have done in our previous work) is expected to further improve this morphological outcome.

Substrate mechanics also play an important role in macrophage polarization. Macrophages typically assume a spread morphology on stiffer substrates and maintain rounded morphology on softer ones.[168] Our HA fibers have an approximate elastic modulus of ~1kPa [140]. This material is much softer than TCP or SCM-coated TCP and therefore stiffness likely contributed to the rounded morphology observed on the fibers.

The immortalized S16 line was generated by repetitive passaging of primary neonatal rat sciatic nerve and was first described in the late 1980s.[195] S16s were chosen for this study because they have previously been studied for their similarities to adult sciatic nerve, especially their level of expression of myelin-associated mRNA and proteins.[196] In the absence of axons, primary Schwann cells rapidly become arrested and begin down-regulating many myelin constituents. This limited number of cells makes functional, metabolic, and cell biology studies challenging. The proliferating S16s are a practical alternative and several characterization studies concluded the S16s are an appropriate model cell line, especially for the study of gene regulation.[196, 197]

Several studies have shown that activation of the Raf/ERK signaling pathway is sufficient to drive dedifferentiation in Schwann cells.[198-200] At the same time, other groups reported that LPS treatment activates the Raf/ERK pathway in RSC96 Schwann cells[201], a comparable line to S16[197], and primary Schwann cells.[202] Given the results of these studies, we hypothesized that LPS could be used to drive the cells towards immaturity/dedifferentiation through Raf/ERK signaling and that our biomaterial cues would direct and accelerate the cells towards a myelinating phenotype. Unfortunately, LPS had no significant effects on gene expression or morphology of the S16. Therefore, we tested the effects of the biomaterials cues on the SCs over time without any LPS. We still hypothesized that our cues would induce markers of maturity/myelination in the cells and our results support this hypothesis, especially for SCs cultured on the HA nanofibers.

As with the macrophages, the HA nanofibers also produced the most significant changes in the Schwann cells. The rearrangement of the cells' cytoskeleton to elongate in the direction of the fibers likely contributed to the observed differences in gene expression. Changes in SC gene expression included significantly decreased GFAP (immature marker) and significantly increased Oct6 and Krox20 (mature markers) at multiple time points. These results are very promising, especially considering the short culture period (significant changes as early as 24 hours). Previous studies have also reported increased expression of myelin-associated genes in SCs when cultured on aligned PCL or poly-lactic-co-glycolic acid (PLGA) fibers but significant differences were only achieved after 5-7 days in culture.[81, 82] All changes, whether up or down, were on the order of 2-fold which also matches these two earlier studies.

While the SCM coating had no significant effects on SC morphology, the SCM did have interesting effects on SC gene expression. By 48 hours Oct6 was downregulated, while Krox20 was upregulated. Krox20 and Oct6 are often co-expressed during initial phases of myelination. However, overexpression of Oct6 can lead to axonal death and therefore it is eventually turned off, a process mediated by Krox20.[203] The possibility that the SCM could direct the SCs towards such an advanced stage of myelination is an interesting prospect and further evaluation of these genes and their regulatory pathways is proposed future work.

Uncoated tissue culture plastic was selected as the control condition, rather than poly-L-lysine coated TCP (as was used during S16 expansion), for several reasons. PLL was excluded in the experimental tests primarily to 1) avoid a confounding chemical/adhesive cue presented to the cells and 2) because we predicted that PLL would keep the cells in an immature state. Maintaining SC immaturity would be ideal for proliferation of the line, but in opposition to our goal of directing SC maturation. PLL had the expected effects on the SCs including significantly decreasing expression of the mature marker Krox20. PLL also significantly influenced cell morphology including increased cell area and reduced elongation. This unipolarized morphology is indicative of SC immaturity.[178] Lastly, the cytokine array results showed that SCs grown on the PLL had

increased release of PDGF-AA, which is an SC autocrine signal for proliferation.[204, 205] A summary of PCR, morphology, proliferation and cytokine array results collected form SCs grown on PLL is provided in Appendix B. PLL appears to keep the SCs in an immature phenotype which supports our choice of experimental control.

Interestingly, the CSA had no statistically significant effects in any of our phenotypical analyses for either cell type. Given that chondroitin sulfates are upregulated following PNI, it follows that they might be able to activate inflammatory programs in the cells. The lack of any CSA-induced changes is a promising result. Furthermore, our results suggest that CSA inhibits neuron outgrowth via direct action on the neurons themselves rather than through modulation of the other cell types.

There are now several great review articles available that discuss using biomaterials to control M1/M2 activation.[206, 207] Despite the vast amount of information now available on this topic, there still exists a lack of exploration into naturally derived polymers, especially the hyaluronic acid (HA) used here. Furthermore, while other groups have studied the effects of decellularized ECM on macrophage activation state, including matrix derived from intestinal submucosa, urinary bladder, brain, liver, skeletal muscle, and skin[208, 209] this was the first look at the effects of ECM specifically derived from spinal cord. Because of the challenges of processed whole nerve allografts, our precipitated SCM proteins provide ECM cues while the fibers can provide the structural component. Here we wanted to delineate the effects of the different cues on the two cell types. However, our results suggest that these two cues could work together synergistically to promote pro-regenerative phenotypes in the macrophages and SCs.

Conclusions

This study adds to the growing collection of literature describing the important role of macrophage activation state for tissue regeneration following injury. This study offers a unique look at macrophage phenotype in response to three cues not previously explored and offers a unique perspective on macrophage phenotype in the context of a peripheral nerve injury. Furthermore,

this study shows for the first time the influence of HA nanofibers, decellularized ECM, and soluble CSA on Schwann cells specifically considering them as neuroimmune cells. Our spinal cord matrix and HA nanofibers successfully directed both cell types towards the intended phenotypes.

The use of a biomaterials to drive macrophages and Schwann cells to a pro-regenerative and pro-myelinating state, respectively, has distinct advantages over previous approaches that are pharmacologically dependent. Drug delivery faces many challenges such as maintaining continuous release at an efficacious dose and preventing unwanted clearance, diffusion, or tissue uptake. Thus, the biomaterials-based approaches presented here could provide simpler translation to the clinic.

It is critical to evaluate the behavior of macrophages and Schwann cells in response to tissue engineered scaffolds to ensure that the chemical and physical cues useful for neuron regeneration also facilitate the normal behaviors of these other repair cells. The approaches presented here could be used by other research groups to study their neural tissue engineered systems and hopefully improve the success of nerve guide conduits *in vivo*.

CHAPTER 5: CONCLUSIONS, FUTURE WORK, AND LONG-TERM GOALS

In the preceding chapters, we have presented several approaches to understanding and engineering the injury microenvironment to improve peripheral nerve regeneration. In Chapter 2, we provide quantified neurite extension and retraction data in response to multiple cues, especially 'negative' Chondroitin sulfate A (CSA). We describe a method for evaluating receptor expression in dorsal root ganglion (DRG) neurons using flow cytometry and provide the first report of the influence of CSA on Syndecan-3. Finally, we demonstrate the ability of a novel biomaterial, isolated porcine spinal cord matrix (SCM), to increase neurite outgrowth through reduced growth cone stalling.

In Chapter 3, we describe methods for methacrylating CSA to CSMA and electrospinning it into nanofibrous scaffolds. Additionally, we describe electrospinning blended scaffolds of SCM and methacrylated hyaluronic acid (MeHA). This is the first report of CSMA and MeHA, and SCM and MeHA, utilized together as electrospun scaffolds for neurite growth. These scaffolds feature two key adhesive cues that successfully improved neurite outgrowth over controls.

In Chapter 4, we explore the ability of CSA, SCM and MeHA nanofibers to modulate the phenotype of other cells in the peripheral nerve injury (PNI) environment. We describe changes in macrophage and Schwann cell morphology, gene expression, and cytokine release over a two-day period following activation of the cells to an injury mimicking state. Our biomaterials cues successfully directed both cells towards pro-regenerative phenotypes (macrophages towards M2 and Schwann cells towards maturation). More importantly changes happened in as little as 24 hours, much faster than other studies have reported.[81, 82, 210, 211] These changes were induced without pharmacological agents as most often described by others.[212, 213] Changes induced by implantable biomaterials rather than diffusible drugs should make for easier and more successful clinical translation. Taken together, our results provide foundational work for creating a single scaffold system, combining multiple biomaterials cues, that could work synergistically to accelerate repair programs in larger peripheral nerve gaps.

Current treatments, including coaptation, autografts and allografts, are insufficient to achieve full functional recovery in large peripheral nerve injuries (transection gaps >3cm). Tissue engineered nerve guide conduits (NGCs) have remained the most promising alternative treatment since their introduction in the clinic in the early 1980s.[40] The typical NGC is a basic, hollow tube into which the two nerve ends are sutured. Unfortunately, currently available NGCs are still hollow. They lack the necessary internal chemical and physical cues to direct axon regeneration.

Short peripheral nerve injuries (<3cm) have great regenerative capacity due to a unique environment that forms following injury. This regeneration program includes de-differentiation, hyperproliferation, and alignment of resident Schwann cells (SCs) into “bridges” (called the Bands of Bungner) that span the gap and provide a substrate for regenerating axons. The Schwann cells also release cytokines to recruit macrophages to the injury site. Pro-inflammatory macrophages initially clean up axonal and myelin debris but transition their phenotype towards a pro-healing state at later stages of repair. The Bands of Bungner take up to 4 days to form and can persist for over 25 days following injury.[214, 215] The average rate of neurite extension (2-5 mm/day in humans) would allow for axons to cross a 3cm gap in this time frame. In large gaps, however, the Bands of Bungner often fail to form completely. A chronic condition develops where Schwann cells remain de-differentiated, macrophages remain pro-inflammatory, and regenerating axon bundles form disorganized neuromas. These patients suffer long-term pain and limited function at their injury site.

Over the past 30 years, several tissue engineering groups have attempted to modify the basic NGC. Modifications include changes to conduit porosity/permeability, material conductivity, growth factor delivery, exogenous cell delivery, and luminal channels. Unfortunately, NGCs, even with these modifications, often fail to match controls (autografts) in animal models.[7, 43] Several examples of these approaches are described in more detail in earlier chapters where we also suggest that current strategies fall short of full repair because of several gaps in the literature. Some of those gaps include understanding the response of neurons to inhibitory cues at the injury

site (e.g. chondroitin sulfate proteoglycans), quantifying real time neuron behavior in response to different cues, exploiting inhibitory cues in scaffold systems, and studying the effect of tissue engineered scaffolds on the other repair cells (macrophages and Schwann cells).

One of the primary goals of this thesis was to study the intrinsic PNI repair environment and to design biomaterials cues that could mimic the Bands of Bungner. We studied both permissive and inhibitory cues present following injury. Effects were studied not only on neuron behavior but especially the behavior of macrophages and Schwann cells. Another key goal was acceleration of the repair programs since time is of the essence in large nerve gaps. The experiments presented here serve as promising tools for studying the PNI environment *in vitro*. We want to further improve this work to be a true PNI model. We want to continue elucidating important repair receptors, monitoring cell behaviors, and identifying key genes and cytokines involved in the repair process. Furthermore, we want to adapt the model to incorporate more and different cells. Below are a few specific experiments that we would explore next.

In this thesis, we successfully define a method for measuring receptor expression in DRG neurons using flow cytometry and demonstrate for the first time that CSA can induce an increase in Syndecan-3 receptors. We propose to expand this investigation to include the other 3 members of the Syndecan family, which have all been investigated for their roles in the nervous system.[216] Murakami et al. showed that 7 days post op, peripheral motor neurons in mice had significantly increased Syndecan-1 expression in the cell bodies and terminals of the regenerating nerve fibers compared to uninjured control neurons.[217] Syndecans-2/4 has been shown to mediate growth promotion of PC12 cells by binding different laminin peptides.[218, 219] We also propose using identification and neutralization antibodies for all 4 of these receptors in combination with time lapse microscopy to confirm their potential roles in neurite extension and retraction. We also propose to confirm the ability of the methacrylated CSA (CMSA), especially when electrospun into nanofibers, to retain its effects on SYN-3 expression in the neurons. Our flow cytometry methods could

be adapted to test a wider variety of receptors in DRG neurons, other neuronal populations, or even the other cell types of the injury environment including SCs and macrophages.

Based on our results from Chapter 2, we recommend a push towards increased video microscopy during experiments involving neurite regeneration. It is especially important to consider not only neurite extension, but stalling and retraction as well in response to different biomaterials. We expect that this could improve development of future tissue engineered treatments for PNI. Interesting future work could also include using time lapse imaging to monitor physical changes (e.g. morphology and migration) in macrophage and Schwann cell phenotype over time.[220] Direct co-culturing of neurons with one or both cell types described here would be ideal but time lapse imaging could present a significant challenge. A possible alternative would be to test the effect of conditioned media from the macrophages, Schwann cells, or co-cultures of both cell types for influencing neurite outgrowth on the scaffolds. Another important cell type releasing factors into the injury environment to promote and direct regeneration are cells of the end organ, for example muscles innervated by motor neurons. End organ responsiveness is increased following nerve injury but the role of CSA on these cells has not been well characterized. The effects of our materials on end organ responsiveness would be an interesting future step. As well as co-culture of the neurons with injured myocytes.

Long-Term Goals

The next steps suggested above are designed to fine tune our model of the PNI environment to further improve *in vitro* testing before moving *in vivo*. The long-term goal of this research, however, is better treatment of large peripheral nerve gaps in the clinic. We ultimately aim to produce a scaffold system that mimics the Bands of Bungner and is an off-the-shell conduit filler that could be implanted inside commercially available devices during normal PNI surgeries. We believe this thesis has successfully evaluated tools that could be combined into such a device for use *in vivo*. To move our materials to animal models and ultimately the clinic, the 2D nanofibers would be formed into 3D cylindrical bridges that could be assembled inside of an implantable

device. To form these 3D bridges, we would use the electrospinning technique described for creating 2D sheets of nanofibers but with a longer spin time to achieve thicker scaffolds. Scaffolds could then be rolled into a cylindrical "bridge." Target diameter of ~1 mm and a minimum of length of 3 cm for these “bridges” represents the size order and length needed for a large nerve gap. Several bridges could be inserted into an existing NGC depending on the diameter of the injured nerve. Peripheral nerve diameters typically range from 1 to 10 mm, but may be as large as 20 mm in the sciatic nerve.[30] Consequently, size mismatch between the injured nerve and donor nerve is a common obstacle to nerve autograft and allograft treatments. This proposed system, in combination with an NGC, could help combat this drawback of grafting.

We anticipate that the bridges could be sutured directly to the nerve stumps using the same suture materials and methods for securing the current conduits into place. However, to avoid introducing additional damage at the repair site with this added suturing, the bridges could also be suspended in place with an injectable gel. Although not presented here, we have previous experience fabricating hyaluronic acid and collagen hydrogels. These gels could be used to embed the electrospun “bridges”. Furthermore, the SCM, used here as an adhesive coating or blended into nanofibers, could also serve as the gel material. Solubilized matrix could be crosslinked using varying concentrations of cytocompatible genipin (0-5mM). Genipin could be mixed into the spinal cord matrix solution and injected into and around the artificial bridges, which once crosslinked, would hold the bridges in place. Furthermore, we have already demonstrated the neurite growth promoting capabilities of the matrix itself. **Figure 5-1** illustrates a proposed nerve guide conduit design. By mimicking the Bands of Bungner that form during regeneration, as opposed to creating open channels, issues such as channel collapse and poor neurite infiltration are eliminated as the bridges are designed to support axon elongation around and on their surface.

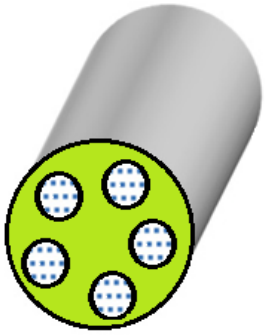

Figure 5-1. Proposed incorporation of HA nanofibers and SCM into a nerve guide conduit
A cross-section illustrating the proposed design of using aligned fibers to mimic the Bands of Bungner/Schwann cell cables that form following injury. The lime green color represents material to be determined, such as HA or collagen hydrogel, or crosslinked spinal cord matrix.

Applications in the Central Nervous System

The experiments in this thesis were specifically designed to explore the native repair processes and environment provided to regenerating peripheral axons. We explore using soluble and adhered, permissive and inhibitory biomolecules and nanofibers. However, these experiments are clearly relevant for testing the extension and retraction behavior of spinal neurons in response to topographical and adhesive cues as well. The MeHA nanofibrous scaffolds can provide a substrate for regenerating axons following SCI. Furthermore, it is possible that our scaffold design would be able to induce phenotypical changes in the glia of the central nervous system (CNS), particularly astrocytes, but also oligodendrocytes (the myelin producing cells of the CNS) and microglia (CNS inflammatory cells), leading to the same accelerated repair that we aimed for in the PNS.

Schwann cells are essential for the regeneration and remyelination of axons following injury in the PNS. Recent studies have also shown that transplantation of Schwann cells is a promising therapy for spinal cord repair.[221, 222] When transplanted into injured spinal cord, a Schwann cell suspension provides trophic support for the regenerating axons. For the Schwann cells to

guide axonal regeneration as a substrate, however, these support cells must be able to proliferate, migrate, and align within the injury site themselves.[223] This process could fail in a SCI in the same way that the Bands of Bungner are often disorganized or absent in large peripheral gaps.

Whole peripheral nerve grafts have also been used to treat spinal cord injuries with considerable success [224, 225]. These results demonstrate that central neurons do not possess a fundamentally different intrinsic ability to regenerate than peripheral neurons. Rather, the substrate/environment provided by the peripheral nerve graft is of critical importance to axonal regeneration. Therefore, we propose applying the scaffold components describe here to the treatment of CNS injuries, especially spinal cord injury (SCI). Schwann cell cables provide for greater flexibility in nerve repair than transplants of whole peripheral nerves as well.[226] A Schwann cell cable mimic could be applied to the spinal cord injury site replicating several of the cues required of all regenerating axons regardless of location.

In this thesis, we studied axon retraction which is an early feature of nearly all neurodegenerative diseases (NDs) including Alzheimer's disease (AD), Parkinson's' disease (PD), Huntington's disease (HD), Multiple Sclerosis (MS), Amyotrophic Lateral Sclerosis (ALS) and more.[118] Combined prevalence of these NDs in the United States exceeds 240 persons per 10,000 as of 2013 (NCHS; NINDS). These and other NDs contribute an estimated $150-200 billion burden to US healthcare annually.[227] Thus the NDs are of particular scientific and clinical interest because of their increasing medical and societal impact.

One issue associated with current ND treatments is increased activation of the microglia. Reducing this activation, and inducing the microglia back to a homeostatic phenotype, with topography and/or adhesive cues on a nanofibrous scaffold, as we've described for macrophages in Aim 3, could also potentially be applied in the brain. In addition, myelin loss is the hallmark of multiple sclerosis. Investigating methods to induce oligodendrocytes into a pro-myelinating phenotype, such as with the topographical approach described here for Schwann cells, might have

potential for treating this disease. An implanted biomaterial scaffold would be a novel treatment option for NDs.

Summary

In a 2009 Nature Review, the regenerating growth cone is compared to a "vehicle" as it encounters many different types of cues. The "vehicle" moves along a "road" of adhesive molecules either presented by neighboring cells or assembled into the extracellular matrix. Anti-adhesive, surface bound molecules, can inhibit the advancement of the growth cone acting as "guard rails" or boundaries. Finally, diffusible chemotropic cues represent "road signs" that present further steering instructions to the growth cone.[13] In this thesis, we explored elements of the “road” (SCM and MeHA nanofibers), “guard rails” (CSMA), and “road signs” (CSA) for their effects on real time neurite behavior and macrophage and Schwann cell phenotype. We aim to engineer better strategies for neural tissue regeneration through deeper understanding of the injury environment and cellular responses to it.

We highlight several tools for studying and manipulating the PNI environment including: flow cytometry, PCR, antibody arrays for cytokine release, time lapse microscopy, fluorescence microscopy, topographical cues created by blend electrospinning (and early potential for dual electrospinning see Appendix B), unique biomaterials cues (soluble CSA, immobilized CSMA, MeHA, SCM as coating and fibers). We applied these tools to several cell types in the PNI environment looking to direct cell responses. The response that we see from the cells are promising results that can lead us to the recommendation that these tools be applied to more cell types (ie. CNS), to combinations of different cell types (direct co-culture or conditioned media) and to evaluate NTE scaffolds in greater detail *in vitro* prior to moving to *in vivo* models which are potentially more expensive and time consuming. We want neural tissue engineered scaffolds to succeed in treating large peripheral nerve gaps. We hope that this thesis can serve as a guideline in the design of other tissue engineered systems and we hope the specific biomaterials explored here will find widespread application in the nervous system.

APPENDIX A: Preliminary Gradient Scaffolds

The ability of soluble and adhered biomolecular gradients to direct neurite outgrowth and growth cone turning has been well established over the last few decades. Furthermore, tissue engineered gradients have become an increasingly popular paradigm for improving axon regeneration following peripheral nerve injury as well as for directing other types of cell migration.[62] This appendix contains preliminary work on creating gradients within our nanofibrous scaffolds using a dual needle electrospinning apparatus.

Polymer Synthesis and Modification

The goal of this work is to deliver molecular gradients of methacrylated Chondroitin Sulfate A (CSMA) and porcine spinal cord matrix (SCM) within our methacrylated hyaluronic acid (MeHA) scaffolds. We previously demonstrated the ability of each of these cues to promote neurite outgrowth individually (see full Methods and Results in Chapter 3). However, in this preliminary work, we have formed gradients of the amino acid sequence RGD (Arg-Gly-Asp) using a method previously described for RGD conjugation to MeHA.[228] Briefly, cysteine-containing RGD peptides (GCGYG*RGD*SPG, Genscript) were conjugated to the MeHA via a Michael's addition reaction between thiols on the peptides and methacrylates on the MeHA. The RGD peptide (1mM) and MeHA (2% w/v) were reacted overnight in triethanolamine buffer (pH 8), dialyzed against DI H_2O for 48 hours, and lyophilized to obtain MeHA+RGD. Un-conjugated methacrylate sites can be linked to one another in the presence of Irgacure 2959 photocrosslinker and UV light to introduce crosslinks that will stabilize the material. **Figure A-1** illustrates the MeHA synthesis and peptide modification reactions.

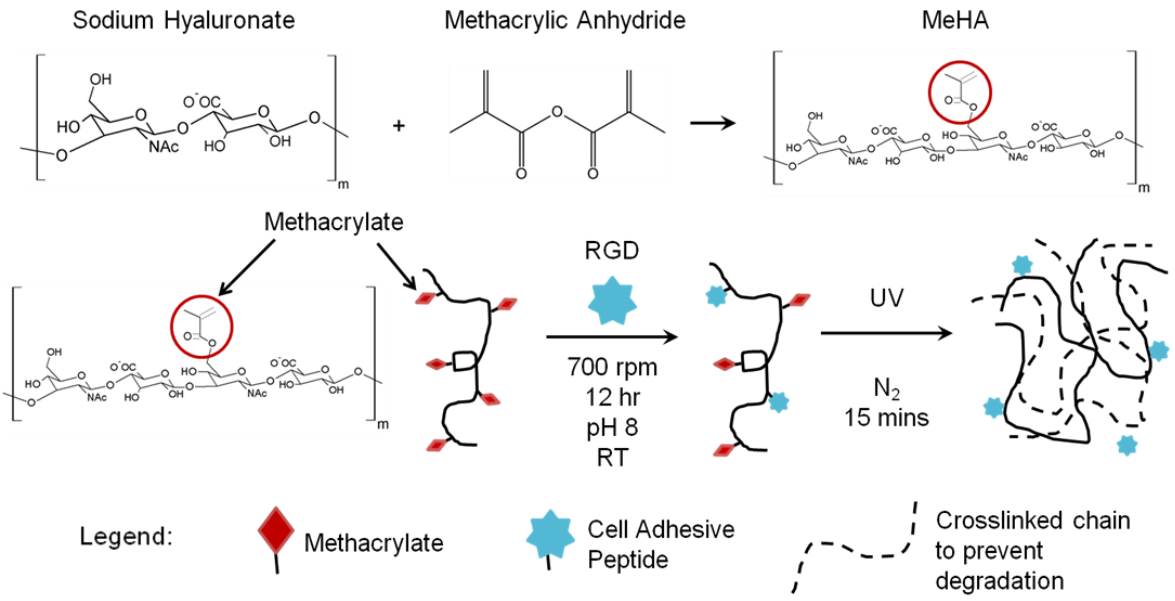

Figure A-1. MeHA synthesis and RGD conjugation.

Methacrylate side groups are added to hyaluronic acid using a Michael's addition reaction. Methacrlyate groups serve as attachment sites for the RGD peptide. Unmodified methacrylate sites are linked to one another in the presence of Irgacure 2959 photocrosslinker and UV light.

Nuclear Magnetic Resonance

Proton nuclear magnetic resonance (NMR) with a Bruker Avance 700 MHz biomolecular NMR was used to assess methacrylation and RGD attachment to the HA following a previously published protocol.[229] Briefly, samples were dissolved at 5 mg/mL in D_2O (Sigma) and the degree of methacrylation was calculated from the NMR spectra as the ratio of the acetylenic protons from the methacrylate groups to the N-acetyl methyl protons from the HA backbone. **Figure A-2** shows NMR spectra collected for two different degrees of HA methacrylation and the MeHA+RGD. These spectra suggest that our methacrylation and peptide modification of the hyaluronic acid was successful. A reaction of 1.11 mL of methacrylic anhydride per gram of HA (**Figure A-2C**) produced ~10% modification, while 2.22 mL of MA per gram of HA (**Figure A-2B**) produced ~25% modification. **Figure A-2A** shows the higher modification MeHA conjugated with 1mM of RGD

peptide. The two peaks at 3.3 and 3.7 ppm are indicative the δH and ξH of the Arginine amino acid, respectively (Biological Magnetic Resonance Data Bank, http://www.bmrb.wisc.edu/).

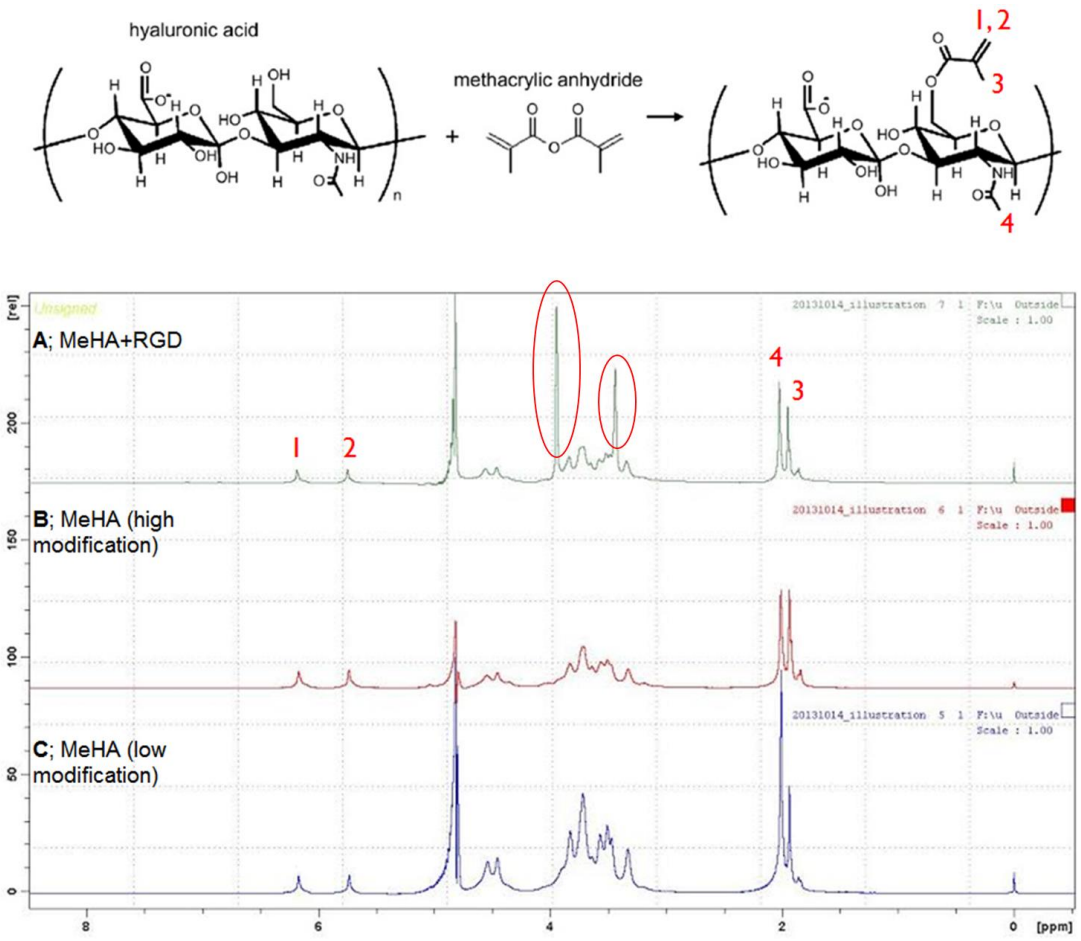

Figure A-2. NMR spectra

The degree of methacrylation is calculated as the ratio of the areas under the proton peaks at 5.6 and 6.1 ppm (acetylenic protons from the methacrylate groups; 1 and 2) to the peak at 2 ppm (N-acetyl methyl protons from the HA backbone, 4).

Electrospinning Gradient Scaffolds

Following synthesis and peptide modification, the following polymer solution was prepared for electrospinning: 2 wt% MeHA+RGD, 3 wt% polyethylene oxide (PEO, MW 900 kDa, Sigma), and 0.05 wt% Irgacure 2959 photoinitiator (BASF) in DI H_2O. Electrospinning apparatus parameters including flow rate, needle gauge, voltage, collection distance, and collection surface/mandrel

dimensions are provided in detail in Chapter 3 and have been adapted from Ifkovits et al 2009. Fibers were collected for 45 minutes (~50μm thick layer) and crosslinked onto methacrylated glass coverslips. Chapter 3 also contains fiber crosslinking, and rinsing methods.

The RGD peptide sequence, derived from fibronectin, is a ubiquitous adhesive cue for all cells. By distributing the RGD in a controlled gradient, the direction of neurite growth can also be controlled. Scaffolds featuring gradients of the RGD peptide were produced by electrospinning two different solutions from needles placed on either side of the spinning mandrel. Mandrel rotation speed was used to form aligned (~2500 rpm) and non-aligned (~700 rpm) nanofibers. The electrospinning set up is illustrated in **Figure A-3** where Polymer A = MeHA with RGD peptide and Polymer B = MeHA without RGD peptide. The offset distance ('x cm') between the two needles was varied to alter the resulting gradient shape.

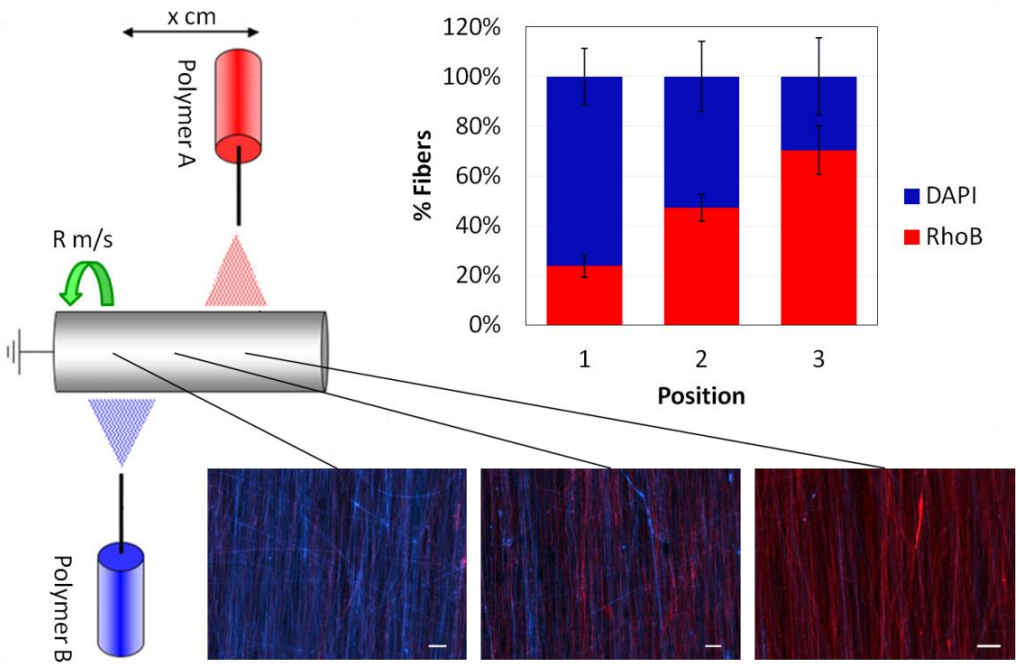

Figure A-3. Schematic of the dual needle electrospinning set up for creating fiber gradients

(A) Schematic of the apparatus used to electrospin gradient scaffolds. **(B)** Resulting gradient obtained with 4cm offset. Percentage of each type of fiber was measured using relative fluorescence of DAPI and Rhodamine stains. **(C)** Fluorescent micrographs of fibers obtained at 3 different positions evenly spaced along the gradient. Scale = 200 μm.

RGD Distribution

To estimate RGD distribution in the gradients, the RGD containing polymer solution was mixed with Rhodamine B (25 μM) prior to spinning and the resulting gradient shape was analyzed using relative fluorescence intensity measurements. The distribution of dyed fibers was used to estimate the spatial distribution of the RGD peptide. 2, 4, 6 and 8 cm offsets between the two needles were tested for producing differently shaped RGD gradients spun onto 22x22mm co-verslips centered between the two needles. The 4cm offset was chosen for the subsequent cell studies because it produced the most linear gradients (see **Figure A-4**) whereas a 2cm offset resulted in a more uniform RhoB distribution and 6 and 8 cm offsets resulted in step-like gradients.

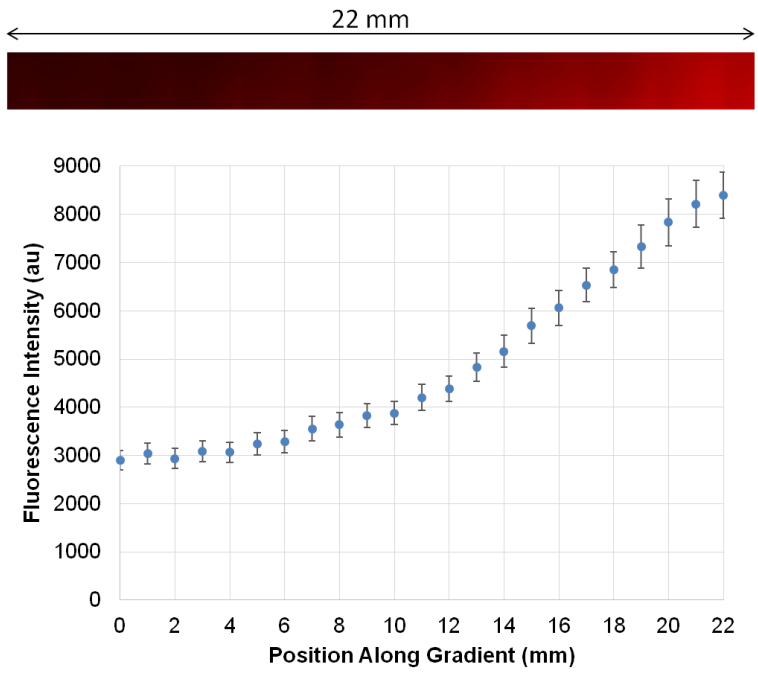

Figure A-4. RGD gradient distribution estimated from Rhodamine B fluorescence intensity

Top: Fluorescent image showing the distribution of Rhodamine B across the width of the nano-fiber scaffold (spun with a 4cm needle offset). **Bottom:** Measured fluorescence intensity across the scaffold. n = 12 scaffolds. Mean ± SEM.

We hypothesize that opposing linear gradients of our two target cues (CSMA and SCM) will produce the most directed neurite outgrowth based on the success of other studies that investigated linear gradients of soluble and adhered biomolecules for directing neurite growth (**Table A-1**). However, many different gradient shapes can be produced with the different needle offset distances. Therefore, many different shapes should be tested in order to optimize the behavior of the DRG neurite outgrowth on the CSMA and SCM gradients, because these two molecules have previously not been tested as gradients for controlling neurite outgrowth.

Cell Type	*Gradient Molecule*	*Threshold Required for Neurite Orientation (Slope)*	*Increased Neurite Growth Rate?*	*Directed Neurite Turning?*	*References*
PC12	NGF	0.133 μg/mL/mm	U	U	230
Chick Embryo DRGs	NGF	0.133 μg/mL/mm	U	Y	231
Chick Embryo DRGs	NGF NT-3	0.08 μg/mL/mm 0.08 μg/mL/mm	U	Y	231
Human Neural Stem Cells	EGF, FGF2 and PDGF	None[a]	Y	U	232
Mouse Hippocampal and DRG Neurons	Netrin-1 (attractant) Slit-2 (repellent)	1 μg/mL[b] 0.250 μg/mL[b]	U U	Y Y	63
Rat DRGs	NGF	U	Y	Y	233
Rat Hippocampal Neurons	Netrin-1	U	Y	U	234
Rat Dorsal Column Lesions	NT-3	U	U	Y	235
Rat Hippocampal Neurons	Laminin	60 μg/mL/μm	N	N	236
Rat PC12	NGF	0.137-0.357 μg/mL/mm	U	U	237
Chick Embryo DRGs	IKVAV	U	Y	Y	50
Chick Embryo DRGs	NGF	0.31 μg/mL/mm	U	U	238
Chick Embryo DRGs	NGF NT-3	0.2 μg/mL/mm 0.2 μg/mL/mm	U	U	238
Chick Embryo DRGs	IKVAV YIGSR	7.44 μg/mL/mm[c] 14.9 μg/mL/mm[c]	Y	N	239
Chick Embryo DRGs	Laminin-1 Isoform	0.017 μg/mL/mm[c]	Y	N	153
Chick Embryo DRGs	PSA HNK-1	U U	Y N	U U	240
Mouse NSC-34 Hybrid Cell Line and Dissociated Rat Spinal Cord Neurons	PSA HNK-1 PSA/HNK-1	U U U	Y Y Y	U U U	240
RSC-96 Rat Schwann cells	PSA HNK-1 PSA/HNK-1	U U U	Y N Y	U U U	240

Table A-1. Neural Cell Responses to Soluble and Immobilized Chemical Gradients

Y = yes; N = no; U = unreported/unavailable; [a] In the concentration range 0–40 ng/mL over a 2.4mm distance, nonlinear slope. [b] Across 1.2mm distance, nonlinear slope. [c] These values do not represent threshold conditions but rather indicate optimal gradient slopes for maximizing outgrowth. PSA/HNK-1 in a 50/50 ratio. Green shaded cells = soluble/chemotactic gradients; Blue shaded cells = immobilized/haptotactic gradients

Gradient Scaffolds for Cell Studies

Scaffolds featuring non-aligned fibers with a gradient of RGD (**Figure A-5A**) were combined with a thin layer of aligned, unmodified fibers in order to assess the additive effect of the adhesive gradient and fiber alignment cues (**Figure A-5B**). Non-aligned scaffolds with a thin layer of aligned fibers, but no RGD, were used as a control (**Figure A-5C**). Whole dorsal root ganglia (DRG) from chick embryos were grown on the scaffolds for 3 days in serum free media and fixed and stained as described in Chapter 3. **Figures A-5D, E** and **F** show examples of DRGs grown on each of the three scaffold types, respectively.

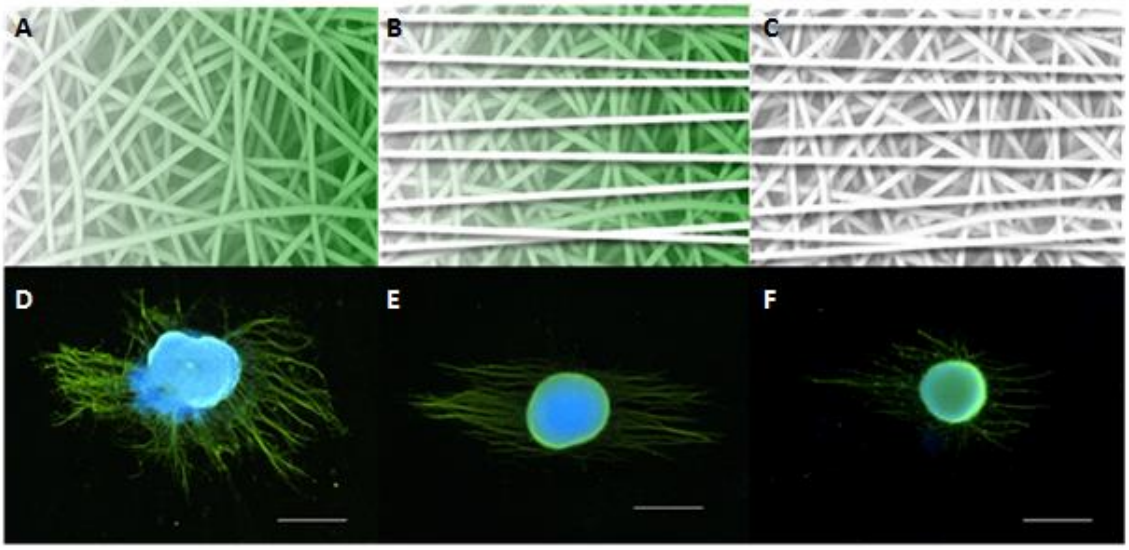

Figure A-5. Gradient scaffold schematics and fluorescence micrographs of DRG outgrowth

A ,B, C) Schematic representations of the non-aligned (NA) gradient, layered gradient, and layered control scaffolds, respectively. Green indicates the direction of increasing RGD peptide. **D, E, F)** Resulting DRG outgrowth on the corresponding gradient and control scaffolds after 3 days. DRGs stained with anti-neurofilament (green) and DAPI (blue). Scale = 500 μm.

NIS Elements and ImageJ software were used to quantify whole DRG outgrowth using two different ratios (**Figure A-6**):

- **Gradient ratio** was used to measure the influence of the RGD peptide. The yellow dashed line represents the area of the DRG body (DAPI staining/blue pixels). The centroid of this area was used to divide the image in half (solid yellow line) so that either side contained an equal area of the DRG body. Next a custom Matlab script was used to measure the area of the neurite outgrowth (FITC staining/green pixels). Briefly, the code uses an automatic threshold to convert a grayscale image to binary and then sums the pixels to quantify the outgrowth area. The ratio of axon outgrowth of the right side to the left side of the image was calculated. A ratio of >1 indicates neurite outgrowth was greater towards the increasing RGD peptide.
- **Modified aspect ratio** was used to measure the influence of fiber alignment. Auto edge detection was used to measure outgrowth in the left/right direction (direction of the gradient and/or fibers) divided by the outgrowth in the top/bottom or perpendicular direction. The red lines in Figure A-6 show an example of these two measurements.

All outgrowth was normalized to body size for each individual DRG.

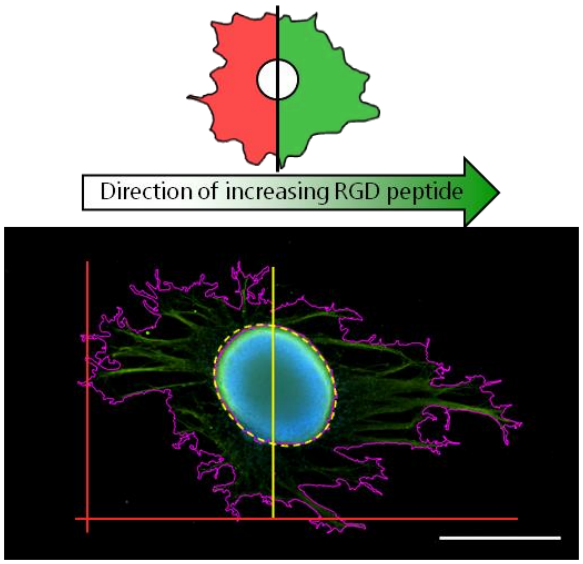

Figure A-6. Measurement techniques and growth ratios of DRGs on gradient scaffolds

Top: Area of outgrowth up (green) or down (red) the gradient of RGD was compared.
Bottom: Sample image of a DRG showing division of the body area for gradient ratio (yellow lines) and maximum outgrowth measurements (red lines) for the modified aspect ratio. Scale = 500 μm.

Scaffolds featuring gradients of RGD peptide produced a ~20% increase in neurite growth towards the direction of increasing RGD over the control scaffold, but the difference was not statistically significant. Furthermore, there was no statistical difference between groups with and without the top layer of aligned fibers. Aspect ratio data revealed that the presence of the aligned fibers significantly increased neurite outgrowth in the fiber (left/right) direction over the non-aligned RGD gradients for both scaffolds with and without RGD. Furthermore, scaffolds with RGD and an aligned fiber layer showed the most overall growth area (data not shown) suggesting a possible additive effect of these two cues. **Figure A-7** quantifies the results of the DRG outgrowth on the gradient scaffolds.

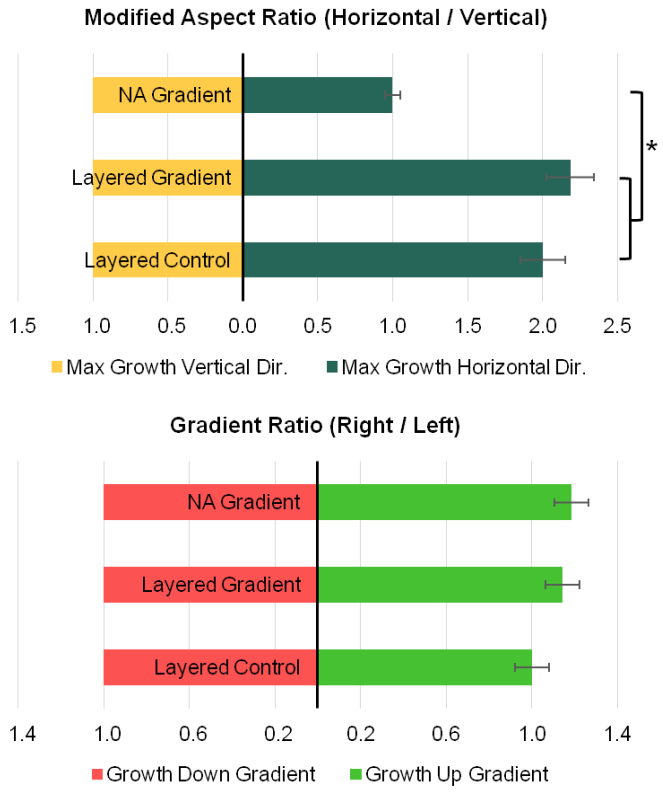

Figure A-7. Quantified outgrowth from DRGs cultured on the gradient scaffolds

Top: Aspect ratio results. * $p < 0.01$, one-way ANOVA, Tukey post hoc. **Bottom:** Gradient ratio results. 3 trials, 3 repeats per condition per trial. n = 9 DRGs measured per condition.

Summary

In this preliminary work RGD peptide was used as an example molecule for creating gradient scaffolds. In the future, the techniques described above could be adapted to deliver the neural specific guidance molecules characterized in this thesis, chondroitin sulfate A and the spinal cord derived matrix. Gradient scaffolds could be delivered *in vivo* to guide growth from the proximal to distal or distal to proximal nerve stumps. The proposed design, featuring dual gradients of both positive and negative adhered guidance molecules, would be a novel approach to controlling the directedness of neurite outgrowth. During nervous system development, chondroitin sulfate proteoglycans (CSPGs) guide neurons to appropriate targets by inhibiting them

from entering inappropriate ones.[28] Our design would exploit the ability of CSPGs to direct neurite outgrowth by avoiding inefficient regeneration, such as misdirected or “wrong way” axons and/or excessive neurite branching. We are especially interested in directing, continuous persistent neurite outgrowth across large peripheral nerve gaps to accelerate repair.

APPENDIX B: Chapter 4 Supplement

Appendix B contains supplementary data and figures from Chapter 4.

A

Each antibody is printed in quadruplicate horizontally								
	1	2	3	4	1	2	3	4
A	POS1				POS2			
B	GM-CSF				IFN-gamma			
C	IL-1 alpha				IL-1 beta			
D	IL-2				IL-3			
E	IL-4				IL-5			
F	IL-6				IL-9			
G	IL-10				IL-12 p70			
H	IL-13				IL-17A			
I	KC (CXCL1)				MCP-1 (CCL2)			
J	M-CSF				RANTES (CCL5)			
K	TNF-alpha				VEGF-A			

B

	A	B	C	D	E	F	G	H	I	J	K	L
1	POS1	POS2	POS3	NEG	Activin A	Agrin	B7-2 / CD86	β-NGF	CINC1	CINC2a	CINC3	CNTF
2	POS1	POS2	POS3	NEG	Activin A	Agrin	B7-2 / CD86	β-NGF	CINC1	CINC2a	CINC3	CNTF
3	FASLG	CX3CL1	CSF2	ICAM1	IFN-γ	IL-1α	IL-1β	IL1 R6	IL-2	IL-4	IL-6	IL-10
4	FASLG	CX3CL1	CSF2	ICAM1	IFN-γ	IL-1α	IL-1β	IL1 R6	IL-2	IL-4	IL-6	IL-10
5	IL-13	Leptin	LIX	SELL	MCP1	MIP-3α	MMP-8	PDGF-AA	PRLR	RAGE	CXCL7	TIMP1
6	IL-13	Leptin	LIX	SELL	MCP1	MIP-3α	MMP-8	PDGF-AA	PRLR	RAGE	CXCL7	TIMP1
7	TNF-α	VEGF-A	NEG	NEG	NEG	NEG	NEG	NEG	NEG	NEG	NEG	POS4
8	TNF-α	VEGF-A	NEG	NEG	NEG	NEG	NEG	NEG	NEG	NEG	NEG	POS4

Figure B-1. Cytokine array maps

Array maps show the position and number of replicates for each cytokine assayed for release from the RAW 264.7 macrophages **(A)** and S16 Schwann cells **(B)** in response to our biomaterials cues. Positive Controls (POS1, POS2, POS3) are equal amounts of biotinylated IgGs printed directly onto the array their intensities should be the same for each sub-array. Negative Control (NEG) spots are a protein-containing buffer. Their signal intensities represent non-specific binding of Biotin-conjugated anti-Cytokines and/or Streptavidin-Fluor. Controls allow for normalization based upon the relative fluorescence signal responses to a known control. CINC1 = CXCL1 (human GRO-α homolog), CINC2a = CXCL3 (human GRO-γ homolog), CINC3 = CXCL2 (human GRO-β homolog), FASLG = Fas Ligand, CX3CL1 = Fractalkine, CSF2 = GM-CSF, LIX = CXCL5, SELL = L-Selectin, PRLR = Prolactin Receptor, RAGE = Receptor for Advanced Glycosylation Endproducts, CXCL7 = Thymus Chemokine 1; VEGF-A detects VEGF(165 aa) and VEGF(121 aa); B7-2 / CD86, PRLR and RAGE detect soluble forms of these proteins.

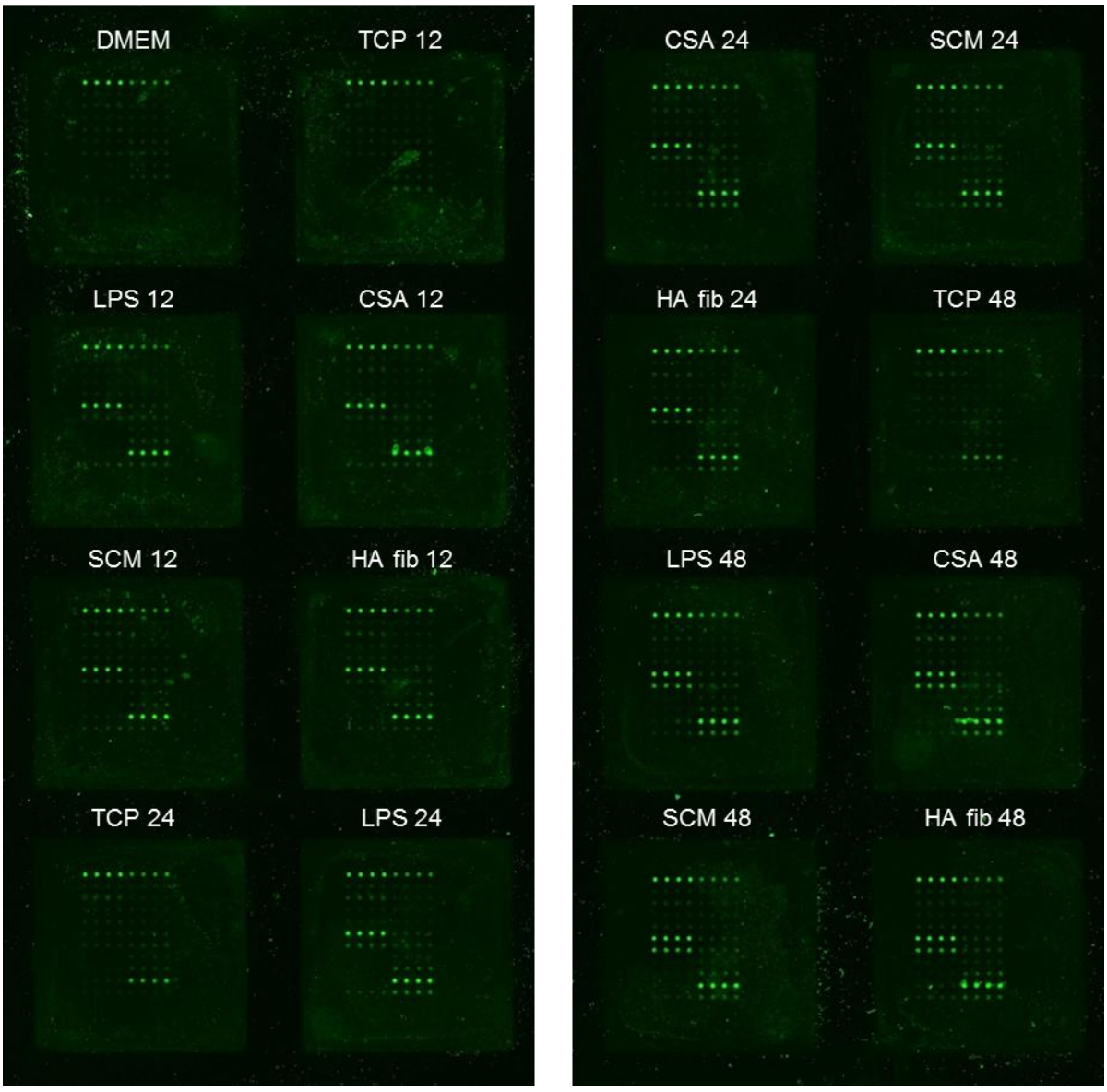

Figure B-2. Macrophage cytokine array images

Laser scanning and data extraction provided by RayBiotech. Headings indicate biomaterial cue being tested and time point in hours. DMEM = media only control/no cells; TCP = tissue culture plastic; LPS = Lipopolysaccharide 1μg/mL; CSA = chondroitin sulfate A at 10μg/mL; SCM = spinal cord matrix coating 5μg/cm^2; HA fib = hyaluronic acid nanofibers.

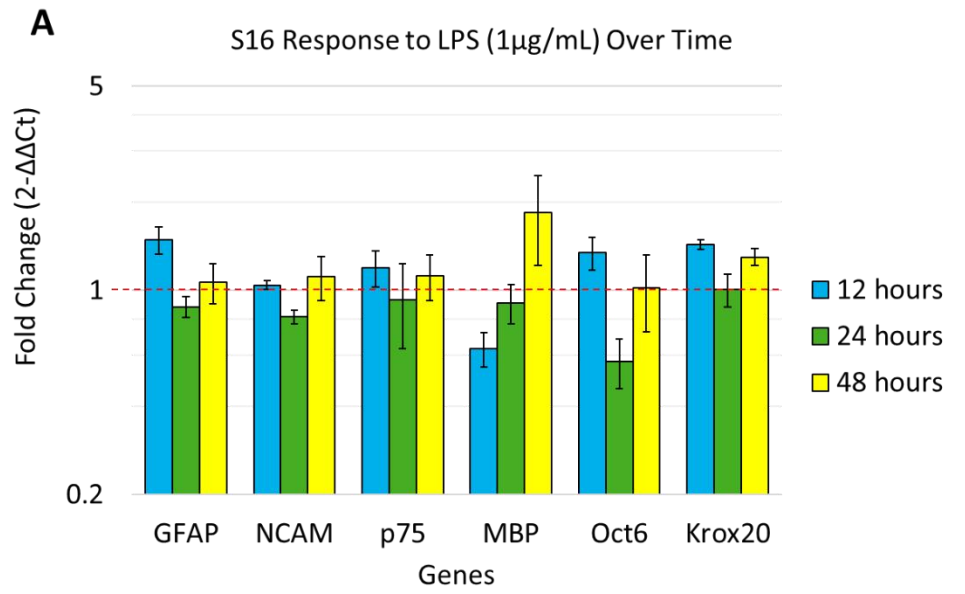

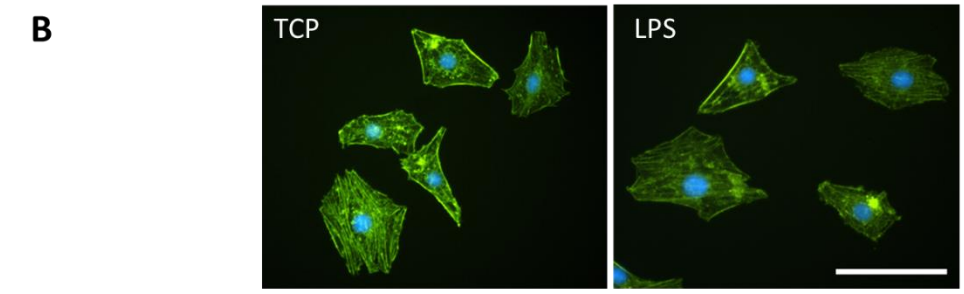

Cell Area (µm²)	2618 ± 109	2507 ± 94
Elongation	1.71 ± 0.04	1.78 ± 0.05
Form Factor/ Circularity	0.55 ± 0.01	0.53 ± 0.01

Figure B-3. Schwann cell response to LPS treatment

LPS had no statistically significant effects on mRNA expression **(A)** or morphology **(B)** of the S16 Schwann cells. Significance considered $p<0.05$ one-way ANOVA + Fisher's LSD post hoc.

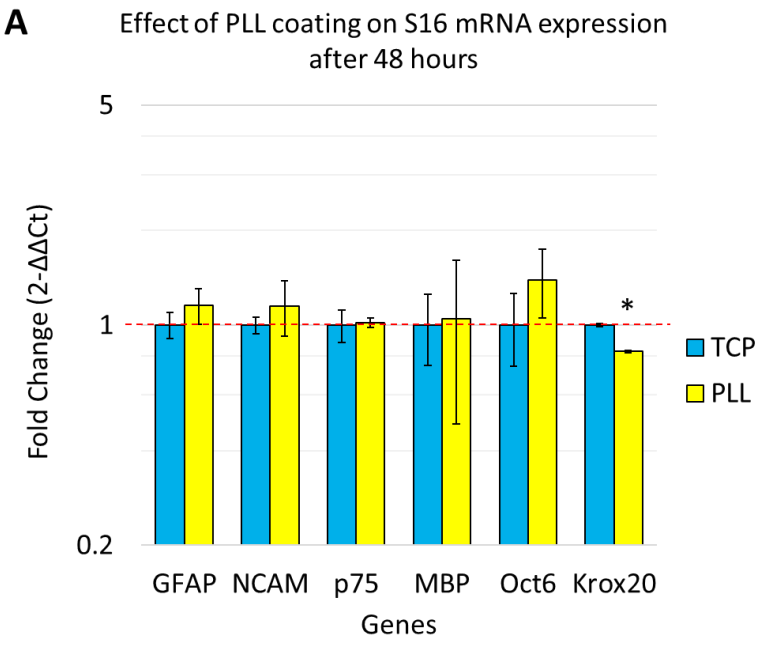

B

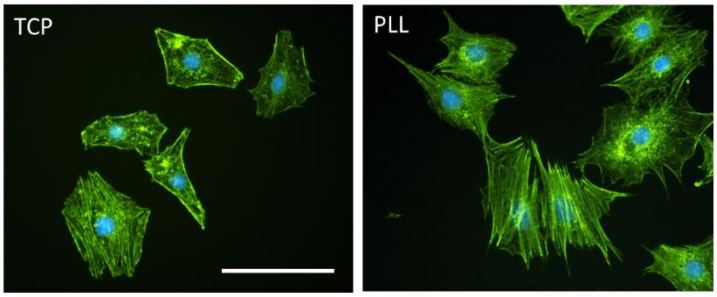

Cell Area (μm²)	2618 ± 109	3235 ± 150*
Elongation	1.71 ± 0.04	1.62 ± 0.04
Form Factor/ Circularity	0.55 ± 0.01	0.40 ± 0.02*

Figure B-4. Schwann cell phenotype on PLL: PCR and Morphology

Poly-L-lysine (PLL) keeps the S16 Schwann cells in an immature state based on statistically significant differences in mRNA expression **(A)** and morphology **(B)** compared to cells grown on TCP without PLL. *p<0.05 one-way ANOVA + Fisher's LSD post hoc.

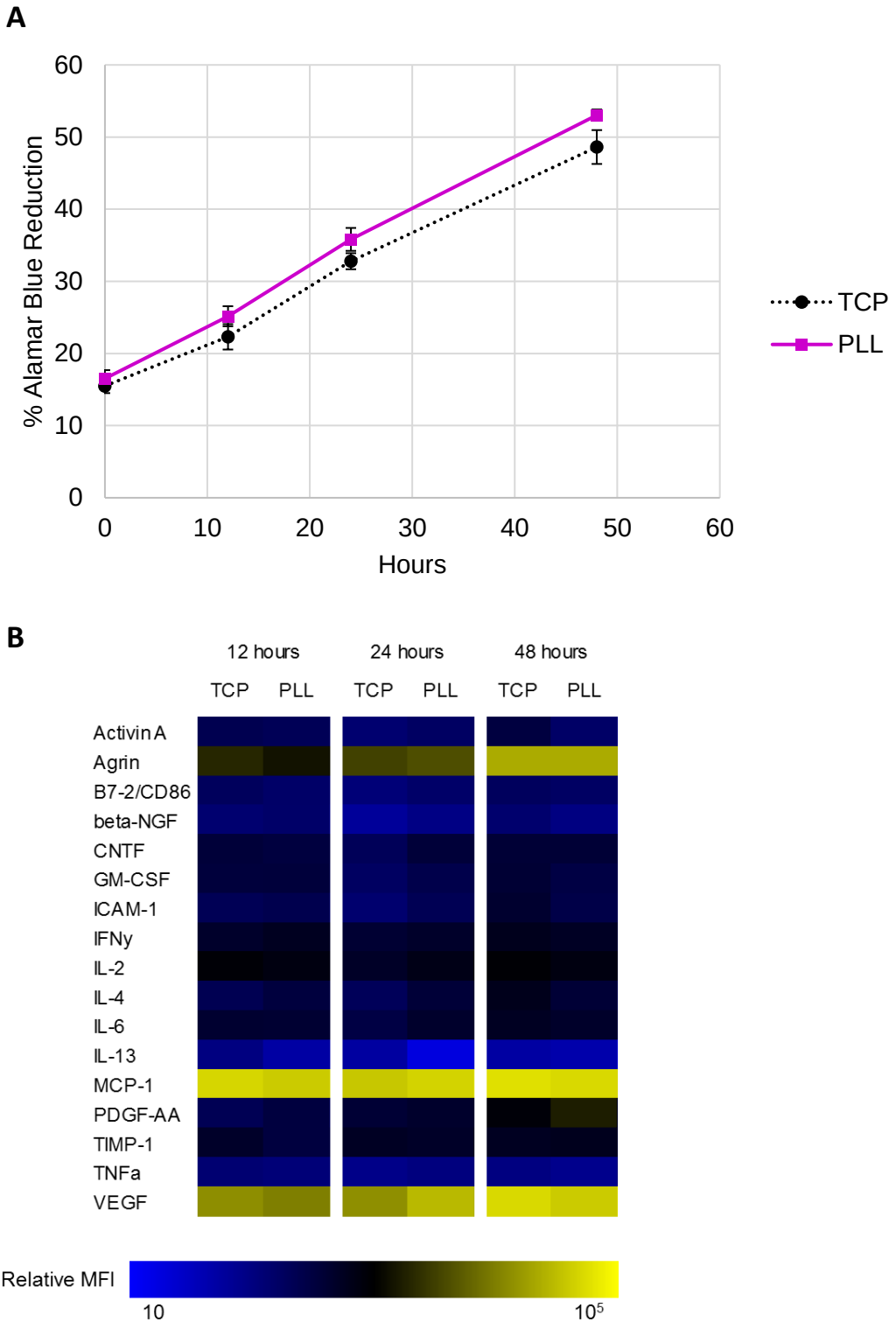

Figure B-5. Schwann cell phenotype on PLL: Proliferation and Cytokine Release

S16 Schwann cells cultured on poly-L-lysine (PLL) have increased proliferation **(A)** and differences in cytokine release **(B)** compared to SCs grown on TCP without PLL.

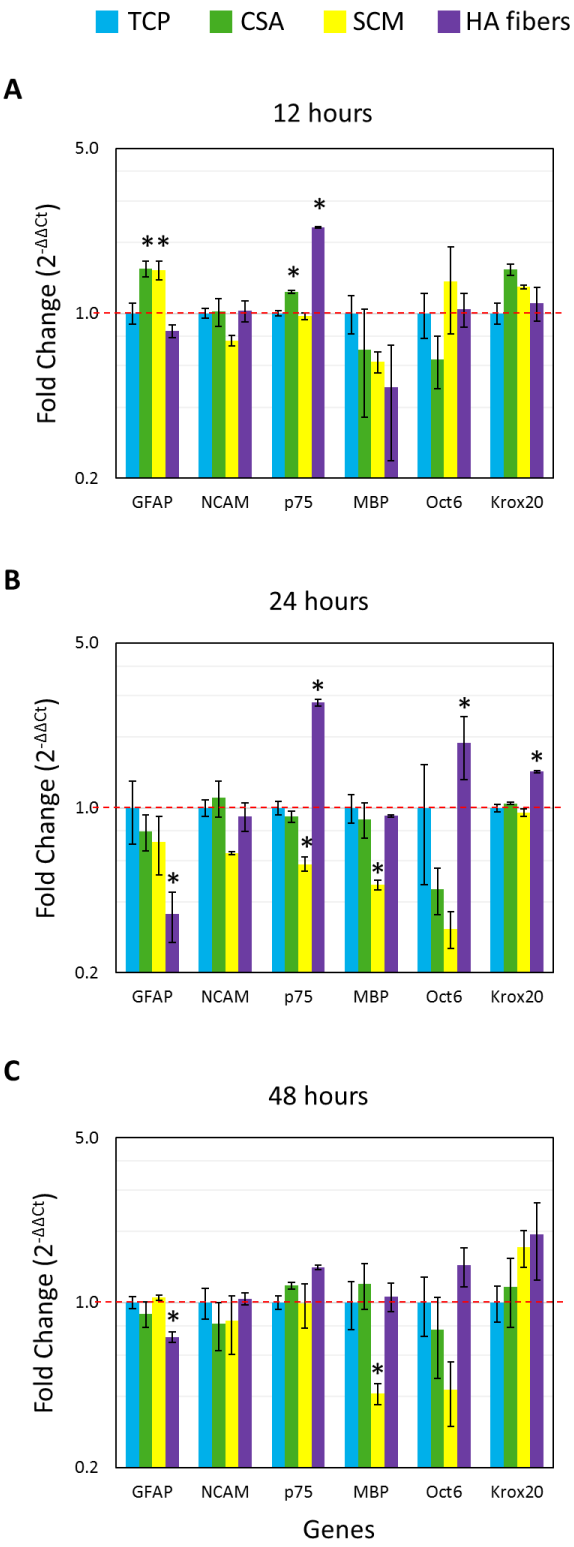

Figure B-6. Schwann cell PCR results

S16 mRNA expression of key markers of maturation/myelination 12 **(A)**, 24 **(B)**, and 48 **(C)** hours following culture with the indicated biomaterials cues. Fold changes reported relative to TCP control and normalized to beta-actin. Mean ± SEM. N = 3 biological replicates. * $p<0.05$ one-way ANOVA + Fisher's LSD post hoc.

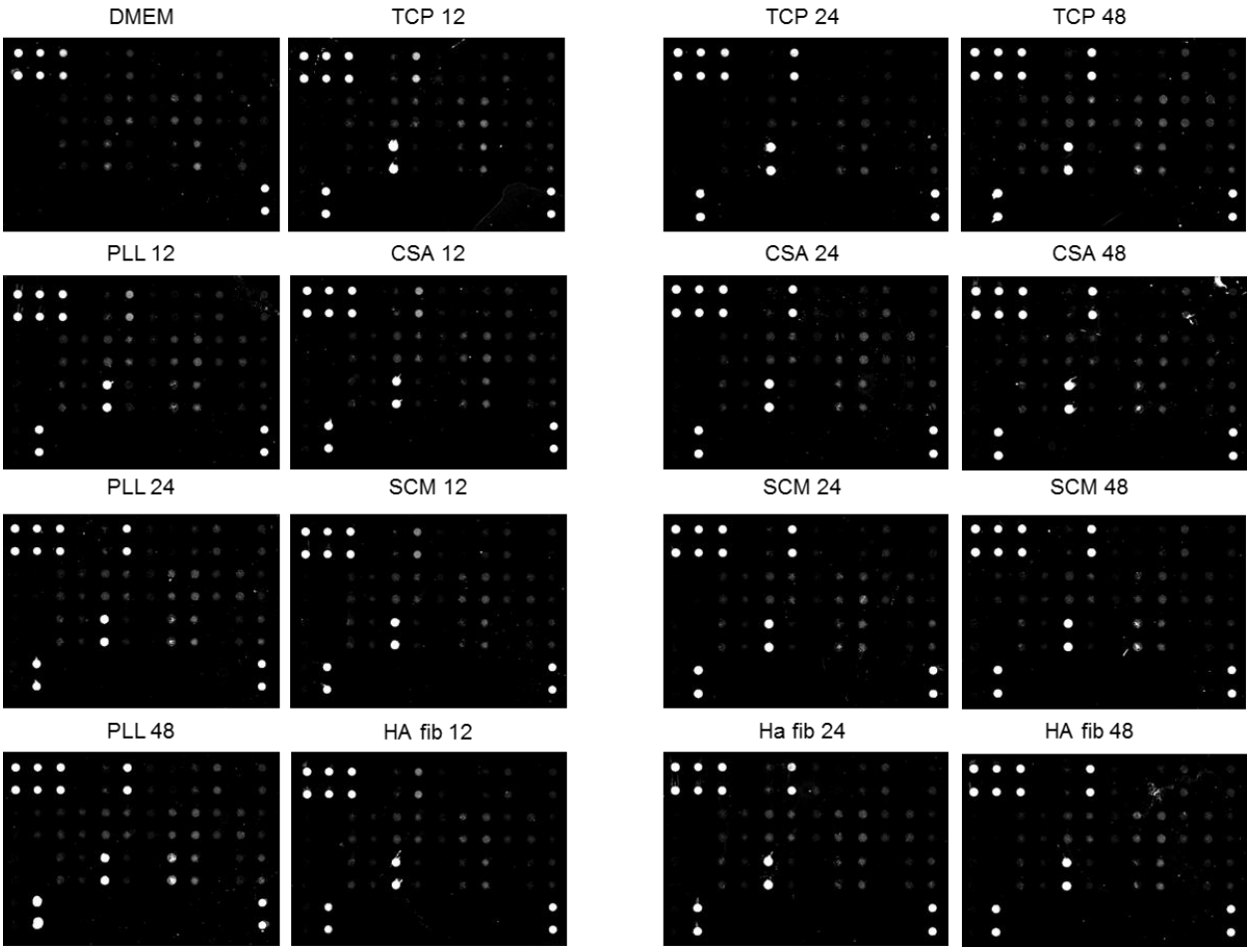

Figure B-7. Schwann cell cytokine array images

Laser scanning and data extraction provided by RayBiotech. Headings indicate biomaterial cue being tested and time point in hours. DMEM = media only control/no cells; TCP = tissue culture plastic; PLL = poly-L-lysine; CSA = chondroitin sulfate A at 10μg/mL; SCM = spinal cord matrix coating 5μg/cm^2; HA fib = hyaluronic acid nanofibers.

REFERENCES

1. Deitch, E.A. and W.R. Grimes, *Experience with 112 shotgun wounds of the extremities.* J Trauma, 1984. **24**(7): p. 600-3.
2. Apel, P.J., J.P. Garrett, P. Sierpinski, J. Ma, A. Atala, T.L. Smith, L.A. Koman, and M.E. Van Dyke, *Peripheral nerve regeneration using a keratin-based scaffold: long-term functional and histological outcomes in a mouse model.* J Hand Surg Am, 2008. **33**(9): p. 1541-7.
3. Yegiyants, S., D. Dayicioglu, G. Kardashian, and Z.J. Panthaki, *Traumatic peripheral nerve injury: a wartime review.* J Craniofac Surg, 2010. **21**(4): p. 998-1001.
4. Burdick, J.A., *Biomaterials for Tissue Engineering Applications*. 2010: Springer.
5. Brattain, K., *Analysis of the Peripheral Nerve Repair Market in the United States*, 2012, Magellan Medical Technology Consultants, Inc.: Minneapolis, MN. p. 1-11.
6. Pfister, L.A., M. Papaloizos, H.P. Merkle, and B. Gander, *Nerve conduits and growth factor delivery in peripheral nerve repair.* J Peripher Nerv Syst, 2007. **12**(2): p. 65-82.
7. Grinsell, D. and C.P. Keating, *Peripheral nerve reconstruction after injury: a review of clinical and experimental therapies.* Biomed Res Int, 2014. **2014**: p. 698256.
8. Chiras, D.D., *Human Biology*. 2013: Jones & Bartlett Learning.
9. Lutz, A.B. and B.A. Barres, *Contrasting the Glial Response to Axon Injury in the Central and Peripheral Nervous Systems.* Developmental Cell, 2014. **28**(1): p. 7-17.
10. Carlson, B.M., *Principles of regenerative biology*. 2007, Amsterdam ; Burlington, Mass.: Elsevier/Academic Press. xix, 379 p.
11. Sicar, S., *Principles of medical physiology*. 2008, Stuttgart ; New York: Thieme. xiii, 793 p.
12. Geuna, S., S. Raimondo, G. Ronchi, F. Di Scipio, P. Tos, K. Czaja, and M. Fornaro, *Chapter 3 Histology of the Peripheral Nerve and Changes Occurring During Nerve*

Regeneration, in *International Review of Neurobiology*, G. Stefano, T. Pierluigi, and B. Bruno, Editors. 2009, Academic Press. p. 27-46.

13. Lowery, L.A. and D. Van Vactor, *The trip of the tip: understanding the growth cone machinery.* Nat Rev Mol Cell Biol, 2009. **10**(5): p. 332-43.
14. Ketschek, A.R., S.L. Jones, and G. Gallo, *Axon extension in the fast and slow lanes: substratum-dependent engagement of myosin II functions.* Dev Neurobiol, 2007. **67**(10): p. 1305-20.
15. Alberts, B., A. Johnson, J. Lewis, D. Morgan, M. Raff, K. Roberts, and P. Walter, *Molecular Biology of the Cell*. 2014: Taylor & Francis.
16. Sherwood, L., *Human Physiology: From Cells to Systems*. 2012: Cengage Learning.
17. Hilliard, M.A., *Axonal degeneration and regeneration: a mechanistic tug-of-war.* J Neurochem, 2009. **108**(1): p. 23-32.
18. Rauch, P., P. Heine, B. Goettgens, and J.A. Kas, *Different modes of growth cone collapse in NG 108-15 cells.* European Biophysics Journal with Biophysics Letters, 2013. **42**(8): p. 591-605.
19. Koike, T., Y. Yang, K. Suzuki, and X. Zheng, *Axon & dendrite degeneration: its mechanisms and protective experimental paradigms.* Neurochem Int, 2008. **52**(4-5): p. 751-60.
20. Beller, J.A., B. Kulengowski, E.M. Kobraei, G. Curinga, C.M. Calulot, A. Bahrami, T.M. Hering, and D.M. Snow, *Comparison of sensory neuron growth cone and filopodial responses to structurally diverse aggrecan variants, in vitro.* Experimental Neurology, 2013. **247**: p. 143-157.
21. Anderson, M., M. Bostrom, K. Pfaller, R. Glueckert, A. Schrott-Fischer, B. Gerdin, and H. Rask-Andersen, *Structure and locomotion of adult in vitro regenerated spiral ganglion growth cones - A study using video microscopy and SEM.* Hearing Research, 2006. **215**(1-2): p. 97-107.

22. Baas, P.W. and F.J. Ahmad, *Force generation by cytoskeletal motor proteins as a regulator of axonal elongation and retraction.* Trends in Cell Biology, 2001. **11**(6): p. 244-249.

23. Gaudet, A.D., P.G. Popovich, and M.S. Ramer, *Wallerian degeneration: gaining perspective on inflammatory events after peripheral nerve injury.* Journal of Neuroinflammation, 2011. **8**: p. 110-110.

24. Luk, H.W., L.J. Noble, and Z. Werb, *Macrophages contribute to the maintenance of stable regenerating neurites following peripheral nerve injury.* J Neurosci Res, 2003. **73**(5): p. 644-58.

25. Beller, J.A. and D.M. Snow, *Proteoglycans: road signs for neurite outgrowth.* Neural Regen Res, 2014. **9**(4): p. 343-55.

26. Man, A.J., J.K. Leach, and P. Bannerman, *Redirection of neurite outgrowth by coupling chondroitin sulfate proteoglycans to polymer membranes.* Ann Biomed Eng, 2014. **42**(6): p. 1271-81.

27. Faissner, A., A. Clement, A. Lochter, A. Streit, C. Mandl, and M. Schachner, *Isolation of a neural chondroitin sulfate proteoglycan with neurite outgrowth promoting properties.* J Cell Biol, 1994. **126**(3): p. 783-99.

28. Treloar, H.B., V. Nurcombe, and B. Key, *Expression of extracellular matrix molecules in the embryonic rat olfactory pathway.* J Neurobiol, 1996. **31**(1): p. 41-55.

29. Seil, J.T. and T.J. Webster, *Electrically active nanomaterials as improved neural tissue regeneration scaffolds.* Wiley Interdiscip Rev Nanomed Nanobiotechnol, 2010. **2**(6): p. 635-47.

30. Maravilla, K.R. and B.C. Bowen, *Imaging of the peripheral nervous system: evaluation of peripheral neuropathy and plexopathy.* AJNR Am J Neuroradiol, 1998. **19**(6): p. 1011-23.

31. Brushart, T.M., *Nerve repair*. 2011, New York: Oxford University Press. ix, 463 p.

32. Sulaiman, W. and T. Gordon, *Neurobiology of peripheral nerve injury, regeneration, and functional recovery: from bench top research to bedside application.* Ochsner J, 2013. **13**(1): p. 100-8.

33. Singh, R., K. Mechelse, W.C. Hop, and R. Braakman, *Long-term results of transplantations to repair median, ulnar, and radial nerve lesions by a microsurgical interfascicular autogenous cable graft technique.* Surg Neurol, 1992. **37**(6): p. 425-31.

34. Ichihara, S., Y. Inada, and T. Nakamura, *Artificial nerve tubes and their application for repair of peripheral nerve injury: an update of current concepts.* Injury, 2008.

35. Willerth, S.M., P.J. Johnson, D.J. Maxwell, S.R. Parsons, M.E. Doukas, and S.E. Sakiyama-Elbert, *Rationally designed peptides for controlled release of nerve growth factor from fibrin matrices.* J Biomed Mater Res A, 2007. **80**(1): p. 13-23.

36. Willerth, S.M. and S.E. Sakiyama-Elbert, *Approaches to neural tissue engineering using scaffolds for drug delivery.* Adv Drug Deliv Rev, 2007.

37. Vasita, R. and D.S. Katti, *Nanofibers and their applications in tissue engineering.* International Journal of Nanomedicine, 2006. **1**(1): p. 15-30.

38. Daly, W., L. Yao, D. Zeugolis, A. Windebank, and A. Pandit, *A biomaterials approach to peripheral nerve regeneration: bridging the peripheral nerve gap and enhancing functional recovery.* J R Soc Interface, 2012. **9**(67): p. 202-21.

39. de Ruiter, G.C., M.J. Malessy, M.J. Yaszemski, A.J. Windebank, and R.J. Spinner, *Designing ideal conduits for peripheral nerve repair.* Neurosurg Focus, 2009.

40. Arslantunali, D., T. Dursun, D. Yucel, N. Hasirci, and V. Hasirci, *Peripheral nerve conduits: technology update.* Med Devices (Auckl), 2014. **7**: p. 405-24.

41. Jones, S., H.M. Eisenberg, and X. Jia, *Advances and Future Applications of Augmented Peripheral Nerve Regeneration.* Int J Mol Sci, 2016. **17**(9).

42. Nectow, A.R., K.G. Marra, and D.L. Kaplan, *Biomaterials for the development of peripheral nerve guidance conduits.* Tissue Eng Part B Rev, 2012. **18**(1): p. 40-50.

43. Pfister, B.J., T. Gordon, J.R. Loverde, A.S. Kochar, S.E. Mackinnon, and D.K. Cullen, *Biomedical engineering strategies for peripheral nerve repair: surgical applications, state of the art, and future challenges.* Crit Rev Biomed Eng, 2011. **39**(2): p. 81-124.

44. Corey, J.M., D.Y. Lin, K.B. Mycek, Q. Chen, S. Samuel, E.L. Feldman, and D.C. Martin, *Aligned electrospun nanofibers specify the direction of dorsal root ganglia neurite growth.* J Biomed Mater Res A, 2007. **83**(3): p. 636-45.

45. Kim, Y.T., V.K. Haftel, S. Kumar, and R.V. Bellamkonda, *The role of aligned polymer fiber-based constructs in the bridging of long peripheral nerve gaps.* Biomaterials, 2008. **29**(21): p. 3117-27.

46. Cunha, C., S. Panseri, and S. Antonini, *Emerging nanotechnology approaches in tissue engineering for peripheral nerve regeneration.* Nanomedicine, 2011. **7**(1): p. 50-9.

47. Jayakumar, R., S.V. Nair, and V. Beachley, *Biomedical applications of polymeric nanofibers*. Advances in polymer science,. 2012, Heidelberg ; New York: Springer. xii, 287 p.

48. Collins, M.N. and C. Birkinshaw, *Hyaluronic acid based scaffolds for tissue engineering--a review.* Carbohydr Polym, 2013. **92**(2): p. 1262-79.

49. Chiono, V., C. Tonda-Turo, and G. Ciardelli, *Chapter 9 Artificial Scaffolds for Peripheral Nerve Reconstruction*, in *International Review of Neurobiology*, G. Stefano, T. Pierluigi, and B. Bruno, Editors. 2009, Academic Press. p. 173-198.

50. Adams, D.N., E.Y. Kao, C.L. Hypolite, M.D. Distefano, W.S. Hu, and P.C. Letourneau, *Growth cones turn and migrate up an immobilized gradient of the laminin IKVAV peptide.* J Neurobiol, 2005. **62**(1): p. 134-47.

51. Lo, C.M., H.B. Wang, M. Dembo, and Y.L. Wang, *Cell movement is guided by the rigidity of the substrate.* Biophys J, 2000. **79**(1): p. 144-52.

52. Knapp, D.M., E.F. Helou, and R.T. Tranquillo, *A fibrin or collagen gel assay for tissue cell chemotaxis: assessment of fibroblast chemotaxis to GRGDSP.* Exp Cell Res, 1999. **247**(2): p. 543-53.

53. Tessier-Lavigne, M., M. Placzek, A.G. Lumsden, J. Dodd, and T.M. Jessell, *Chemotropic guidance of developing axons in the mammalian central nervous system.* Nature, 1988. **336**(6201): p. 775-8.

54. Li Jeon, N., H. Baskaran, S.K. Dertinger, G.M. Whitesides, L. Van de Water, and M. Toner, *Neutrophil chemotaxis in linear and complex gradients of interleukin-8 formed in a microfabricated device.* Nat Biotechnol, 2002. **20**(8): p. 826-30.

55. Babensee, J.E., L.V. McIntire, and A.G. Mikos, *Growth factor delivery for tissue engineering.* Pharm Res, 2000. **17**(5): p. 497-504.

56. Wang, C.Y., J.J. Liu, C.Y. Fan, X.M. Mo, H.J. Ruan, and F.F. Li, *The effect of aligned core-shell nanofibres delivering NGF on the promotion of sciatic nerve regeneration.* J Biomater Sci Polym Ed, 2012. **23**(1-4): p. 167-84.

57. Ji, W., Y. Sun, F. Yang, J.J. van den Beucken, M. Fan, Z. Chen, and J.A. Jansen, *Bioactive electrospun scaffolds delivering growth factors and genes for tissue engineering applications.* Pharm Res, 2011. **28**(6): p. 1259-72.

58. McCaig, C.D., A.M. Rajnicek, B. Song, and M. Zhao, *Has electrical growth cone guidance found its potential?* Trends Neurosci, 2002. **25**(7): p. 354-9.

59. Dodla, M.C. and R.V. Bellamkonda, *Anisotropic scaffolds facilitate enhanced neurite extension in vitro.* J Biomed Mater Res A, 2006. **78**(2): p. 213-21.

60. Ramón y Cajal, S., J. DeFelipe, and E.G. Jones, *Cajal's degeneration and regeneration of the nervous system*. History of neuroscience. 1991, New York: Oxford University Press. xvi, 769 p.

61. Park, S.Y., T.H. Kim, H.I. Kim, Y.K. Shin, C.S. Lee, M. Park, and J.H. Song, *Celecoxib inhibits Na+ currents in rat dorsal root ganglion neurons.* Brain Res, 2007. **1148**: p. 53-61.

62. Wrobel, M.R. and H.G. Sundararaghavan, *Directed migration in neural tissue engineering.* Tissue Eng Part B Rev, 2014. **20**(2): p. 93-105.

63. Kothapalli, C.R., E. van Veen, S. de Valence, S. Chung, I.K. Zervantonakis, F.B. Gertler, and R.D. Kamm, *A high-throughput microfluidic assay to study neurite response to growth factor gradients.* Lab Chip, 2011. **11**(3): p. 497-507.

64. Moore, A.M., M. MacEwan, K.B. Santosa, K.E. Chenard, W.Z. Ray, D.A. Hunter, S.E. Mackinnon, and P.J. Johnson, *Acellular nerve allografts in peripheral nerve regeneration: a comparative study.* Muscle Nerve, 2011. **44**(2): p. 221-34.

65. Szynkaruk, M., S.W. Kemp, M.D. Wood, T. Gordon, and G.H. Borschel, *Experimental and clinical evidence for use of decellularized nerve allografts in peripheral nerve gap reconstruction.* Tissue Eng Part B Rev, 2013. **19**(1): p. 83-96.

66. Neubauer, D., J.B. Graham, and D. Muir, *Chondroitinase treatment increases the effective length of acellular nerve grafts.* Exp Neurol, 2007. **207**(1): p. 163-70.

67. Whitlock, E.L., S.H. Tuffaha, J.P. Luciano, Y. Yan, D.A. Hunter, C.K. Magill, A.M. Moore, A.Y. Tong, S.E. Mackinnon, and G.H. Borschel, *Processed allografts and type I collagen conduits for repair of peripheral nerve gaps.* Muscle Nerve, 2009. **39**(6): p. 787-99.

68. Muir, D., *The potentiation of peripheral nerve sheaths in regeneration and repair.* Exp Neurol, 2010. **223**(1): p. 102-11.

69. Jesuraj, N.J., K.B. Santosa, P. Newton, Z. Liu, D.A. Hunter, S.E. Mackinnon, S.E. Sakiyama-Elbert, and P.J. Johnson, *A systematic evaluation of Schwann cell injection into acellular cold-preserved nerve grafts.* J Neurosci Methods, 2011. **197**(2): p. 209-15.

70. Wang, Y., Z. Zhao, Z. Ren, B. Zhao, L. Zhang, J. Chen, W. Xu, S. Lu, Q. Zhao, and J. Peng, *Recellularized nerve allografts with differentiated mesenchymal stem cells promote peripheral nerve regeneration.* Neurosci Lett, 2012. **514**(1): p. 96-101.

71. Kofron, C.M., Y. Liu, C. Lopez-Fagundo, J.A. Mitchel, and D. Hoffman-Kim, *Neurite Outgrowth at the Biomimetic Interface.* Annals of Biomedical Engineering, 2010. **38**(6): p. 2210–2225.

72. Lopez-Fagundo, C., J.A. Mitchel, T.D. Ramchal, Y.T. Dingle, and D. Hoffman-Kim, *Navigating neurites utilize cellular topography of Schwann cell somas and processes for optimal guidance.* Acta Biomater, 2013. **9**(7): p. 7158-68.

73. Georgiou, M., S.C. Bunting, H.A. Davies, A.J. Loughlin, J.P. Golding, and J.B. Phillips, *Engineered neural tissue for peripheral nerve repair.* Biomaterials, 2013. **34**(30): p. 7335-43.

74. Suri, S. and C.E. Schmidt, *Cell-laden hydrogel constructs of hyaluronic acid, collagen, and laminin for neural tissue engineering.* Tissue Eng Part A, 2010. **16**(5): p. 1703-16.

75. Kigerl, K.A., J.C. Gensel, D.P. Ankeny, J.K. Alexander, D.J. Donnelly, and P.G. Popovich, *Identification of two distinct macrophage subsets with divergent effects causing either neurotoxicity or regeneration in the injured mouse spinal cord.* J Neurosci, 2009. **29**(43): p. 13435-44.

76. Mokarram, N. and R.V. Bellamkonda, *A perspective on immunomodulation and tissue repair.* Ann Biomed Eng, 2014. **42**(2): p. 338-51.

77. Franz, S., F. Allenstein, J. Kajahn, I. Forstreuter, V. Hintze, S. Moller, and J.C. Simon, *Artificial extracellular matrices composed of collagen I and high-sulfated hyaluronan promote phenotypic and functional modulation of human pro-inflammatory M1 macrophages.* Acta Biomater, 2013. **9**(3): p. 5621-9.

78. McWhorter, F.Y., T.T. Wang, P. Nguyen, T. Chung, and W.F. Liu, *Modulation of macrophage phenotype by cell shape.* Proceedings of the National Academy of Sciences of the United States of America, 2013. **110**(43): p. 17253-17258.

79. Bartneck, M., K.H. Heffels, Y. Pan, M. Bovi, G. Zwadlo-Klarwasser, and J. Groll, *Inducing healing-like human primary macrophage phenotypes by 3D hydrogel coated nanofibres.* Biomaterials, 2012. **33**(16): p. 4136-46.

80. Potas, J.R., F. Haque, F.L. Maclean, and D.R. Nisbet, *Interleukin-10 conjugated electrospun polycaprolactone (PCL) nanofibre scaffolds for promoting alternatively activated (M2) macrophages around the peripheral nerve in vivo.* J Immunol Methods, 2015. **420**: p. 38-49.

81. Chew, S.Y., R. Mi, A. Hoke, and K.W. Leong, *The effect of the alignment of electrospun fibrous scaffolds on Schwann cell maturation.* Biomaterials, 2008. **29**(6): p. 653-61.

82. Radhakrishnan, J., A.A. Kuppuswamy, S. Sethuraman, and A. Subramanian, *Topographic Cue from Electrospun Scaffolds Regulate Myelin-Related Gene Expressions in Schwann Cells.* J Biomed Nanotechnol, 2015. **11**(3): p. 512-21.

83. Gu, Y., Y. Ji, Y. Zhao, Y. Liu, F. Ding, X. Gu, and Y. Yang, *The influence of substrate stiffness on the behavior and functions of Schwann cells in culture.* Biomaterials, 2012. **33**(28): p. 6672-81.

84. Birchmeier, C. and K.A. Nave, *Neuregulin-1, a key axonal signal that drives Schwann cell growth and differentiation.* Glia, 2008. **56**(14): p. 1491-7.

85. Chernousov, M.A., W.M. Yu, Z.L. Chen, D.J. Carey, and S. Strickland, *Regulation of Schwann cell function by the extracellular matrix.* Glia, 2008. **56**(14): p. 1498-507.

86. di Summa, P.G., D.F. Kalbermatten, W. Raffoul, G. Terenghi, and P.J. Kingham, *Extracellular matrix molecules enhance the neurotrophic effect of Schwann cell-like differentiated adipose-derived stem cells and increase cell survival under stress conditions.* Tissue Eng Part A, 2013. **19**(3-4): p. 368-79.

87. Martens, W., K. Sanen, M. Georgiou, T. Struys, A. Bronckaers, M. Ameloot, J. Phillips, and I. Lambrichts, *Human dental pulp stem cells can differentiate into Schwann cells and promote and guide neurite outgrowth in an aligned tissue-engineered collagen construct in vitro.* FASEB J, 2014. **28**(4): p. 1634-43.

88. Webber, C. and D. Zochodne, *The nerve regenerative microenvironment: Early behavior and partnership of axons and Schwann cells.* Experimental Neurology, 2010. **223**(1): p. 51-59.

89. Silver, J. and J.H. Miller, *Regeneration beyond the glial scar.* Nature Reviews Neuroscience, 2004. **5**(2): p. 146-156.

90. Zuo, J., Y.J. Hernandez, and D. Muir, *Chondroitin sulfate proteoglycan with neurite-inhibiting activity is up-regulated following peripheral nerve injury.* J Neurobiol, 1998. **34**(1): p. 41-54.

91. Liu, T., J. Xu, B.P. Chan, and S.Y. Chew, *Sustained release of neurotrophin-3 and chondroitinase ABC from electrospun collagen nanofiber scaffold for spinal cord injury repair.* J Biomed Mater Res A, 2012. **100**(1): p. 236-42.

92. Fass, J.N. and D.J. Odde, *Tensile force-dependent neurite elicitation via anti-beta1 integrin antibody-coated magnetic beads.* Biophys J, 2003. **85**(1): p. 623-36.

93. Loverde, J.R., V.C. Ozoka, R. Aquino, L. Lin, and B.J. Pfister, *Live imaging of axon stretch growth in embryonic and adult neurons.* J Neurotrauma, 2011. **28**(11): p. 2389-403.

94. Francisco, H., B.B. Yellen, D.S. Halverson, G. Friedman, and G. Gallo, *Regulation of axon guidance and extension by three-dimensional constraints.* Biomaterials, 2007. **28**(23): p. 3398-407.

95. Franze, K., J. Gerdelmann, M. Weick, T. Betz, S. Pawlizak, M. Lakadamyali, J. Bayer, K. Rillich, M. Gogler, Y.B. Lu, A. Reichenbach, P. Janmey, and J. Kas, *Neurite branch*

retraction is caused by a threshold-dependent mechanical impact. Biophys J, 2009. **97**(7): p. 1883-90.

96. Sur, S., C.J. Newcomb, M.J. Webber, and S.I. Stupp, *Tuning supramolecular mechanics to guide neuron development.* Biomaterials, 2013. **34**(20): p. 4749-57.

97. Stroissnigg, H., A. Trancikova, L. Descovich, J. Fuhrmann, W. Kutschera, J. Kostan, A. Meixner, F. Nothias, and F. Propst, *S-nitrosylation of microtubule-associated protein 1B mediates nitric-oxide-induced axon retraction.* Nat Cell Biol, 2007. **9**(9): p. 1035-45.

98. Horn, K.P., S.A. Busch, A.L. Hawthorne, N. van Rooijen, and J. Silver, *Another barrier to regeneration in the CNS: activated macrophages induce extensive retraction of dystrophic axons through direct physical interactions.* J Neurosci, 2008. **28**(38): p. 9330-41.

99. Hodgkinson, G.N., P.A. Tresco, and V. Hlady, *The role of well-defined patterned substrata on the regeneration of DRG neuron pathfinding and integrin expression dynamics using chondroitin sulfate proteoglycans.* Biomaterials, 2012. **33**(17): p. 4288-97.

100. Agius, E., Y. Sagot, A.M. Duprat, and P. Cochard, *Antibodies directed against the beta 1-integrin subunit and peptides containing the IKVAV sequence of laminin perturb neurite outgrowth of peripheral neurons on immature spinal cord substrata.* Neuroscience, 1996. **71**(3): p. 773-86.

101. Carey, D.J., *Syndecans: multifunctional cell-surface co-receptors.* Biochem J, 1997. **327 (Pt 1)**: p. 1-16.

102. Rapraeger, A.C., *Syndecan-regulated receptor signaling.* J Cell Biol, 2000. **149**(5): p. 995-8.

103. Chung, H., H.A. Multhaupt, E.S. Oh, and J.R. Couchman, *Minireview: Syndecans and their crucial roles during tissue regeneration.* FEBS Lett, 2016. **590**(15): p. 2408-17.

104. Swarup, V.P., C.P. Mencio, V. Hlady, and B. Kuberan, *Sugar glues for broken neurons.* Biomol Concepts, 2013. **4**(3): p. 233-57.

105. Buettner, H.M. and R.N. Pittman, *Quantitative effects of laminin concentration on neurite outgrowth in vitro.* Dev Biol, 1991. **145**(2): p. 266-76.

106. Gundersen, R.W., *Response of sensory neurites and growth cones to patterned substrata of laminin and fibronectin in vitro.* Dev Biol, 1987. **121**(2): p. 423-31.

107. Gonzalez-Perez, F., E. Udina, and X. Navarro, *Extracellular matrix components in peripheral nerve regeneration.* Int Rev Neurobiol, 2013. **108**: p. 257-75.

108. Coulson-Thomas, V.J. and T.F. Gesteira, *Dimethylmethylene Blue Assay (DMMB).* Bio Protoc, 2014. **4**(18): p. e1236.

109. Kliment, C.R., J.M. Englert, L.P. Crum, and T.D. Oury, *A novel method for accurate collagen and biochemical assessment of pulmonary tissue utilizing one animal.* Int J Clin Exp Patho, 2011. **4**(4): p. 349-355.

110. Song, M. and K.E. Uhrich, *Optimal micropattern dimensions enhance neurite outgrowth rates, lengths, and orientations.* Ann Biomed Eng, 2007. **35**(10): p. 1812-20.

111. Walwyn, W., C.J. Evans, and T.G. Hales, *Beta-arrestin2 and c-Src regulate the constitutive activity and recycling of mu opioid receptors in dorsal root ganglion neurons.* J Neurosci, 2007. **27**(19): p. 5092-104.

112. Walwyn, W., N.T. Maidment, M. Sanders, C.J. Evans, B.L. Kieffer, and T.G. Hales, *Induction of delta opioid receptor function by up-regulation of membrane receptors in mouse primary afferent neurons.* Mol Pharmacol, 2005. **68**(6): p. 1688-98.

113. Medberry, C.J., P.M. Crapo, B.F. Siu, C.A. Carruthers, M.T. Wolf, S.P. Nagarkar, V. Agrawal, K.E. Jones, J. Kelly, S.A. Johnson, S.S. Velankar, S.C. Watkins, M. Modo, and S.F. Badylak, *Hydrogels derived from central nervous system extracellular matrix.* Biomaterials, 2013. **34**(4): p. 1033-1040.

114. Dou, C.L. and J.M. Levine, *Differential effects of glycosaminoglycans on neurite growth on laminin and L1 substrates.* J Neurosci, 1995. **15**(12): p. 8053-66.

115. Snow, D.M., E.M. Brown, and P.C. Letourneau, *Growth cone behavior in the presence of soluble chondroitin sulfate proteoglycan (CSPG), compared to behavior on CSPG bound to laminin or fibronectin.* International Journal of Developmental Neuroscience, 1996. **14**(3): p. 331-349.

116. Castro, C. and D.P. Kuffler, *Membrane-bound CSPG mediates growth cone outgrowth and substrate specificity by Schwann cell contact with the DRG neuron cell body and not via growth cone contact.* Exp Neurol, 2006. **200**(1): p. 19-25.

117. Bockelmann, J., K. Klinkhammer, A. von Holst, N. Seiler, A. Faissner, G.A. Brook, D. Klee, and J. Mey, *Functionalization of electrospun poly(epsilon-caprolactone) fibers with the extracellular matrix-derived peptide GRGDS improves guidance of schwann cell migration and axonal growth.* Tissue Eng Part A, 2011. **17**(3-4): p. 475-86.

118. Neukomm, L.J. and M.R. Freeman, *Diverse cellular and molecular modes of axon degeneration.* Trends in Cell Biology, 2014. **24**(9): p. 515-523.

119. Ozturk, G., N. Cengiz, E. Erdogan, A. Him, E.K. Oguz, E. Yenidunya, and N. Aysit, *Two distinct types of dying back axonal degeneration in vitro.* Neuropathology and Applied Neurobiology, 2013. **39**(4): p. 362-376.

120. Portera-Cailliau, C., R.M. Weimer, V. De Paola, P. Caroni, and K. Svoboda, *Diverse modes of axon elaboration in the developing neocortex.* PLoS Biol, 2005. **3**(8): p. e272.

121. Bao, F., C.S. Bailey, K.R. Gurr, S.I. Bailey, M.P. Rosas-Arellano, A. Brown, G.A. Dekaban, and L.C. Weaver, *Human spinal cord injury causes specific increases in surface expression of beta integrins on leukocytes.* J Neurotrauma, 2011. **28**(2): p. 269-80.

122. Lopes, C.C., C.P. Dietrich, and H.B. Nader, *Specific structural features of syndecans and heparan sulfate chains are needed for cell signaling.* Braz J Med Biol Res, 2006. **39**(2): p. 157-67.

123. Fuentes, E.O., J. Leemhuis, G.B. Stark, and E.M. Lang, *Rho kinase inhibitors Y27632 and H1152 augment neurite extension in the presence of cultured Schwann cells.* J Brachial Plex Peripher Nerve Inj, 2008. **3**: p. 19.

124. Monnier, P.P., A. Sierra, J.M. Schwab, S. Henke-Fahle, and B.K. Mueller, *The Rho/ROCK pathway mediates neurite growth-inhibitory activity associated with the chondroitin sulfate proteoglycans of the CNS glial scar.* Molecular and Cellular Neuroscience, 2003. **22**(3): p. 319-330.

125. Chan, C.C., K. Khodarahmi, J. Liu, D. Sutherland, L.W. Oschipok, J.D. Steeves, and W. Tetzlaff, *Dose-dependent beneficial and detrimental effects of ROCK inhibitor Y27632 on axonal sprouting and functional recovery after rat spinal cord injury.* Exp Neurol, 2005. **196**(2): p. 352-64.

126. Chan, C.C.M., C.R. Roberts, J.D. Steeves, and W. Tetzlaff, *Aggrecan components differentially modulate nerve growth factor-responsive and neurotrophin-3-responsive dorsal root ganglion neurite growth.* Journal of Neuroscience Research, 2008. **86**(3): p. 581-592.

127. Inatani, M., M. Honjo, Y. Otori, A. Oohira, N. Kido, Y. Tano, Y. Honda, and H. Tanihara, *Inhibitory effects of neurocan and phosphacan on neurite outgrowth from retinal ganglion cells in culture.* Investigative Ophthalmology & Visual Science, 2001. **42**(8): p. 1930-1938.

128. Schmalfeldt, M., C.E. Bandtlow, M.T. Dours-Zimmermann, K.H. Winterhalter, and D.R. Zimmermann, *Brain derived versican V2 is a potent inhibitor of axonal growth.* Journal of Cell Science, 2000. **113**(5): p. 807-816.

129. Gopalakrishnan, S.M., N. Teusch, C. Imhof, M.H. Bakker, M. Schurdak, D.J. Burns, and U. Warrior, *Role of Rho kinase pathway in chondroitin sulfate proteoglycan-mediated inhibition of neurite outgrowth in PC12 cells.* J Neurosci Res, 2008. **86**(10): p. 2214-26.

130. Hynds, D.L. and D.M. Snow, *Neurite outgrowth inhibition by chondroitin sulfate proteoglycan: stalling/stopping exceeds turning in human neuroblastoma growth cones.* Exp Neurol, 1999. **160**(1): p. 244-55.

131. Muzzarelli, R.A., F. Greco, A. Busilacchi, V. Sollazzo, and A. Gigante, *Chitosan, hyaluronan and chondroitin sulfate in tissue engineering for cartilage regeneration: a review.* Carbohydr Polym, 2012. **89**(3): p. 723-39.

132. Derakhshan, Z.H., B. Shaghaghi, M.P. Asl, M. Majidi, L. Ghazizadeh, A. Chegini, and S. Bonakdar, *In Situ Forming Hydrogel Based on Chondroitin Sulfate-Hydroxyapatite for Bone Tissue Engineering.* International Journal of Polymeric Materials and Polymeric Biomaterials, 2015. **64**(17): p. 919-26.

133. Wang, T.W., H.C. Wu, Y.C. Huang, J.S. Sun, and F.H. Lin, *Biomimetic bilayered gelatin-chondroitin 6 sulfate-hyaluronic acid biopolymer as a scaffold for skin equivalent tissue engineering.* Artif Organs, 2006. **30**(3): p. 141-9.

134. Allodi, I., E. Udina, and X. Navarro, *Specificity of peripheral nerve regeneration: interactions at the axon level.* Prog Neurobiol, 2012. **98**(1): p. 16-37.

135. Lanza, R.P., R.S. Langer, and J. Vacanti, *Principles of tissue engineering*. Fourth edition / ed. 2014, Amsterdam: Academic Press, an imprint of Elsevier. xlviii, 1887 pages.

136. Whitehead, T.J. and H.G. Sundararaghavan, *Electrospinning growth factor releasing microspheres into fibrous scaffolds.* J Vis Exp, 2014(90).

137. Bryant, S.J., K.A. Davis-Arehart, N. Luo, R.K. Shoemaker, J.A. Arthur, and K.S. Anseth, *Synthesis and Characterization of Photopolymerized Multifunctional Hydrogels: Water-Soluble Poly(Vinyl Alcohol) and Chondroitin Sulfate Macromers for Chondrocyte Encapsulation.* Macromolecules, 2004. **37**: p. 6726-33.

138. Burdick, J.A., C. Chung, X. Jia, M.A. Randolph, and R. Langer, *Controlled degradation and mechanical behavior of photopolymerized hyaluronic acid networks.* Biomacromolecules, 2005. **6**(1): p. 386-91.

139. Ifkovits, J.L., H.G. Sundararaghavan, and J.A. Burdick, *Electrospinning fibrous polymer scaffolds for tissue engineering and cell culture.* J Vis Exp, 2009(32).

140. Sundararaghavan, H.G. and J.A. Burdick, *Gradients with depth in electrospun fibrous scaffolds for directed cell behavior.* Biomacromolecules, 2011. **12**(6): p. 2344-50.

141. Li, W.J., R.L. Mauck, J.A. Cooper, X. Yuan, and R.S. Tuan, *Engineering controllable anisotropy in electrospun biodegradable nanofibrous scaffolds for musculoskeletal tissue engineering.* J Biomech, 2007. **40**(8): p. 1686-93.

142. Snow, D.M., V. Lemmon, D.A. Carrino, A.I. Caplan, and J. Silver, *Sulfated proteoglycans in astroglial barriers inhibit neurite outgrowth in vitro.* Exp Neurol, 1990. **109**(1): p. 111-30.

143. Guo, Y., T. Yuan, Z. Xiao, P. Tang, Y. Xiao, Y. Fan, and X. Zhang, *Hydrogels of collagen/chondroitin sulfate/hyaluronan interpenetrating polymer network for cartilage tissue engineering.* J Mater Sci Mater Med, 2012. **23**(9): p. 2267-79.

144. Levett, P.A., F.P. Melchels, K. Schrobback, D.W. Hutmacher, J. Malda, and T.J. Klein, *A biomimetic extracellular matrix for cartilage tissue engineering centered on photocurable gelatin, hyaluronic acid and chondroitin sulfate.* Acta Biomater, 2014. **10**(1): p. 214-23.

145. Jiang, T., X.J. Ren, J.L. Tang, H. Yin, K.J. Wang, and C.L. Zhou, *Preparation and characterization of genipin-crosslinked rat acellular spinal cord scaffolds.* Mater Sci Eng C Mater Biol Appl, 2013. **33**(6): p. 3514-21.

146. Coburn, J., M. Gibson, P.A. Bandalini, C. Laird, H.Q. Mao, L. Moroni, D. Seliktar, and J. Elisseeff, *Biomimetics of the Extracellular Matrix: An Integrated Three-Dimensional Fiber-Hydrogel Composite for Cartilage Tissue Engineering.* Smart Struct Syst, 2011. **7**(3): p. 213-222.

147. Baiguera, S., C. Del Gaudio, E. Lucatelli, E. Kuevda, M. Boieri, B. Mazzanti, A. Bianco, and P. Macchiarini, *Electrospun gelatin scaffolds incorporating rat decellularized brain extracellular matrix for neural tissue engineering.* Biomaterials, 2014. **35**(4): p. 1205-14.

148. Wen, X., Y. Wang, Z. Guo, H. Meng, J. Huang, L. Zhang, B. Zhao, Q. Zhao, Y. Zheng, and J. Peng, *Cauda equina-derived extracellular matrix for fabrication of nanostructured hybrid scaffolds applied to neural tissue engineering.* Tissue Eng Part A, 2015. **21**(5-6): p. 1095-105.

149. Wrobel, M.R. and H.G. Sundararaghavan, *Positive and negative cues for modulating neurite dynamics and receptor expression.* Biomed Mater, 2017. **12**(2): p. 025016.

150. Balgude, A.P., X. Yu, A. Szymanski, and R.V. Bellamkonda, *Agarose gel stiffness determines rate of DRG neurite extension in 3D cultures.* Biomaterials, 2001. **22**(10): p. 1077-84.

151. Clements, I.P., Y.T. Kim, A.W. English, X. Lu, A. Chung, and R.V. Bellamkonda, *Thin-film enhanced nerve guidance channels for peripheral nerve repair.* Biomaterials, 2009. **30**(23-24): p. 3834-46.

152. Mukhatyar, V.J., M. Salmeron-Sanchez, S. Rudra, S. Mukhopadaya, T.H. Barker, A.J. Garcia, and R.V. Bellamkonda, *Role of fibronectin in topographical guidance of neurite extension on electrospun fibers.* Biomaterials, 2011. **32**(16): p. 3958-68.

153. Dodla, M.C. and R.V. Bellamkonda, *Differences between the effect of anisotropic and isotropic laminin and nerve growth factor presenting scaffolds on nerve regeneration across long peripheral nerve gaps.* Biomaterials, 2008. **29**(1): p. 33-46.

154. Mokarram, N., A. Merchant, V. Mukhatyar, G. Patel, and R.V. Bellamkonda, *Effect of modulating macrophage phenotype on peripheral nerve repair.* Biomaterials, 2012. **33**(34): p. 8793-801.

155. Tan, K.S., L. Qian, R. Rosado, P.M. Flood, and L.F. Cooper, *The role of titanium surface topography on J774A.1 macrophage inflammatory cytokines and nitric oxide production.* Biomaterials, 2006. **27**(30): p. 5170-7.

156. Hotchkiss, K.M., G.B. Reddy, S.L. Hyzy, Z. Schwartz, B.D. Boyan, and R. Olivares-Navarrete, *Titanium surface characteristics, including topography and wettability, alter macrophage activation.* Acta Biomater, 2016. **31**: p. 425-34.

157. Luu, T.U., S.C. Gott, B.W. Woo, M.P. Rao, and W.F. Liu, *Micro- and Nanopatterned Topographical Cues for Regulating Macrophage Cell Shape and Phenotype.* ACS Appl Mater Interfaces, 2015. **7**(51): p. 28665-72.

158. Barth, K.A., J.D. Waterfield, and D.M. Brunette, *The effect of surface roughness on RAW 264.7 macrophage phenotype.* Journal of Biomedical Materials Research Part A, 2013. **101**(9): p. 2679-2688.

159. Lamers, E., X.F. Walboomers, M. Domanski, L. Prodanov, J. Melis, R. Luttge, L. Winnubst, J.M. Anderson, H.J. Gardeniers, and J.A. Jansen, *In vitro and in vivo evaluation of the inflammatory response to nanoscale grooved substrates.* Nanomedicine, 2012. **8**(3): p. 308-17.

160. Malheiro, V., F. Lehner, V. Dinca, P. Hoffmann, and K. Maniura-Weber, *Convex and concave micro-structured silicone controls the shape, but not the polarization state of human macrophages.* Biomater Sci, 2016. **4**(11): p. 1562-1573.

161. Schaub, N.J., T. Britton, R. Rajachar, and R.J. Gilbert, *Engineered nanotopography on electrospun PLLA microfibers modifies RAW 264.7 cell response.* ACS Appl Mater Interfaces, 2013. **5**(20): p. 10173-84.

162. Saino, E., M.L. Focarete, C. Gualandi, E. Emanuele, A.I. Cornaglia, M. Imbriani, and L. Visai, *Effect of electrospun fiber diameter and alignment on macrophage activation and secretion of proinflammatory cytokines and chemokines.* Biomacromolecules, 2011. **12**(5): p. 1900-11.

163. Fex Svennigsen, A. and L.B. Dahlin, *Repair of the Peripheral Nerve-Remyelination that Works.* Brain Sci, 2013. **3**(3): p. 1182-97.

164. Livak, K.J. and T.D. Schmittgen, *Analysis of relative gene expression data using real-time quantitative PCR and the 2(-Delta Delta C(T)) Method.* Methods, 2001. **25**(4): p. 402-8.

165. Willems, E., L. Leyns, and J. Vandesompele, *Standardization of real-time PCR gene expression data from independent biological replicates.* Anal Biochem, 2008. **379**(1): p. 127-9.

166. Spandidos, A., X. Wang, H. Wang, S. Dragnev, T. Thurber, and B. Seed, *A comprehensive collection of experimentally validated primers for Polymerase Chain Reaction quantitation of murine transcript abundance.* BMC Genomics, 2008. **9**: p. 633.

167. Laskin, D.L., *Macrophages and inflammatory mediators in chemical toxicity: a battle of forces.* Chem Res Toxicol, 2009. **22**(8): p. 1376-85.

168. Blakney, A.K., M.D. Swartzlander, and S.J. Bryant, *The effects of substrate stiffness on the in vitro activation of macrophages and in vivo host response to poly(ethylene glycol)-based hydrogels.* J Biomed Mater Res A, 2012. **100**(6): p. 1375-86.

169. Patel, N.R., M. Bole, C. Chen, C.C. Hardin, A.T. Kho, J. Mih, L. Deng, J. Butler, D. Tschumperlin, J.J. Fredberg, R. Krishnan, and H. Koziel, *Cell elasticity determines macrophage function.* PLoS One, 2012. **7**(9): p. e41024.

170. Sieweke, M.H. and J.E. Allen, *Beyond stem cells: self-renewal of differentiated macrophages.* Science, 2013. **342**(6161): p. 1242974.

171. Martinez, F.O. and S. Gordon, *The M1 and M2 paradigm of macrophage activation: time for reassessment.* F1000Prime Rep, 2014. **6**: p. 13.

172. Mills, C.D. and K. Ley, *M1 and M2 macrophages: the chicken and the egg of immunity.* J Innate Immun, 2014. **6**(6): p. 716-26.

173. Banchereau, J., V. Pascual, and A. O'Garra, *From IL-2 to IL-37: the expanding spectrum of anti-inflammatory cytokines.* Nat Immunol, 2012. **13**(10): p. 925-31.

174. Wu, W.K., O.P. Llewellyn, D.O. Bates, L.B. Nicholson, and A.D. Dick, *IL-10 regulation of macrophage VEGF production is dependent on macrophage polarisation and hypoxia.* Immunobiology, 2010. **215**(9-10): p. 796-803.

175. Jaguin, M., N. Houlbert, O. Fardel, and V. Lecureur, *Polarization profiles of human M-CSF-generated macrophages and comparison of M1-markers in classically activated macrophages from GM-CSF and M-CSF origin.* Cell Immunol, 2013. **281**(1): p. 51-61.

176. Yamane, K. and K.P. Leung, *Rabbit M1 and M2 macrophages can be induced by human recombinant GM-CSF and M-CSF.* FEBS Open Bio, 2016. **6**(9): p. 945-53.

177. Yang, Y., J. Qin, L. Lan, N. Li, C. Wang, P. He, F. Liu, H. Ni, and Y. Wang, *M-CSF cooperating with NFkappaB induces macrophage transformation from M1 to M2 by upregulating c-Jun.* Cancer Biol Ther, 2014. **15**(1): p. 99-107.

178. Lopez-Fagundo, C., E. Bar-Kochba, L.L. Livi, D. Hoffman-Kim, and C. Franck, *Three-dimensional traction forces of Schwann cells on compliant substrates.* J R Soc Interface, 2014. **11**(97): p. 20140247.

179. Brady, S.T., G.J. Siegel, R.W. Albers, D.L. Price, and J. Benjamins, *Basic neurochemistry : principles of molecular, cellular, and medical neurobiology*. 8th ed. 2012, Amsterdam ; Boston: Elsevier/Academic Press. xxiv, 1096 p.

180. Fernandez-Valle, C., D. Gorman, A.M. Gomez, and M.B. Bunge, *Actin plays a role in both changes in cell shape and gene-expression associated with Schwann cell myelination.* J Neurosci, 1997. **17**(1): p. 241-50.

181. Menorca, R.M., T.S. Fussell, and J.C. Elfar, *Nerve physiology: mechanisms of injury and recovery.* Hand Clin, 2013. **29**(3): p. 317-30.

182. Mobasseri, S.A., G. Terenghi, and S. Downes, *Schwann cell interactions with polymer films are affected by groove geometry and film hydrophilicity.* Biomed Mater, 2014. **9**(5): p. 055004.

183. Dewitt, D.D., S.N. Kaszuba, D.M. Thompson, and J.P. Stegemann, *Collagen I-matrigel scaffolds for enhanced Schwann cell survival and control of three-dimensional cell morphology.* Tissue Eng Part A, 2009. **15**(10): p. 2785-93.

184. Zhou, W., J.M. Stukel, H.L. Cebull, and R.K. Willits, *Tuning the Mechanical Properties of Poly(Ethylene Glycol) Microgel-Based Scaffolds to Increase 3D Schwann Cell Proliferation.* Macromol Biosci, 2016. **16**(4): p. 535-44.

185. Eggers, R., F. de Winter, S.A. Hoyng, K.C. Roet, E.M. Ehlert, M.J. Malessy, J. Verhaagen, and M.R. Tannemaat, *Lentiviral vector-mediated gradients of GDNF in the injured peripheral nerve: effects on nerve coil formation, Schwann cell maturation and myelination.* PLoS One, 2013. **8**(8): p. e71076.

186. Yang, J.F., G. Cao, S. Koirala, L.V. Reddy, and C.P. Ko, *Schwann cells express active agrin and enhance aggregation of acetylcholine receptors on muscle fibers.* J Neurosci, 2001. **21**(24): p. 9572-84.

187. Cui, Y., C. Lu, D. Meng, Z. Xiao, X. Hou, W. Ding, D. Kou, Y. Yao, B. Chen, Z. Zhang, J. Li, J. Pan, and J. Dai, *Collagen scaffolds modified with CNTF and bFGF promote facial nerve regeneration in minipigs.* Biomaterials, 2014. **35**(27): p. 7819-27.

188. Hu, Y., S.G. Leaver, G.W. Plant, W.T. Hendriks, S.P. Niclou, J. Verhaagen, A.R. Harvey, and Q. Cui, *Lentiviral-mediated transfer of CNTF to schwann cells within reconstructed peripheral nerve grafts enhances adult retinal ganglion cell survival and axonal regeneration.* Mol Ther, 2005. **11**(6): p. 906-15.

189. Kim, Y., A.G. Remacle, A.V. Chernov, H. Liu, I. Shubayev, C. Lai, J. Dolkas, S.A. Shiryaev, V.S. Golubkov, A.P. Mizisin, A.Y. Strongin, and V.I. Shubayev, *The MMP-*

9/TIMP-1 axis controls the status of differentiation and function of myelin-forming Schwann cells in nerve regeneration. PLoS One, 2012. **7**(3): p. e33664.

190. Moore, C.S., R. Milner, A. Nishiyama, R.F. Frausto, D.R. Serwanski, R.R. Pagarigan, J.L. Whitton, R.H. Miller, and S.J. Crocker, *Astrocytic tissue inhibitor of metalloproteinase-1 (TIMP-1) promotes oligodendrocyte differentiation and enhances CNS myelination.* J Neurosci, 2011. **31**(16): p. 6247-54.

191. Naureckiene, S., W. Edris, S.K. Ajit, A.H. Katz, K. Sreekumar, K.E. Rogers, J.D. Kennedy, and P.G. Jones, *Use of a murine cell line for identification of human nitric oxide synthase inhibitors.* J Pharmacol Toxicol Methods, 2007. **55**(3): p. 303-13.

192. Bailey, L.O., N.R. Washburn, C.G. Simon, Jr., E.S. Chan, and F.W. Wang, *Quantification of inflammatory cellular responses using real-time polymerase chain reaction.* J Biomed Mater Res A, 2004. **69**(2): p. 305-13.

193. Salitsky, A., *The raw 264.7 cell line : a valid candidate for studying macrophage activation*, in *Microbiology and Immunology*1983, Hahnemann University: Philadelphia, PA.

194. Keller, M., J. Mazuch, U. Abraham, G.D. Eom, E.D. Herzog, H.D. Volk, A. Kramer, and B. Maier, *A circadian clock in macrophages controls inflammatory immune responses.* Proceedings of the National Academy of Sciences of the United States of America, 2009. **106**(50): p. 21407-21412.

195. Porter, S., L. Glaser, and R.P. Bunge, *Release of autocrine growth factor by primary and immortalized Schwann cells.* Proc Natl Acad Sci U S A, 1987. **84**(21): p. 7768-72.

196. Toda, K., J.A. Small, S. Goda, and R.H. Quarles, *Biochemical and cellular properties of three immortalized Schwann cell lines expressing different levels of the myelin-associated glycoprotein.* J Neurochem, 1994. **63**(5): p. 1646-57.

197. Hai, M., N. Muja, G.H. DeVries, R.H. Quarles, and P.I. Patel, *Comparative analysis of Schwann cell lines as model systems for myelin gene transcription studies.* Journal of Neuroscience Research, 2002. **69**(4): p. 497-508.

198. Harrisingh, M.C., E. Perez-Nadales, D.B. Parkinson, D.S. Malcolm, A.W. Mudge, and A.C. Lloyd, *The Ras/Raf/ERK signalling pathway drives Schwann cell dedifferentiation.* Embo Journal, 2004. **23**(15): p. 3061-3071.

199. Napoli, I., L.A. Noon, S. Ribeiro, A.P. Kerai, S. Parrinello, L.H. Rosenberg, M.J. Collins, M.C. Harrisingh, I.J. White, A. Woodhoo, and A.C. Lloyd, *A central role for the ERK-signaling pathway in controlling Schwann cell plasticity and peripheral nerve regeneration in vivo.* Neuron, 2012. **73**(4): p. 729-42.

200. Yang, D.P., J. Kim, N. Syed, Y.J. Tung, A. Bhaskaran, T. Mindos, R. Mirsky, K.R. Jessen, P. Maurel, D.B. Parkinson, and H.A. Kim, *p38 MAPK activation promotes denervated Schwann cell phenotype and functions as a negative regulator of Schwann cell differentiation and myelination.* J Neurosci, 2012. **32**(21): p. 7158-68.

201. Wang, H.B., C. Cheng, Y.W. Qin, S.Q. Niu, S.F. Gao, X. Li, T. Tao, and A.G. Shen, *Role of Mitogen-Activated Protein Kinase Cascades in Inducible Nitric Oxide Synthase Expression by Lipopolysaccharide in a Rat Schwann Cell Line.* Neurochemical Research, 2009. **34**(3): p. 430-437.

202. Qin, Y.W., M.H. Hua, Y.N. Duan, Y.J. Gao, X.Y. Shao, H.B. Wang, T. Tao, A.G. Shen, and C. Cheng, *TNF-alpha Expression in Schwann Cells is Induced by LPS and NF-kappa B-Dependent Pathways.* Neurochemical Research, 2012. **37**(4): p. 722-731.

203. Stolt, C.C. and M. Wegner, *Schwann cells and their transcriptional network: Evolution of key regulators of peripheral myelination.* Brain Res, 2016. **1641**(Pt A): p. 101-10.

204. Chen, Y.J., J.X. Zhang, L. Shen, Q. Qi, X.X. Cheng, Z.R. Zhong, Z.Q. Jiang, R. Wang, H.Z. Lu, and J.G. Hu, *Schwann cells induce Proliferation and Migration of*

Oligodendrocyte Precursor Cells Through Secretion of PDGF-AA and FGF-2. J Mol Neurosci, 2015. **56**(4): p. 999-1008.

205. Watabe, K., T. Fukuda, J. Tanaka, H. Honda, K. Toyohara, and O. Sakai, *Spontaneously immortalized adult mouse Schwann cells secrete autocrine and paracrine growth-promoting activities.* J Neurosci Res, 1995. **41**(2): p. 279-90.
206. Sridharan, R., A.R. Cameron, D.J. Kelly, C.J. Kearney, and F.J. O'Brien, *Biomaterial based modulation of macrophage polarization: a review and suggested design principles.* Materials Today, 2015. **18**(6): p. 313-25.
207. Vishwakarma, A., N.S. Bhise, M.B. Evangelista, J. Rouwkema, M.R. Dokmeci, A.M. Ghaemmaghami, N.E. Vrana, and A. Khademhosseini, *Engineering Immunomodulatory Biomaterials To Tune the Inflammatory Response.* Trends Biotechnol, 2016. **34**(6): p. 470-82.
208. Dziki, J.L., D.S. Wang, C. Pineda, B.M. Sicari, T. Rausch, and S.F. Badylak, *Solubilized extracellular matrix bioscaffolds derived from diverse source tissues differentially influence macrophage phenotype.* J Biomed Mater Res A, 2017. **105**(1): p. 138-147.
209. Sicari, B.M., J.L. Dziki, B.F. Siu, C.J. Medberry, C.L. Dearth, and S.F. Badylak, *The promotion of a constructive macrophage phenotype by solubilized extracellular matrix.* Biomaterials, 2014. **35**(30): p. 8605-12.
210. Park-Min, K.H., T.T. Antoniv, and L.B. Ivashkiv, *Regulation of macrophage phenotype by long-term exposure to IL-10.* Immunobiology, 2005. **210**(2-4): p. 77-86.
211. Tarique, A.A., J. Logan, E. Thomas, P.G. Holt, P.D. Sly, and E. Fantino, *Phenotypic, functional, and plasticity features of classical and alternatively activated human macrophages.* Am J Respir Cell Mol Biol, 2015. **53**(5): p. 676-88.
212. Mantovani, A., S.K. Biswas, M.R. Galdiero, A. Sica, and M. Locati, *Macrophage plasticity and polarization in tissue repair and remodelling.* J Pathol, 2013. **229**(2): p. 176-85.

213. Tedesco, S., C. Bolego, A. Toniolo, A. Nassi, G.P. Fadini, M. Locati, and A. Cignarella, *Phenotypic activation and pharmacological outcomes of spontaneously differentiated human monocyte-derived macrophages.* Immunobiology, 2015. **220**(5): p. 545-54.

214. Gillingwater, T.H. and R.R. Ribchester, *Compartmental neurodegeneration and synaptic plasticity in the Wld(s) mutant mouse.* J Physiol, 2001. **534**(Pt 3): p. 627-39.

215. Wood, M.D., S.W. Kemp, C. Weber, G.H. Borschel, and T. Gordon, *Outcome measures of peripheral nerve regeneration.* Ann Anat, 2011. **193**(4): p. 321-33.

216. Schmidt, S. and P. Friedl, *Interstitial cell migration: integrin-dependent and alternative adhesion mechanisms.* Cell Tissue Res, 2010. **339**(1): p. 83-92.

217. Murakami, K. and S. Yoshida, *Nerve injury induces the expression of syndecan-1 heparan sulfate proteoglycan in peripheral motor neurons.* Neurosci Lett, 2012. **527**(1): p. 28-33.

218. Hienola, A., S. Tumova, E. Kulesskiy, and H. Rauvala, *N-syndecan deficiency impairs neural migration in brain.* J Cell Biol, 2006. **174**(4): p. 569-80.

219. Toba, Y., M. Horie, K. Sango, A. Tokashiki, F. Matsui, A. Oohira, and H. Kawano, *Expression and immunohistochemical localization of heparan sulphate proteoglycan N-syndecan in the migratory pathway from the rat olfactory placode.* Eur J Neurosci, 2002. **15**(9): p. 1461-73.

220. Redd, M.J., G. Kelly, G. Dunn, M. Way, and P. Martin, *Imaging macrophage chemotaxis in vivo: Studies of microtubule function in zebrafish wound inflammation.* Cell Motility and the Cytoskeleton, 2006. **63**(7): p. 415-422.

221. Guest, J., A.J. Santamaria, and F.D. Benavides, *Clinical translation of autologous Schwann cell transplantation for the treatment of spinal cord injury.* Curr Opin Organ Transplant, 2013. **18**(6): p. 682-9.

222. Zhang, S.X., F. Huang, M. Gates, and E.G. Holmberg, *Role of endogenous Schwann cells in tissue repair after spinal cord injury.* Neural Regen Res, 2013. **8**(2): p. 177-85.

223. Wang, Y., H.L. Teng, and Z.H. Huang, *Intrinsic migratory properties of cultured Schwann cells based on single-cell migration assay.* PLoS One, 2012. **7**(12): p. e51824.

224. Cote, M.P., A.A. Amin, V.J. Tom, and J.D. Houle, *Peripheral nerve grafts support regeneration after spinal cord injury.* Neurotherapeutics, 2011. **8**(2): p. 294-303.

225. Tom, V.J., H.R. Sandrow-Feinberg, K. Miller, C. Domitrovich, J. Bouyer, V. Zhukareva, M.C. Klaw, M.A. Lemay, and J.D. Houle, *Exogenous BDNF enhances the integration of chronically injured axons that regenerate through a peripheral nerve grafted into a chondroitinase-treated spinal cord injury site.* Exp Neurol, 2013. **239**: p. 91-100.

226. Vikhanski, L., *In search of the lost cord : solving the mystery of spinal cord regeneration*. 2001, Washington, D.C.: Joseph Henry Press. xiii, 269 p.

227. Kabanov, A.V. and H.E. Gendelman, *Nanomedicine in the diagnosis and therapy of neurodegenerative disorders.* Prog Polym Sci, 2007. **32**(8-9): p. 1054-1082.

228. Kim, I.L., S. Khetan, B.M. Baker, C.S. Chen, and J.A. Burdick, *Fibrous hyaluronic acid hydrogels that direct MSC chondrogenesis through mechanical and adhesive cues.* Biomaterials, 2013. **34**(22): p. 5571-80.

229. Ananthanarayanan, B., Y. Kim, and S. Kumar, *Elucidating the mechanobiology of malignant brain tumors using a brain matrix-mimetic hyaluronic acid hydrogel platform.* Biomaterials, 2011. **32**(31): p. 7913-23.

230. Cao, X. and M.S. Shoichet, *Defining the concentration gradient of nerve growth factor for guided neurite outgrowth.* Neuroscience, 2001. **103**(3): p. 831-40.

231. Cao, X. and M.S. Shoichet, *Investigating the synergistic effect of combined neurotrophic factor concentration gradients to guide axonal growth.* Neuroscience, 2003. **122**(2): p. 381-9.

232. Chung, B.G., L.A. Flanagan, S.W. Rhee, P.H. Schwartz, A.P. Lee, E.S. Monuki, and N.L. Jeon, *Human neural stem cell growth and differentiation in a gradient-generating microfluidic device.* Lab Chip, 2005. **5**(4): p. 401-6.

233. Webber, C.A., Y. Xu, K.J. Vanneste, J.A. Martinez, V.M. Verge, and D.W. Zochodne, *Guiding adult Mammalian sensory axons during regeneration.* J Neuropathol Exp Neurol, 2008. **67**(3): p. 212-22.

234. Pinato, G., T. Raffaelli, E. D'Este, F. Tavano, and D. Cojoc, *Optical delivery of liposome encapsulated chemical stimuli to neuronal cells.* J Biomed Opt, 2011. **16**(9): p. 095001.

235. Alto, L.T., L.A. Havton, J.M. Conner, E.R. Hollis, 2nd, A. Blesch, and M.H. Tuszynski, *Chemotropic guidance facilitates axonal regeneration and synapse formation after spinal cord injury.* Nat Neurosci, 2009. **12**(9): p. 1106-13.

236. Dertinger, S.K., X. Jiang, Z. Li, V.N. Murthy, and G.M. Whitesides, *Gradients of substrate-bound laminin orient axonal specification of neurons.* Proc Natl Acad Sci U S A, 2002. **99**(20): p. 12542-7.

237. Kapur, T.A. and M.S. Shoichet, *Immobilized concentration gradients of nerve growth factor guide neurite outgrowth.* J Biomed Mater Res A, 2004. **68**(2): p. 235-43.

238. Moore, K., M. MacSween, and M. Shoichet, *Immobilized concentration gradients of neurotrophic factors guide neurite outgrowth of primary neurons in macroporous scaffolds.* Tissue Eng, 2006. **12**(2): p. 267-78.

239. Sundararaghavan, H.G., S.N. Masand, and D.I. Shreiber, *Microfluidic Generation of Haptotactic Gradients through 3D Collagen Gels for Enhanced Neurite Growth.* J Neurotrauma, 2011.

240. Masand, S.N., I.J. Perron, M. Schachner, and D.I. Shreiber, *Neural cell type-specific responses to glycomimetic functionalized collagen.* Biomaterials, 2012. **33**(3): p. 790-7.

ABSTRACT

BIOMATERIALS APPROACHES FOR UTILIZING THE REGENERATIVE POTENTIAL OF THE PERIPHERAL NERVE INJURY MICROENVIRONMENT

by

MELISSA RENEE WROBEL

August 2017

Advisor: Dr. Harini Sundararaghavan

Major: Biomedical Engineering

Degree: Doctor of Philosophy

Clinically available treatments are insufficient to achieve full functional recovery in large (>3cm) peripheral nerve injuries (PNI). The objectives in this thesis were 1) to study often overlooked elements of intrinsic PNI repair including release of inhibitory CSPGs and post-injury responses of inflammatory macrophages and dedifferentiated Schwann cells; 2) to create biomaterial scaffolds featuring topographical and adhesive cues to enhance neurite outgrowth; and 3) to test the ability of those cues to direct macrophages and Schwann cells towards a pro-regenerative phenotype. It is hypothesized that recapitulating the positive *and* negative cues of the PNI microenvironment can better improve regeneration. The effect of a characteristic CSPG, Chondroitin Sulfate A (CSA), was tested on neurite dynamics of dissociated chick embryo dorsal root ganglion (DRG) neurons using time lapse video microscopy. DRG growth was recorded on different adhesive substrates, including a novel, porcine-derived spinal cord matrix (SCM). The SCM significantly increased neurite extension, reduced neurite stalling, and mitigated CSA inhibition. Flow cytometry was used to measure changes in cell-substrate binding receptor expression in the neurons. Results showed a significant increase in Syndecan-3 receptor expression in neurons treated with CSA, suggesting a possible priming of the cells for regrowth. The CSA was successfully immobilized within electrospun hyaluronic acid (HA) nanofibers using a methacrylation reaction. Blended electrospinning was used to create scaffolds featuring the CSA and SCM cues.

Results showed significantly increased neurite outgrowth on scaffolds with the SCM and low levels of CSA. Higher incorporation of CSA maintained its inhibitory properties. Next the CSA, SCM, and HA fiber cues were tested for their effects on macrophage and Schwann cell phenotype. It was hypothesized that one or more of the cues would accelerate the macrophages return to rest following classical activation (M1/pro-inflammatory) with lipopolysaccharide (LPS; 1μg/mL) and would accelerate the transformation of Schwann cells from an immature state following injury to a mature/pro-myelinating one. Cell phenotypes were functionally assessed using quantified reverse transcription polymerase chain reaction (qRT-PCR), immunofluorescence, and sandwich-ELISA based antibody arrays to measure changes in mRNA expression, morphology, and cytokine release, respectively. Macrophages cultured with the SCM and HA fibers had significantly reduced M1 gene expression, released lower levels of M1 cytokines (IL-1a, RANTES and TFN-a) and assumed an elongated morphology indicative of M2. These cues also induced changes in the Schwann cells including significantly reduced area, increased elongation, decreased expression of immature genes (GFAP) and increased expression of mature genes (Krox20 and Oct6). These results suggest that the SCM and HA nanofibers could trigger non-neuronal cells towards regenerative programs more quickly than traditional PNI interventions. Changes induced by biomaterials have distinct benefits over the use of immunomodulatory cytokines and would be a novel approach to direct repair. Our collective studies offer improved insight into the endogenous potential of the injured peripheral nerve and offer ways to incorporate intrinsic repair cues into a biomaterial system for treating large gaps.

AUTOBIOGRAPHICAL STATEMENT

EDUCATION

- **PhD Biomedical Engineering** Wayne State University, Detroit, MI, 2013 – 2017
- **MS Biomedical Engineering** Wayne State University, Detroit, MI, 2010 – 2013 *GPA: 3.97*
- **BS Materials Science Engineering** University of Michigan, Ann Arbor, MI, 2006 – 2010 *GPA: 3.59*

EXPERIENCE

- **Graduate Research Assistant** Wayne State University, June 2012 – Date *Neural Tissue Engineering Lab*
- **Instructor** Wayne State University, Spring/Summer 2015 *Design Lab Jumpstart I (BME 1925)*
- **Graduate Teaching Assistant** Wayne State University, 2012 – 2013

PRESENTATIONS (5 most recent of 14)

1. **Wrobel, M.R.**, Sundararaghavan, H.G. *Biomaterial Cues for Modulating Macrophage and Schwann Cell Phenotype Following Peripheral Nerve Injury*. Oral Presentation. Society for Biomaterials Annual Meeting. April 2017. Minneapolis, MN.
2. **Wrobel, M.R.**, Sundararaghavan, H.G. *Using Spinal Cord Matrix Proteins and Hyaluronic Acid Nanofibers to Direct a Pro-Regenerative Phenotype in Macrophages and Schwann Cells*. Poster. Graduate and Postdoc Research Symposium. Mar 2017. Wayne State University, Graduate School. Detroit, MI.
3. **Wrobel, M.R.**, Sundararaghavan, H.G. *Positive and Negative Cues for Modulating Neurite Dynamics and Receptor Expression to Improve Peripheral Nerve Regeneration.* Oral Presentation. Summer Biomechanics, Bioengineering and Biotransport Conference. July 2016. National Harbor, MD.
4. **Wrobel, M.R.**, Sundararaghavan, H.G. *Measuring Chondroitin Sulfate-Induced Receptor Upregulation in Peripheral Neurons with Flow Cytometry*. Poster. Graduate and Postdoc Research Symposium. Mar 2016. Wayne State University, Graduate School. Detroit, MI.
5. **Wrobel, M.R.**, Sundararaghavan, H.G. *Flow Cytometric Analysis of Chondroitin Sulfate-Induced Syndecan Receptor Upregulation in Peripheral Neurons.* Oral Presentation. Graduate Student Research Day XIV. Sept 2015. Wayne State University, School of Medicine. Detroit, MI.

PUBLICATIONS

1. **Wrobel, M.R.** and H.G. Sundararaghavan, *Directed Migration in Neural Tissue Engineering*. Tissue Engineering Part B-Reviews, 2014. 20(2): p. 93-105
2. **Wrobel, M.R.** and H.G. Sundararaghavan, *Positive and Negative Cues for Modulating Neurite Dynamics and Receptor Expression.* Biomedical Materials, 2017. 12(2): 025016

AWARDS & HONORS

- Summer Dissertation Fellowship, Wayne State University, 2016
- Diversity Travel Award, Summer Bioengineering, Biomechanics and Biotransport Conference (SB^3C), 2016
- Thomas C. Rumble Graduate Fellowship, Wayne State University, 2013-2014 and 2015-2016
- Graduate Student Professional Travel Award, Wayne State University, 2013 and 2017
- First Prize Oral Presentation, Graduate Student Research Day, Wayne State School of Medicine, 2014
- First Place Poster, Graduate and Postdoc Research Symposium, Wayne State University Graduate School, 2014 and 2017
- Third Place Poster, Graduate and Postdoc Research Symposium, Wayne State University Graduate School, 2016
- B.S. awarded with Magna Cum Laude honors, University of Michigan, 2010
- Girl Scout Gold Award (Topic: Breast Cancer Awareness and Prevention; 150 hours of service), 2006

ACTIVITIES & AFFILIATIONS

- Society for Biomaterials, Student Member 2017 - present
- Society of Women Engineers, Student Member 2015 - present
- Tau Beta Pi Engineering Honor Society, Officer 2013 - present
- Biomedical Engineering Society, Student Member 2012 - present
- Girl Scouts, 1995 – 2006